2011

An Assessment of the Accuracy of Magnetic Resonance Phase Velocity Mapping in Turbulent Flow Through Orifices

Sahitya Pidaparthi
Cleveland State University

AN ASSESSMENT OF THE ACCURACY OF MAGENTIC RESONANCE PHASE VELOCITY MAPPING IN TURBULENT FLOW THROUGH ORIFICES

SAHITYA PIDAPARTHI

Bachelor of Engineering in Chemical Engineering

Jawaharlal Nehru Technological University, India

May, 2007

Submitted in partial fulfillment of requirements for the degree

MASTER OF SCIENCE IN CHEMICAL ENGINEERING

at the

CLEVELAND STATE UNIVERSITY

May, 2011

This thesis has been approved
for the Department of Chemical and Biomedical Engineering
and the College of Graduate Studies by

Thesis Committee Chairperson, Dr. George P. Chatzimavroudis

Chemical and Biomedical Engineering

Department Date

Dr. Randolph M. Setser

Chemical and Biomedical Engineering

Department Date

Dr. Sandra S. Halliburton

Chemical and Biomedical Engineering

Department Date

This thesis is dedicated to my beloved grandfather

Venkateswara Reddy V

ACKNOWLEDGEMENTS

First of all I would like to thank Dr. George P Chatzimavroudis and Dr. Randolph M Setser for providing me with the opportunity to work on this exciting project. They have been very helpful and encouraging throughout my Masters and it is just because of their constant support this thesis has been made possible.

Many thanks also go to Dr. Sandra S Halliburton for all the help and guidance she has offered every time I needed.

I would like to thank the Department of Chemical and Biomedical Engineering and the college of graduate studies for supporting me with tuition waivers throughout my Master's education.

I would also like to thank the entire cardiovascular image group at the Cleveland Clinic Foundation for giving me an opportunity to use the MRI scanner and helping me in getting trained to use the scanner.

My heartfelt thanks go to Ms. Becky Laird and Ms. Darlene for all the help and affection all through these years.

I am thankful to my fellow members of the Biofluid Mechanics & Cardiovascular Imaging Laboratory for their helpful and friendly nature. I would also like to thank Uma Numburi and Navneeth for guiding me at various stages of my thesis.

A special note of thanks goes to Pujitha, Pooja and Rakshith for their invaluable support and encouragement.

I am thankful to all my friends Kiran, Ramesh, Mehmet, Srikanth, Serge, and Mitya for their help throughout my masters.

Finally, I would like to thank my parents, Ramakrishna Reddy Pidaparthi and Vijaya Lakshmi, paternal and maternal grandparents and my beloved brother Chanakya for their continuous love and support all through my life without whom I would have never been heretoday.

AN ASSESSMENT OF THE ACCURACY OF MAGENTIC RESONANCE PHASE VELOCITY MAPPING IN TURBULENT FLOW THROUGH ORIFICES

SAHITYA PIDAPARTHI

ABSTRACT

Magnetic resonance phase velocity mapping (MRPVM) is an established clinical technique to measure blood flow. The acquired information can be used to diagnose a variety of cardiovascular disease. One of the main limitations of MRPVM is that it cannot quantify the flow under turbulent flow conditions. Such conditions develop in certain cases such as in heart valve stenosis and arterial stenosis. Specifically, heart valve stenosis is a serious disease in which the valve does not open as much as necessary for blood to pass through. As a result, the heart has to overwork to overcome the increased resistance. If untreated, the disease can lead to death. One of the diagnostic problems related to stenosis is that the flow through the stenotic orifice becomes turbulent, associated with velocity fluctuations, flow separation and recirculation downstream of the stenosis. Clinically, it is difficult to quantify turbulent flow. Especially in the case of MRPVM, turbulent flow leads to signal loss in the images, resulting in loss of valuable diagnostic information.

This study aimed at investigating the effects of imaging parameters on the ability of MRPVM for turbulent flow quantification. Two orifice models were used, one with a

75% area reduction and another with a 94% area reduction. Axial MRPVM acquisitions were performed (flow rate: 1.2-10.5 L/min; upstream Re: 1271-11124, orifice Re: 2542–44497) inside a 1.5 Tesla whole-body clinical MRI scanner. Three in-plane spatial resolutions (0.9 x 0.9, 1.5 x 1.5, and 2.0 x 2.0 mm^2) and five echo times (2.65, 3.5, 5.0, 7.5, 10.0 msec) were studied. Images were acquired in both models at five locations: 6.0 cm upstream from the orifice; at the orifice; 1.0 cm downstream from the orifice; 3.0 cm downstream from the orifice; and 5.0 cm downstream from the orifice. The MRPVM-measured flow rates were compared with the true flow rates known from rotameters to determine the accuracy.

The results confirmed that MRPVM is highly accurate under laminar flow conditions, but under turbulent flow conditions, the accuracy was reduced. Signal loss caused an underestimation in the flow rate which was higher in the 94% area reduction orifice model as compared to the 75% model. As Re increased, the signal loss and the underestimation in the flow rate increased. Overall, increasing the spatial resolution and shortening the echo time had an effect on improving the accuracy of the measurements, although the effect of resolution was smaller when compared to that of the echo time. Further in vitro studies using additional geometries and a larger range of Re as well as clinical studies are necessary to further investigate ways to improve the ability of MRPVM under turbulent flow conditions.

ABSTRACT ..... **VI**

LIST OF TABLES ..... **X**

LIST OF FIGURES ..... **XV**

NOMENCLATURE ..... **XXX**

CHAPTER

I. INTRODUCTION **1**

II. LITERATURE REVIEW **4**

2.1 Previous and Current Techniques to Measure Flow through Valvular Stenosis **4**

2.2 Magnetic Resonance Imaging and Magnetic Resonance Phase Velocity mapping **5**

2.3 MRPVM of Stenotic Turbulent Flows **11**

III. HYPOTHESIS AND SPECIFIC AIMS **18**

IV. METHODS **21**

4.1 Experimental Apparatus **21**

4.2 Models **23**

4.3 Flow Conditions **26**

4.4 Imaging Procedures and Parameters **27**

4.5 Image Data Analysis 33

V. RESULTS 35

75% Area Reduction Orifice Model – True Flow Rate = 1.2 L/min 35

75% Area Reduction Orifice Model – True Flow Rate = 5.5 L/min 45

75% Area Reduction Orifice Model – True Flow Rate = 10.5 L/min 56

94 % Area Reduction Orifice Model – True Flow Rate = 5.5 L/min 67

94% Area Reduction Orifice Model – True Flow Rate = 8.5 lpm 76

VI. DISCUSSION 96

The Effects of TE 99

The Effects of In-plane Resolution 110

Effect of Imaging Parameters and Geometry on MRPVM Flow Measurements 114

VII. LIMITATIONS AND FUTURE RECOMMENDATIONS 116

VIII. CONCLUSIONS 118

REFERENCES 120

APPENDIX 128

APPENDIX A 129

APPENDIX B 137

LIST OF TABLES

Table **Page**

Table 4.1: Flow rates, Average cross-sectional velocity values and Reynolds numbers in 75% orifice models...…….26

Table 4.2: Flow rates, Average cross-sectional velocity values and Reynolds numbers in 94% orifice models……..……..27

Table 4.3: Imaging parameters used for the transverse MRPVM through-plane acquisitions in the 75% Orifice model - flow rate: 1.2 L/min……..……..28

Table 4.4: Imaging parameters used for the transverse MRPVM through-plane acquisitions in the 75% Orifice model - flow rate: 5.5 L/min……..…….29

Table 4.5: Imaging parameters used for the transverse MRPVM through-plane acquisitions in the 75% Orifice model - flow rate: 10.5 L/min…..……...30

Table 4.6: Imaging parameters used for the transverse MRPVM through-plane acquisitions in the 94% Orifice model - flow rate: 5.5 L/min……..…….31

Table 4.7: Imaging parameters used for the transverse MRPVM through-plane acquisitions in the 94% Orifice model - flow rate: 8.5 L/min.……..32

Table 5.1: Measured flow rates (L/min) at five TEs and three in-plane spatial resolutions; Slice location: 6 cm upstream from the orifice; True flow rate = 1.2 L/min; 75% orifice model……..36

Table 5.2: Measured flow rates (L/min) at five TEs and three in-plane spatial resolutions; Slice location: at the orifice; True flow rate = 1.2 L/min; 75% orifice model……..37

Table 5.3: Measured flow rates (L/min) at five TEs and three in-plane spatial resolutions; Slice location: 1 cm downstream from the orifice; True flow rate = 1.2 L/min; 75% orifice model……..38

Table 5.4: Measured flow rates (L/min) at five TEs and three in-plane spatial resolutions; Slice location: 3 cm downstream from the orifice; True flow rate = 1.2 L/min; 75% orifice model……..……39

Table 5.5: Measured flow rates (L/min) at five TEs and three in-plane spatial resolutions; Slice location: 5 cm downstream from the orifice; True flow rate = 1.2 L/min; 75% orifice model……..……40

Table 5.6: Measured flow rates (L/min) at five TEs and three in-plane spatial resolutions; Slice location: 6 cm upstream from the orifice; True Flow Rate =5.5 L/min; 75% orifice model…….……45

Table 5.7: Measured flow rates (L/min) at five TEs and three in-plane spatial resolutions; Slice location: at the orifice; True Flow Rate =5.5 L/min; 75% orifice model…….46

Table 5.8: Measured flow rates (L/min) at five TEs and three in-plane spatial resolutions; Slice location: 1 cm downstream from the orifice; True Flow Rate =5.5 L/min; 75% orifice model……..47

Table 5.9: Measured flow rates (L/min) at five TEs and three in-plane spatial resolutions; Slice location: 3 cm downstream from the orifice; True Flow Rate =5.5 L/min; 75% orifice model…...……...48

Table 5.10: Measured flow rates (L/min) at five TEs and three in-plane spatial resolutions; Slice location: 5 cm downstream from the orifice; True Flow Rate =5.5 L/min; 75% orifice model……..…….……...49

Table 5.11: Measured flow rates (L/min) at five TEs and three in-plane spatial resolutions; Slice location: 6.0 cm upstream from the orifice; True Flow Rate = 10.5 Lpm; 75% orifice model……..……..56

Table 5.12: Measured flow rates (L/min) at five TEs and three in-plane spatial resolutions; Slice location: at the orifice; True Flow Rate = 10.5 Lpm; 75% orifice model……...……...57

Table 5.13: Measured flow rates (L/min) at five TEs and three in-plane spatial resolutions; Slice location: 1.0 cm downstream from the orifice; True Flow Rate = 10.5 Lpm; 75% orifice model…….……...58

Table 5.14: Measured flow rates (L/min) at five TEs and three in-plane spatial resolutions; Slice location: 3.0 cm downstream from the orifice; True Flow Rate = 10.5 Lpm; 75% orifice model……..……..59

Table 5.15: Measured flow rates (L/min) at five TEs and three in-plane spatial resolutions; Slice location: 5.0 cm downstream from the orifice; True Flow Rate = 10.5 Lpm; 75% orifice model……..……...60

Table 5.16: Measured flow rates (L/min) at five TEs and three in-plane spatial resolutions; Slice location: 6.0 cm upstream from the orifice; True Flow Rate = 5.5 Lpm; 94% orifice model……...……...67

Table 5.17: Measured flow rates (L/min) at five TEs and three in-plane spatial resolutions; Slice location: At the orifice; True Flow Rate = 5.5 Lpm; 94% orifice model……...……...68

Table 5.18: Measured flow rates (L/min) at five TEs and three in-plane spatial resolutions; Slice location: 1.0 cm downstream from the orifice; True Flow Rate = 5.5 Lpm; 94% orifice model……..……..69

Table 5.19: Measured flow rates (L/min) at five TEs and three in-plane spatial resolutions; Slice location: 3.0 cm downstream from the orifice; True flow rate = 5.5 L/min; 94% orifice model……...……...70

Table 5.20: Measured flow rates (L/min) at five TEs and three in-plane spatial resolutions; Slice location: 5.0 cm downstream from the orifice; True flow rate = 5.5 L/min; 94% orifice model…...……..76

Table 5.21: Measured flow rates (L/min) at five TEs and three in-plane spatial resolutions; Slice location: 6 cm upstream from the orifice; True flow rate = 8.5 L/min; 94% orifice model……...……..77

Table 5.22: Measured flow rates (L/min) at five TEs and three in-plane spatial resolutions; Slice location: At the orifice; True flow rate = 8.5 L/min; 94% orifice model……75

Table 5.23: Measured flow rates (L/min) at five TEs and three in-plane spatial resolutions; Slice location: 1.0 cm downstream from the orifice; True flow rate = 8.5 L/min; 94% orifice model……..……78

Table 5.24: Measured flow rates (L/min) at five TEs and three in-plane spatial resolutions; Slice location: 3.0 cm downstream from the orifice; True flow rate = 8.5 L/min; 94% orifice model……79

Table 5.25: Measured flow rates (L/min) at five TEs and three in-plane spatial resolutions; Slice location: 5.0 cm downstream from the orifice; True flow rate = 8.5 L/min; 94% orifice model……80

LIST OF FIGURES

Figure **Page**

Figure 2.1: Gradient Echo Pulse Sequence diagram...……10

Figure 4.1: Schematic of the Steady State Flow loop...……...22

Figure 4.2: Schematic of the 75% Orifice model……...……...24

Figure 4.3: Schematic of the 94% Orifice model……..25

Figure 4.4: Sample Magnitude and Phase images…...……..33

Figure 5.1: Magnitude and phase images of the 75 % orifice model at 1.2 L/min; in-plane resolution: 0.9 x 0.9 mm^2; TE = 2.65 msec. (a) 6.0 cm upstream from the orifice, (b) at the orifice, (c) 1.0 cm downstream from the orifice, (d) 3.0 cm downstream from the orifice, and (e) 5.0 cm downstream from the orifice…….41

Figure 5.2: Percent error in flow rate measurement as a function of TE for the 75% orifice model, at each slice position for a true flow rate of 1.2 L/min; In-plane resolution: 0.9 x 0.9 mm^2…….42

Figure 5.3: Percent error in flow rate measurement as a function of TE for the 75% orifice model, at each slice position for a true flow rate of 1.2 L/min; In-plane resolution: 1.5 x 1.5 mm^2…….42

Figure 5.4: Percent error in flow rate measurement as a function of TE for the 75% orifice model, at each slice position for a true flow rate of 1.2 L/min; In-plane resolution: 2.0 x 2.0 mm^2……...……..43

Figure 5.5: Percentage error in flow rate measurement as a function of in-plane resolution for the 75% orifice model; Slice position: 6.0 cm upstream; for a true flow rate of 1.2 L/min……..44

Figure 5.6: Percentage error in flow rate measurement as a function of in-plane resolution for the 75% orifice model; Slice position: at the orifice; for a true flow rate of 1.2 L/min……..44

Figure 5.7: Magnitude and phase images of the 75% orifice model at 1.2 L/min; in-plane resolution: 0.9 x 0.9 mm^2; TE = 2.65 msec. (a) 6.0 cm upstream from the orifice, (b) at the orifice, (c) 1.0 cm downstream from the orifice, (d) 3.0 cm downstream from the orifice and (e) 5.0 cm downstream from the orifice……..50

Figure 5.8: Percent error in flow rate measurement as a function of TE for the 75% orifice model, at each slice position for a true flow rate of 5.5 L/min; In-plane resolution: 0.9 x 0.9 mm^2……..……51

Figure 5.9: Percent error in flow rate measurement as a function of TE for the 75% orifice model, at each slice position for a true flow rate of 5.5 L/min; In-plane resolution: 1.5 x 1.5 mm^2……..……52

Figure 5.10: Percent error in flow rate measurement as a function of TE for the 75% orifice model, at each slice position for a true flow rate of 5.5 L/min; In-plane resolution: 2.0 x 2.0 mm^2……..……53

Figure 5.11: Percentage error in flow rate measurement as a function of in-plane resolution for the 75% orifice model; Slice position: 6.0 cm upstream; for a true flow rate of 5.5 L/min……...……54

Figure 5.12: Percentage error in flow rate measurement as a function of in-plane resolution for the 75% orifice model; Slice position: at the orifice; for a true flow rate of 5.5 L/min……55

Figure 5.13: Percentage error in flow rate measurement as a function of in-plane resolution for the 75% orifice model; Slice position: 1.0 cm downstream; for a true flow rate of 5.5 L/min……55

Figure 5.14: Magnitude and phase images of the 75% orifice model at 10.5 L/min; in-plane resolution: 0.9 x 0.9 mm^2; at TE = 2.65 msec. (a) 6.0 cm upstream from the orifice, (b) at the orifice, (c) 1.0 cm downstream from the orifice, (d) 3.0 cm downstream from the orifice and (e) 5.0 cm downstream from the orifice.……...61

Figure 5.15: Percent error in flow rate measurement as a function of TE for 75% orifice model, at each slice position for a true flow rate of 10.5 L/min; In-plane resolution: 0.9 x 0.9 mm^2.……...……..62

Figure 5.16: Percent error in flow rate measurement as a function of TE for 75% orifice model, at each slice position for a true flow rate of 10.5 L/min; In-plane resolution: 1.5 x 1.5 mm^2……..63

Figure 5.17: Percent error in flow rate measurement as a function of TE for 75% orifice model, at each slice position for a true flow rate of 10.5 L/min; In-plane resolution: 2.0 x 2.0 mm^2……..64

Figure 5.18: Percentage error in flow rate measurement as a function of in-plane resolution for the 75% orifice model; Slice position: 6.0 cm upstream; for a true flow rate of 10.5 L/min……...……..65

Figure 5.19: Percentage error in flow rate measurement as a function of in-plane resolution for the 75% orifice model; Slice position: at the orifice; for a true flow rate of 10.5 L/min……..65

Figure 5.20: Percentage error in flow rate measurement as a function of in-plane resolution for the 75% orifice model; Slice position: 1.0 cm downstream; for a true flow rate of 10.5 L/min……..66

Figure 5.21: Magnitude and phase images of the 94 % orifice model at 5.5 L/min; in-plane resolution: 0.9 x 0.9 mm^2; TE = 2.65 msec. (a) 6.0 cm upstream from the orifice, (b) at the orifice, (c) 1.0 cm downstream from the orifice, (d) 3.0 cm downstream from the orifice and (e) 5.0 cm downstream from the orifice...…….....72

Figure 5.22: Percentage error in the flow rate measurement as a function of TE for 94% orifice model at each slice position for a true flow rate of 5.5 L/min; In-plane resolution: 0.9 x 0.9 mm^2…….....73

Figure 5.23: Percentage error in flow rate measurement as a function of in-plane resolution for the 94% orifice model; Slice position: 1.0 cm downstream; for a true flow rate of 5.5 L/min……...…….....74

Figure 5.24: Percentage error in flow rate measurement as a function of in-plane resolution for the 94% orifice model; Slice position: 5.0 cm downstream; for a true flow rate of 5.5 L/min……...…….....75

Figure 5.25: Magnitude and phase images of the 94% orifice model at 8.5 L/min; in-plane resolution: 0.9 x 0.9 mm^2; TE = 2.65 msec. (a) 6.0 cm upstream from the orifice, (b) at the orifice, (c) 1.0 cm downstream from the orifice, (d) 3.0 cm downstream from the orifice and (e) 5.0 cm downstream from the orifice.…….....81

Figure 5.26: Percentage error in the flow rate measurement as a function of TE for 94% orifice model at each slice position for a true flow rate of 8.5 L/min; In-plane resolution: 0.9 x 0.9 mm^2…….82

Figure 5.27: Percentage error in flow rate measurement as a function of in-plane resolution for the 94% orifice model; Slice position: at the orifice; for a true flow rate of 8.5 L/min……..……..83

Figure 5.28: Percentage error in flow rate measurement as a function of in-plane resolution for the 94% orifice model; Slice position: 1.0 cm downstream; for a true flow rate of 8.5 L/min……84

Figure 5.29: Percentage error in flow rate measurement as a function of in-plane resolution for the 94% orifice model; Slice position: 3.0 cm downstream; for a true flow rate of 8.5 L/min……..…..84

Figure 5.30: Percentage error in flow rate measurement as a function of in-plane resolution for the 94% orifice model; Slice position: 5.0 cm downstream; for a true flow rate of 8.5 L/min……...…….....85

Figure 5.31: Relationship between the measured flow rate and the true flow rate for all TEs, at 6.0 cm upstream from the 75% orifice; In-plane resolution = 0.9 x 0.9 mm^2.....86

Figure 5.32: Relationship between the measured flow rate and the true flow rate for all TEs, at the Orifice, from the 75% orifice; In-plane resolution = 0.9 x 0.9 mm^2……..…..87

Figure 5.33: Relationship between the measured flow rate and the true flow rate for all TEs, at the 1 cm downstream from the 75% orifice; In-plane resolution = 0.9 x 0.9 mm^2 ……88

Figure 5.34: Relationship between the measured flow rate and the true flow rate for all TEs, at the 3 cm downstream from the 75% orifice; In-plane resolution = 0.9 x 0.9 mm^2……..**.....**89

Figure 5.35: Relationship between the measured flow rate and the true flow rate for all TEs, at the 5 cm downstream from the 75% orifice; In-plane resolution = 0.9 x 0.9 mm^2……...…….....90

Figure 5.36: Relationship between the measured flow rate and the true flow rate for all TEs, at 6.0 cm upstream from the 94% orifice; In-plane resolution = 0.9 x 0.9 mm^2…...91

Figure 5.37: Relationship between the measured flow rate and the true flow rate for all TEs, at the Orifice, from the 94% orifice; In-plane resolution = 0.9 x 0.9 mm^2…...……92

Figure 5.38: Relationship between the measured flow rate and the true flow rate for all TEs, at the 1 cm downstream from the 94% orifice; In-plane resolution = 0.9 x 0.9 mm^2……93

Figure 5.39: Relationship between the measured flow rate and the true flow rate for all TEs, at the 3 cm downstream from the 94% orifice; In-plane resolution = 0.9 x 0.9 mm^2……..…….94

Figure 5.40: Relationship between the measured flow rate and the true flow rate for all TEs, at the 5 cm downstream from the 94% orifice; In-plane resolution = 0.9 x 0.9 mm^2…….……..94

Figure 6.1: Set of magnitude (top) and phase images (bottom) from the 75% orifice model; Slice location: at the orifice; Flow Rate = 1.2 L/min, Re = 2543; Spatial Resolution: 0.9x0.9 mm^2; TE: (a) 2.65, (b) 3.5, (c) 5.0, (d) 7.5, and (e) 10.0 msec…...101

Figure 6.2: Set of magnitude (top) and phase images (bottom) from the 75% orifice model; Slice location: 1.0 cm downstream from the orifice, Flow Rate = 1.2 L/min, Re =

1271; Spatial Resolution: 0.9x0.9 mm^2; TE: (a) 2.65, (b) 3.5, (c) 5.0, (d) 7.5 and (e) 10.0 msec……101

Figure 6.3: Set of magnitude (top) and phase images (bottom) from the 75% orifice model; Slice location: at the orifice, Flow Rate = 5.5 L/min, Re = 11654; Spatial Resolution: 0.9x0.9 mm^2; TE: (a) 2.65, (b) 3.5, (c) 5.0, (d) 7.5 and (e) 10.0 msec…….102

Figure 6.4: Set of magnitude (top) and phase images (bottom) from the 75% orifice model; Slice location: 1.0 cm downstream from the orifice, Flow Rate = 5.5 L/min, Re = 5827; Spatial Resolution: 0.9x0.9 mm^2; TE: (a) 2.65, (b) 3.5, (c) 5.0, (d) 7.5 and (e) 10.0 msec……...……..103

Figure 6.5: Set of magnitude (top) and phase images (bottom) from the 75% orifice model; Slice location: at the orifice, Flow Rate = 10.5 L/min, Re = 22248; Spatial Resolution: 0.9x0.9 mm^2; TE: (a) 2.65, (b) 3.5, (c) 5.0, (d) 7.5 and (e) 10.0 msec…....104

Figure 6.6: Set of magnitude (top) and phase images (bottom) from the 75% orifice model; Slice location: 1.0 cm downstream from the orifice, Flow Rate = 10.5 L/min, Re = 11124; Spatial Resolution: 0.9x0.9 mm^2; TE: (a) 2.65, (b) 3.5, (c) 5.0, (d) 7.5 and (e) 10.0 msec……104

Figure 6.7: Set of magnitude (top) and phase images (bottom) from the 94% orifice model; Slice location: At the orifice; Flow Rate = 5.5 L/min, Re = 23308; Spatial Resolution: 0.9x0.9 mm^2; TE: (a) 2.65, (b) 3.5, (c) 5.0, (d) 7.5 and (e) 10.0 msec…….106

Figure 6.8: Set of magnitude (top) and phase images (bottom) from the 94% orifice model; Slice location: 1.0 cm downstream from the orifice; Flow Rate = 5.5 L/min, Re =

5827; Spatial Resolution: 0.9x0.9 mm^2; TE: (a) 2.65, (b) 3.5, (c) 5.0, (d) 7.5 and (e) 10.0 msec……106

Figure 6.9: Set of magnitude (top) and phase images (bottom) from the 94% orifice model; Slice location: 3.0 cm downstream from the orifice; Flow Rate = 5.5 L/min, Re = 5827; Spatial Resolution: 0.9x0.9 mm^2; TE: (a) 2.65, (b) 3.5, (c) 5.0, (d) 7.5 and (e) 10.0 msec……107

Figure 6.10: Set of magnitude (top) and phase images (bottom) from the 94% orifice model; Slice location: 5.0 cm downstream from the orifice; Flow Rate = 5.5 L/min, Re = 5827; Spatial Resolution: 0.9x0.9 mm^2; TE: (a) 2.65, (b) 3.5, (c) 5.0, (d) 7.5 and (e) 10.0 msec……108

Figure 6.11: Set of magnitude (top) and phase images (bottom) from the 94% orifice model; Slice location: At the orifice; Flow Rate = 8.5 L/min, Re = 44496; Spatial Resolution: 0.9x0.9 mm^2; TE: (a) 2.65, (b) 3.5, (c) 5.0, (d) 7.5 and (e) 10.0 msec…….108

Figure 6.12: Set of magnitude (top) and phase images (bottom) from the 94% orifice model; Slice location: 1.0 cm downstream from the orifice; Flow Rate = 8.5 L/min, Re = 11124; Spatial Resolution: 0.9x0.9 mm^2; TE: (a) 2.65, (b) 3.5, (c) 5.0, (d) 7.5 and (e) 10.0 msec……109

Figure 6.13: Set of magnitude (top) and phase images (bottom) from the 94% orifice model; Slice location: 3.0 cm downstream from the orifice; Flow Rate = 8.5 L/min, Re = 11124; Spatial Resolution: 0.9x0.9 mm^2; TE: (a) 2.65, (b) 3.5, (c) 5.0, (d) 7.5 and (e) 10.0 msec……109

Figure 6.14: Set of magnitude (top) and phase images (bottom) from the 94% orifice model; Slice location: 5.0 cm downstream from the orifice; Flow Rate = 8.5 L/min, Re = 11124; Spatial Resolution: 0.9x0.9 mm^2; TE: (a) 2.65, (b) 3.5, (c) 5.0, (d) 7.5 and (e) 10.0 msec……110

Figure 6.15: Percentage error in flow rate measurement as a function of in-plane resolution for the 75% orifice model; Slice position: at the orifice; for a true flow rate of 5.5 L/min……..111

Figure 6.16: Percentage error in flow rate measurement as a function of in-plane resolution for the 75% orifice model; Slice position: at the orifice; for a true flow rate of 10.5 L/min……111

Figure 6.17: Percentage error in flow rate measurement as a function of in-plane resolution for the 94% orifice model; Slice position: 5.0 cm downstream; for a true flow rate of 5.5 L/min……..112

Figure 6.18: Percentage error in flow rate measurement as a function of in-plane resolution for the 94% orifice model; Slice position: at the orifice; for a true flow rate of 8.5 L/min……..113

Figure 6.19: Percentage error in flow rate measurement as a function of in-plane resolution for the 94% orifice model; Slice position: 1.0 cm downstream; for a true flow rate of 8.5 L/min……..114

Figure A.1: Percentage error in flow rate measurement as a function of in-plane resolution for the 75% orifice model; Slice position: 1.0 cm downstream; for a true flow rate of 1.2 L/min……..129

Figure A.2: Percentage error in flow rate measurement as a function of in-plane resolution for the 75% orifice model; Slice position: 3.0 cm downstream; for a true flow rate of 1.2 L/min……..130

Figure A.3: Percentage error in flow rate measurement as a function of in-plane resolution for the 75% orifice model; Slice position: 5.0 cm downstream; for a true flow rate of 1.2 L/min……..130

Figure A.4: Percentage error in flow rate measurement as a function of in-plane resolution for the 75% orifice model; Slice position: 3.0 cm downstream; for a true flow rate of 5.5 L/min……..131

Figure A.5: Percentage error in flow rate measurement as a function of in-plane resolution for the 75% orifice model; Slice position: 5.0 cm downstream; for a true flow rate of 5.5 L/min……..131

Figure A.6: Percentage error in flow rate measurement as a function of in-plane resolution for the 75% orifice model; Slice position: 3.0 cm downstream; for a true flow rate of 10.5 L/min……132

Figure A.7: Percentage error in flow rate measurement as a function of in-plane resolution for the 75% orifice model; Slice position: 5.0 cm downstream; for a true flow rate of 10.5 L/min……132

Figure A.8: Percentage error in the flow rate measurement as a function of TE for 94% orifice model at each slice position for a true flow rate of 5.5 L/min; In-plane resolution: 1.5 x 1.5 mm^2……...133

Figure A.9: Percentage error in the flow rate measurement as a function of TE for 94% orifice model at each slice position for a true flow rate of 5.5 L/min; In-plane resolution: 2.0 x 2.0 mm^2……...133

Figure A.10: Percentage error in flow rate measurement as a function of in-plane resolution for the 94% orifice model; Slice position: 6.0 cm upstream; for a true flow rate of 5.5 L/min…….134

Figure A.11: Percentage error in flow rate measurement as a function of in-plane resolution for the 94% orifice model; Slice position: At the orifice; for a true flow rate of 5.5 L/min……..134

Figure A.12: Percentage error in flow rate measurement as a function of in-plane resolution for the 94% orifice model; Slice position: 3.0 cm downstream; for a true flow rate of 5.5 L/min…….…….135

Figure A.13: Percentage error in the flow rate measurement as a function of TE for 94% orifice model at each slice position for a true flow rate of 8.5 L/min; In-plane resolution: 1.5 x 1.5 mm^2……..135

Figure A.14: Percentage error in the flow rate measurement as a function of TE for 94% orifice model at each slice position for a true flow rate of 8.5 L/min; In-plane resolution: 1.5 x 1.5 mm^2……...136

Figure A.15: Percentage error in flow rate measurement as a function of in-plane resolution for the 94% orifice model; Slice position: 6.0 cm upstream; for a true flow rate of 8.5 L/min…….136

Figure B.1: Relationship between the measured flow rate and the true flow rate for all TEs, at 6.0 cm upstream from the 75% orifice; In-plane resolution = 1.5 x 1.5 mm^2….137

Figure B.2: Relationship between the measured flow rate and the true flow rate for all TEs, at 6.0 cm upstream from the 75% orifice; In-plane resolution = 2.0 x 2.0 mm^2….137

Figure B.3: Relationship between the measured flow rate and the true flow rate for all TEs, at the orifice, from the 75% orifice; In-plane resolution = 1.5 x 1.5 mm^2……..138

Figure B.4: Relationship between the measured flow rate and the true flow rate for all TEs, at the orifice, from the 75% orifice; In-plane resolution = 2.0 x 2.0 mm^2……..138

Figure B.5: Relationship between the measured flow rate and the true flow rate for all TEs, at 1.0 cm downstream from the 75% orifice; In-plane resolution = 1.5 x 1.5 mm^2……..139

Figure B.6: Relationship between the measured flow rate and the true flow rate for all TEs, at 1.0 cm downstream from the 75% orifice; In-plane resolution = 2.0 x 2.0 mm^2……..139

Figure B.7: Relationship between the measured flow rate and the true flow rate for all TEs, at 3.0 cm downstream from the 75% orifice; In-plane resolution = 1.5 x 1.5 mm^2……..140

Figure B.8: Relationship between the measured flow rate and the true flow rate for all TEs, at 3.0 cm downstream from the 75% orifice; In-plane resolution = 2.0 x 2.0 mm^2……..140

Figure B.9: Relationship between the measured flow rate and the true flow rate for all TEs, at 5.0 cm downstream from the 75% orifice; In-plane resolution = 1.5 x 1.5 mm^2……..141

Figure B.10: Relationship between the measured flow rate and the true flow rate for all TEs, at 5.0 cm downstream from the 75% orifice; In-plane resolution = 2.0 x 2.0 mm^2…..……141

Figure B.11: Relationship between the measured flow rate and the true flow rate for all TEs, at 6.0 cm upstream from the 94% orifice; In-plane resolution = 1.5 x 1.5 mm^2. ……..142

Figure B.12: Relationship between the measured flow rate and the true flow rate for all TEs, at 6.0 cm upstream from the 94% orifice; In-plane resolution = 2.0 x 2.0 mm^2……..142

Figure B.13: Relationship between the measured flow rate and the true flow rate for all TEs, at the orifice, from the 94% orifice; In-plane resolution = 1.5 x 1.5 mm^2……..143

Figure B.14: Relationship between the measured flow rate and the true flow rate for all TEs, at the orifice, from the 94% orifice; In-plane resolution = 2.0 x 2.0 mm^2……..143

Figure B.15: Relationship between the measured flow rate and the true flow rate for all TEs, at 1.0 cm from the 94% orifice; In-plane resolution = 1.5 x 1.5 mm^2…….144

Figure B.16: Relationship between the measured flow rate and the true flow rate for all TEs, at 1.0 cm from the 94% orifice; In-plane resolution = 2.0 x 2.0 mm^2…….144

Figure B.17: Relationship between the measured flow rate and the true flow rate for all TEs, at 3.0 cm from the 94% orifice; In-plane resolution = 1.5 x 1.5 mm^2…….145

Figure B.18: Relationship between the measured flow rate and the true flow rate for all TEs, at 30 cm from the 94% orifice; In-plane resolution = 2.0 x 2.0 mm^2……..145

Figure B.19: Relationship between the measured flow rate and the true flow rate for all TEs, at 5.0 cm from the 94% orifice; In-plane resolution = 1.5 x 1.5 mm^2…….146

Figure B.20: Relationship between the measured flow rate and the true flow rate for all TEs, at 5.0 cm from the 94% orifice; In-plane resolution = 2.0 x 2.0 mm^2…….146

NOMENCLATURE

CFD	**Computational Fluid Dynamics**
ID	**Internal Diameter**
MR	**Magnetic Resonance**
MRPVM	**Magnetic Resonance Phase Velocity Mapping**
RF	**Radio Frequency**
TE	**Echo Time**
TR	**Repetition Time**

CHAPTER I

INTRODUCTION

The number of individuals suffering from various types of cardiovascular disease has been increasing. Approximately, 81 million Americans have been suffering from various types of heart and blood vessel diseases [1]. Cardiac malformation is the most common abnormality and roughly 0.5 % of the infants around the world are born with congenital cardiac malformation. Amongst these valvular defects account for 25% of the malformations [2]. Heart valve stenosis plays a significant role in many types of heart diseases. Valvular diseases have a high mortality rate and approximately 82000 valvular replacements are performed in United States every year [2]. Valvular heart diseases occur when the heart valves stop functioning normally. It can be either due to valvular stenosis or regurgitation. In case of stenosis, the valve leaflets become harder narrowing the valve opening. Based on the severity of the stenosis, the heart function is reduced. Valvular stenosis (atrioventricular valves or outflow tract valves) leads to an increase in the pressure gradient across the valve, whose magnitude depends on the degree of stenosis

and the blood flow rate across the valve. In case of higher degree of stenosis, there is a possibility for turbulent blood flow patterns across the valve. Mitral valve stenosis, tricuspid valve stenosis, aortic valve stenosis and pulmonic valve stenosis are examples for valvular stenosis. In all the cases, the valve opening is reduced, creating high resistance for blood flow across the valves. This increases the pressure across the valve and thereby increasing the blood flow velocity leading to complex turbulent flow conditions [3]. So it is very important to develop a reliable and practical diagnostic protocol which will accurately quantify the severity of the stenosis.

Clinically it has been very difficult to quantify turbulent flow. Among all the clinical modalities, hydrogen based magnetic resonance (MR) imaging is a widely used imaging modality which provides important information about cardiovascular anatomy and function non-invasively without using ionizing radiation. Magnetic resonance phase velocity mapping (MRPVM) is a special MR technique able to accurately quantify blood flow. MRPVM is the only clinical technique which can measure the flow velocity in all of the three spatial directions. Although it has been shown to be accurate and precise under laminar flow conditions, it has limitations under turbulent flow conditions.

The first blood flow measurement was reported by Moran in 1982. He used a velocity encoding gradient along with the conventional MR and obtained flow images [4]. Later, phase changes were used for blood flow measurements by Van Dijk in 1983 [37]. The first clinical measurement of blood flow was reported by Bryant et al in 1984. By using phase difference technique in combination with gradient recalled echo sequence flow measurements were carried out in femoral and carotid arteries in vivo. Results were

validated in vitro using a continuous flow water phantom and in vivo using Doppler ultrasound [38]. Studies conducted by Yokosawa et al in the year 2005 showed that 2D cine phase contrast MRI can be used to study complex blood flow patterns in human body. Their results confirmed that 2D cine PCMRI was accurate only at lower flow rates [5].

This study aimed at determining the effects of vessel geometry and imaging parameters, such as echo time (TE) and spatial resolution, on the quality of the acquired MRPVM data under turbulent flow conditions. Axial MR images were acquired for two area reduction orifice models (75% and 94% area reduction) under steady flow conditions in a 1.5T Siemens MR scanner for different flow rates (1.2 L/min – 10.5 L/min), five slice locations and varying imaging parameters (echo times and in-plane spatial resolutions). The images were then analyzed at Cleveland Clinic Foundation using Argus software and at Cleveland State University using Transform software. The results were then compared to study the effect of geometry and imaging parameters on MRPVM measurements.

CHAPTER II

LITERATURE REVIEW

This chapter provides details about the history of flow measurements through valvular stenosis as well as the principles and some history about MRPVM.

2.1 Previous and Current Techniques to Measure Flow through Valvular Stenosis

Doppler echocardiography played a significant role in evaluating the valvular heart disease [6-9]. Analyzing the Doppler blood velocity data can be useful in determining the severity of valvular stenosis. The detection of presence or absence of stenosis is usually based on detection of turbulence and increased flow in the stenosis area [10]. 3D echocardiography can be very useful in the assessment of complex cardiac morphology. Specially using 3D echocardiography, additional slices can be generated with the same volume of data available but at a later time [11]. The use of cardiac catheterization has been limited to preoperative evaluation of the coronary arteries or to find the discrepancies between clinical findings and echocardiographic data [12]. The main issue

in echocardiography is to collect the data accurately as the velocity is calculated from Doppler frequency shift. For this the ultrasound must be aligned parallel to the flow. But the direction of the stenotic jet is unpredictable, so it is very important to take every precaution to avoid the error [13]. The 3D MR imaging, being a non-invasive technique, serves as an alternative to echocardiography [14-16]. MR imaging allows accurate measurement of velocity profiles similar to color Doppler ultrasonography or duplex Doppler and doesn't have any limitations to acoustic penetrations to various regions of the heart [17, 18]. Study conducted by Bluestein and Einav using Laser Doppler Anemometry in a pulse duplicator system using prosthetic heart valves at mitral and aortic valve positions showed that the highest level of turbulence was closely related to degree of stenosis, valve position and was observed in the decelerating phase. The flow was later laminar in the accelerating phase [19]. Study conducted by Caruthers et al proved that velocity encoded MRI can be used as a reliable technique to evaluate the flow through stenotic aortic valves [20].

2.2 Magnetic Resonance Imaging and Magnetic Resonance Phase Velocity mapping

MR imaging is a clinical imaging modality whose principles are based on nuclear magnetic resonance. Very few nuclei containing an odd number of protons and neutrons exhibit those specific magnetic properties [22]. One such nucleus is the hydrogen proton. Human body is largely composed of water, and each water molecule contains two hydrogen nuclei. Thus hydrogen protons are in abundance in human body. NMR potential has been exploited in late 1946 by two different groups, however Felin Bloch

and Edward Purcell were the persons who identified its applications in natural science and were awarded the noble prize for the same in the year 1952 [34-36].

Each proton in the hydrogen nuclei carries an electric charge and spin around its own axis. This creates a small electromagnetic field and the proton behaves like a small bar magnet. Thus hydrogen proton has two energy states (-1/2 0r +1/2). It can either be in a low or high energy state, resulting in protons being aligned in parallel or antiparallel to the direction of an externally-applied static magnetic field. In the absence of a strong external magnetic field, the protons will be aligned in random direction. However, when an external magnetic field B_0 is applied, more than 50% of the protons have their magnetic moment vector being aligned in the direction of the applied magnetic field. Each proton starts wobbling or precessing as a result of its spin (angular momentum) and the external magnetic field. The frequency of the precession of the proton is given by the "Larmor Equation" [23]:

$$\boldsymbol{\omega = \gamma B_0} \qquad \textbf{Eq: 2.1}$$

where,

B_0 is the external magnetic field (T)

ω is the precession frequency (Hz) and

$\boldsymbol{\gamma}$ is the gyromagnetic ratio (Hz/T)

The gyromagnetic ratio depends on the element; for example, it is equal to 42.58 MHz/T for the hydrogen nucleus.

The imaging cycle consists of the following different steps:

1. Application of the radio frequency (RF) energy pulse
2. Creating gradients in the magnetic field and slice selection
3. Phase and frequency encoding
4. Signal readout
5. Image reconstruction

The first step in MR imaging is the excitation of protons in the object of interest. This can be achieved by the application of an RF pulse perpendicular to the main magnetic field. Let B_1 be the magnetic field strength of the RF pulse. Now the protons start precessing about the axis of B_1at a frequency $\omega_1 = \gamma B_1$. So, the protons are precessing at a frequency of ω about B_0 field and at a frequency of ω_1 about the B_1 field resulting in flipping the net magnetization vector from z-axis into x-y plane [23]. For the RF pulse to have any effect on the protons, the frequency of RF pulse should be same as the proton precession frequencyω. In order to select the protons in a particular slice, the frequency of the precession of the protons in this slice should differ from the frequency of precession of the other protons. This can be achieved by applying a gradient which creates a variation of precessional frequency, thus allowing RF pulse to excite the protons in particular slice of interest. Thus slice selection is achieved [21].

Once the RF pulse is turned off, the protons have to give up their excess energy and start realigning in the direction of external magnetic field. This process of the protons returning to their lower energy states is termed as relaxation. The time taken for the protons to realign along the longitudinal or the z-axis is called as the longitudinal (T1) or spin-lattice relaxation and the time taken for the decay of magnetization along the x-y plane is called as the spin-spin or transverse (T2) relaxation. Due to spin dephasing in T2 relaxation, it occurs five to ten times faster than the T1 recovery. External magnetic filed inhomogeneties, changing the TR and TE can change the T1 and T2 relaxation times [23].

Now, it is time for phase and frequency encoding of the signal. This is achieved by applying two different gradients Gx and Gy in X and Y directions respectively. Gy is applied for phase encoding and Gx is applied for frequency encoding. Gy is applied prior to Gx. Application of Gy gradient causes a difference in precessional frequency of the protons at different Y levels and application of Gx gradient causes a difference in precessional frequency of the protons at different X levels, thus leading to spatial encoding of the signal. This fills one line in the k-space. The entire process is repeated, with the only change being the Gy gradient, to get required amount of data to fill the k-space. The information in the k-space is in time domain and an inverse 2D discrete Fourier transform gives the final reconstructed image [23].

In addition to its ability as a reliable clinical imaging modality, MR imaging provides valuable flow related information in various applications [24-26]. The major advantage of MR over other clinical modalities is its unique ability to measure the

velocity in all the three spatial directions. By applying a proper bipolar gradient, the velocity of the moving proton is encoded into the phase of the received signal [4]. Each acquisition produces two images, one magnitude image and one phase image. The velocity can be calculated from the phase image due to the linear relation between the velocity of the protons and the encoded phase signal. However, to avoid errors in velocity information it is recommended that the flow is non-accelerated. Phase is also affected by several other factors like magnetic field inhomogeneties, RF pulse effects, turbulence and reverse flow effects [27]. In order to eliminate some of these errors, a set of two images is acquired for each of the velocity encoding direction. Both the images have all the phase inhomogeneties but with a phase shift. Subtracting the two images results in a phase difference image where the irregularities are minimized and the intensity of the pixel is directly proportional to the velocity in the encoded direction [28].

There are two basic imaging pulse sequences used for acquiring images in MR imaging: spin echo and gradient echo. Spin echo pulse sequence eliminates the dephasing effects due to the inhomogeneties in the external magnetic field by the application of one or more 180 degree rephasing pulses after the 90 degree RF pulse. It gives a high signal to noise ratio but has longer scan times. On the other hand, the gradient echo pulse sequence has a shorter TR, thus allowing it to do 3D imaging. It can also acquire the images of flowing blood. The two important parameters in gradient echo pulse sequence are TR and TE. TR is defined as the time interval between two consecutive RF pulses and echo time (TE) is defined as the time between the application of RF pulse and the signal readout [23]. The gradient echo pulse sequence is schematically represented below.

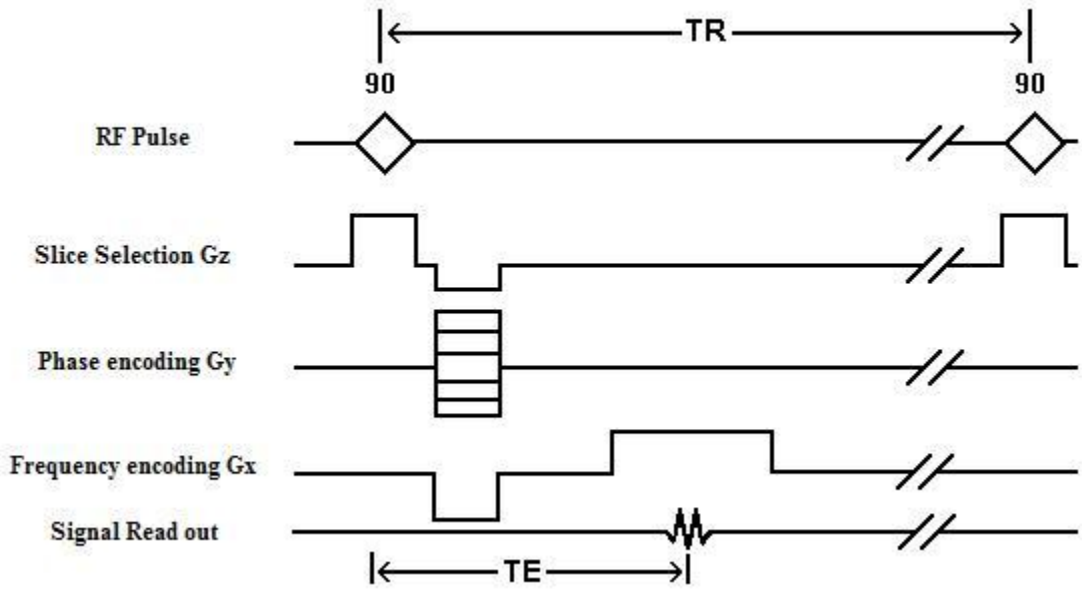

Fig 2.1: Gradient Echo Pulse Sequence diagram

Where,

RF -- Radiofrequency

Gz – Slice selection

Gy – Phase encoding

Gx – Frequency encoding

TE – Echo time

TR – Repetition time

In a gradient echo sequence the bipolar gradient is usually applied in the z-direction or the slice selection direction. The phase is calculated using the following equation [29]:

$$\varphi = (\gamma M_1)\, v = (\gamma \int_0^{TE} G(t)tdt)\, v = (\gamma A_g T)\, v \qquad \textbf{Eq:2.2}$$

where,

φ is Phase of the received signal (radian), γ is Gyromagnetic ratio (Hz/T), ν is Velocity (m/s), M_1 is first moment of the gradient waveform (T s^2/m) at TE, G (t) is Magnetic field gradient (T/m), A_g is area of each lobe of the bipolar gradient (T/m s) and T is time between the centers of the two lobes of the gradient.

The velocity can be calculated from the phase values using the following equation:

$$v = \Delta\varphi\ (Venc/\ \pi) \qquad \textbf{Eq:2.3}$$

There is a critical velocity value above which aliasing occurs and that limiting velocity is called as velocity encoding limit or simply Venc. Venc values should not be too high and be chosen in such a way to ensure high sensitivity and avoid aliasing [30].

2.3 MRPVM of Stenotic Turbulent Flows

In general, turbulent flow is defined as a form of irregular viscous flow in which pressure and velocity of the fluid fluctuates at random in both time and space. It can be characterized by Reynolds number (Re) which is defined by the following equation:

$$Re = \rho * V * L\ /\ \mu \qquad \textbf{Eq: 2.4}$$

where,

Re - Reynolds number

ρ - Density (Kg/m^3)

V - Velocity (m/s)

L - Characteristic linear dimension (m)

μ - Dynamic viscosity ($N\text{-}s/m^2$)

The Reynolds number is a dimensionless number that gives a measure of ratio of inertial forces to viscous forces. It is used to characterize different flow regimes. Laminar flow occurs when the Reynolds number is less than 2100, where viscous forces are dominant, and is characterized by smooth, constant fluid motion. Transitional flow occurs when Re ranges from 2100 – 4000. Turbulent flow occurs at Re greater than 4000 and is dominated by inertial forces, which produce eddies, vortices and other flow instabilities [31].

Blood flow in human body is laminar under healthy conditions. But presence of orifice in the blood vessels leads to the narrowing of blood vessels and thereby creating turbulence in the blood flow. These turbulent blood flows can have adverse effects on human health. MR imaging is being used for flow measurements since three decades [4, 32, 33].

Several studies have been conducted to understand the complexities involved with using MR for measuring turbulent blood flow, yet its effectiveness in valvular stenosis remains unclear [39-45]. In gradient echo imaging turbulence can be detected by the signal loss observed in the images. Signal loss is induced because of the velocity fluctuations in both time and space. In gradient echo imaging flowing blood appears

bright and the signal intensity is usually proportional to the fluid velocity [46]. Study conducted by two separate groups concluded that turbulent flow through valves and vascular stenosis may be associated with signal loss. Also no signal loss was observed in straight tubes under steady state conditions at higher turbulence; whereas signal loss was observed at the same Re in a flow through orifice [47, 48]. Podolak et al conducted a study on the affect of signal intensity of flowing fluid in a simulated vascular stenosis. Various stenotic models with 25%, 51% and 73% area reduction were studied. They concluded that in a stenosis of 51% area reduction and higher, the systolic signal intensity decreases. Negligible affect is seen through a 25% area reduction. They also predicted that turbulence might be the reason for signal loss [39]. A study conducted by Gatehouse et al showed that the signal loss can be reduced by using rapid k-space sampling in MRPVM. They acquired both in plane and through plane velocity acquisitions in volunteers and their results showed that early acquisition of center k-space reduced the signal loss [49].

Various studies have been conducted to study the effects of turbulence in spin echo images. Studies carried out by two individual groups suggest that there may be an increase or decrease in the signal intensity in spin echo imaging due to turbulence [50, 51]. Later conducted studies proved that in disturbed flow, velocity and acceleration differences and loss of phase coherence with in a voxel are important factors for signal loss in vascular flow [52-54]. In spin echo imaging, the signal intensity decreases with an increase in flow unlike the gradient flow where the signal intensity increases with an increase in flow. This is because of the replacement of partially saturated spins with fully

magnetized spins. Hence the gradient echo imaging can be used for studying the effects of turbulence. Turbulence need not create signal loss. In transition flow through orifice signal intensity is not affected; however as the level of turbulence increases a threshold value is reached where signal loss occurs. For the same Re, signal loss is highest in the smallest orifice [48].

Stahlberg et al conducted in vitro experiments under steady flow conditions to see the effect of imaging parameters on phase contrast imaging and found that the phase contrast measurements were not reliable in turbulent jets due to acceleration and increased intravoxel dephasing effects. They concluded that reducing the TEs reduced these dephasing effects [55]. Another set of in vitro studies were performed by Sondergaard et al under steady flow conditions in stenotic jets. They found that there was an error of approximately 24% in phase contrast velocity measurements in stenotic valve area [56]. The area of signal loss helps in effectively estimating the aortic valve area [32]. The main issue with phase contrast imaging is the longer scan duration because of the need for acquisition of multiple images to produce the final image. In order to overcome this, Chee-man proposed the estimation of velocity in flow encoded image only, thereby reducing the scan time by more than fifty percent. The study concluded that leakage of flow phase into the background phase is the main reason for the underestimation of velocities [57].

A group of researchers conducted studies to compare the phase contrast MR measurements with the CFD computations in a flow through step stenosis. Their results showed that at Re = 100, 90% of the phase contrast MR measurements lied within an

error of 10% of the measurements from CFD and at Re = 258, 94% of the phase contrast MR measurements lied within an error of 10% of the measurements from CFD. Thus phase contrast MR data is well in agreement with the CFD computational results [58]. Moran et al conducted studies on accuracy of phase contrast MR angiography in intravoxel velocity distributions and found that, the method was accurate in determining the velocity in unidirectional flow but results in errors in case of bidirectional flow [42]. Studies were conducted to evaluate the fast segmented k-space MRPVM in quantifying flow through mitral regurgitant orifices. Experiments were performed under steady and pulsatile flow conditions. The results were then compared to the results from non-segmented MRPVM results and they were well matched in both steady and pulsatile flow conditions with errors lying under 5% [59].

Oshinski and group investigated the cause of signal loss in MR images due to turbulent flow effects in a 90% stenosis. The results suggested that reducing the gradient durations and TEs may reduce the signal loss. Also fluids with physiological properties similar to blood should be used in future studies [60]. Sederman and group used the gradient echo rapid velocity and acceleration imaging sequence and acquired three component velocity images of turbulent flow pipe. They conducted the experiments in a long tube at Re ranging from 1250 to 5000, thus both laminar and turbulent flow conditions were taken care of. Laminar flow results were well in agreement with the predicted values where as the turbulent puffs were observed in case of turbulent flow results [61].

O'Brien et al conducted studies on MR phase contrast velocity and errors in turbulent stenotic jets. Their research concluded that flow errors in turbulent flows were mainly due to signal loss. Also TE = 2.0 msec can be used for accurate flow measurements till 600 ml/sec. Another set of experiments were conducted to study the effect of TE on stenotic jets and found that shorter TEs reduce the intra-voxel dephasing and thereby reducing the signal loss in stenotic jets [21, 43, 62]. In valvular stenosis irregular flow types and turbulence can induce signal loss. In such cases shortening of TEs reduces the amount of signal loss by increasing the threshold of turbulence intensity for signal loss. The experiments conducted by Kilner and group confirmed that velocities upto 6 m/sec can be accurately measured with TE = 3.6 msec [63].

Recently, Navneeth conducted experiments on two stenosis models with 75 % area reduction and 94 % area reduction. The experiments were carried out at five TEs [2.65, 3.4, 4.2, 5, 6 msec] and three in plane spatial resolutions [0.9x0.9, 1.3x1.3, 1.7x1.7 mm^2]. The results showed that MRPVM is accurate in turbulent flow conditions and consistently underestimated the flow in turbulent flow conditions. This underestimation is due to signal loss. Lower TEs [2.65 and 3.4] provided accurate results when compared to higher TEs. The underestimation of flow rates increased with an increase in flow rate and with an increase in degree of stenosis [66].

Looking at the previous studies, there is a need to conduct extensive research to see the accuracy of MR in measuring flow rates in different geometries and study the effect of various imaging parameters on these measurements. This study aims at determining

the ability of MRPVM to quantify flow in turbulent flow regions with various degrees of stenosis stressing on the effect of different imaging parameters.

CHAPTER III

HYPOTHESIS AND SPECIFIC AIMS

Medical Imaging has experienced a lot of advancement in clinical and technological fields. The main aim of these developments is to acquire adequate diagnostic information without compromising the care provided to the patients. With the number of patients suffering from heart diseases increasing day by day, it is really important to find a reliable imaging technique that can provide accurate information for proper diagnosis. Narrowing of blood vessels is one of the most common among all the heart diseases faced by people today. This narrowing of blood vessels results in complex blood flow patterns inside the arteries. Thus it is very essential to find an imaging technique that can provide accurate information in these complex blood flow patterns. MR phase velocity mapping (MRPVM) is one such development in medical imaging, which can measure flow velocities in all the three spatial directions. MRPVM can accurately measure velocities under laminar flow conditions; however it has several limitations in turbulent flow regions due to signal loss. The main aim of this study was to examine the ability of MRPVM to measure flow in two orifice models under a variety of flow conditions.

The following hypothesis were tested in this study-

1. The lower the TE, the higher the accuracy of MRPVM under turbulent flow conditions
2. The higher the spatial resolution, the higher the accuracy of MRPVM under turbulent flow conditions

These hypotheses were tested by achieving the following specific aims:

Specific Aim 1:

To determine the effect of TE on the accuracy of MRPVM under turbulent flow conditions

Experiments were conducted in a 1.5T Siemens MRI scanner under steady flow conditions. Axial MR images were acquired for 75% area reduction and 94% area reduction orifice models at five different TE's (2.65, 3.5, 5.0, 7.5, 10.0 msec). The acquisitions were performed at five different positions for both the models: 6.0 cm upstream from the orifice, at the orifice, 1.0 cm downstream from the orifice, 3.0 cm downstream from the orifice and 5.0 cm downstream from the orifice. Flow rates ranging between 1.2 L/min and 10.5 L/min (Re ranging from 1271-11124 at upstream and 2543-22248 at the orifice) were used in the experiments. Flow rates were calculated from the acquired phase images using the Argus software. These flow rates were then compared with the true flow rates from the rotameter to see the effect of TE on the MRPVM measurements.

Specific Aim 2:

To determine the effect of spatial resolution on the accuracy of MRPVM under turbulent flow conditions

Experiments were conducted in a 1.5T Siemens MRI scanner under steady flow conditions. Axial MR images were acquired for 75% area reduction and 94% area reduction orifice models at three different spatial resolutions (0.9x0.9, 1.5x1.5, 2.0x2.0 mm^2). The acquisitions were performed at five different positions for both the models: 6.0 cm upstream from the orifice, at the orifice, 1.0 cm downstream from the orifice, 3.0 cm downstream from the orifice and 5.0 cm downstream from the orifice. Flow rates ranging between 1.2 L/min and 10.5 L/min (Re ranging from 1271-11124 at upstream and 2543-22248 at the orifice) were used in the experiments. Flow rates were calculated from the acquired phase images using the Argus software. These flow rates were then compared with the true flow rates from the rotameter to see the effect of TE on the MRPVM measurements.

CHAPTER IV

METHODS

4.1 Experimental Apparatus

All the experiments were carried out in a 1.5T MR scanner (Magnetom Sonata, Siemens Medical solutions Inc, Germany). A steady flow loop (Figure 4.1) was constructed for conducting the experiments. The flow loop consisted of a steady state sump pump (Flotec V4 HP; Delavan WI), a rotameter (Dakota Instruments, 0-12 lpm), a reservoir, PVC pipes, flexible tubing, polycarbonate box and the orifice model. Water was used as the working fluid throughout the experiments.

The orifice model was placed inside the polycarbonate box. The box was then filled with water to ensure a good MR signal. The pump was placed in the 50 L reservoir filled with water. A rotameter was used to measure the true Flow rates. Flexible tubes and ¾" diameter PVC pipes were used to transport water to the model and back to the reservoir. A graded cylinder and a stopwatch were used to calibrate the rotameter. The flow rate was adjusted using valves. The flow loop was thoroughly tested in the laboratory at

Cleveland State University to ensure there were no leaks and other problems and it was transferred to the Cleveland Clinic for the experiments.

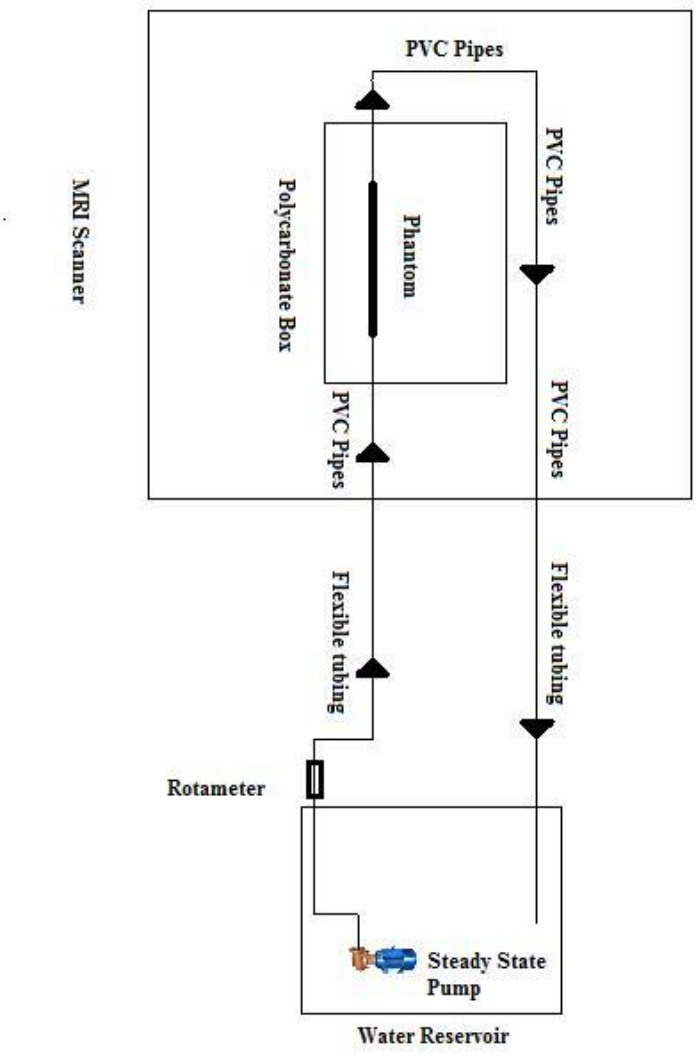

Figure 4.1: Schematic of the Steady State Flow loop

4.2 Models

75% Area Reduction Orifice Model:

Pyrex glass was the material used to make the model. It had an internal diameter (ID) of 2.0 cm both upstream and downstream from the orifice and it was 30.0 cm in length. The area of the orifice was 25 % the area of the unoccluded part, resulting in an orifice ID of 1.0 cm. Thus the cross-sectional area is 0.785 cm^2 at the throat of the orifice and 3.14 cm^2 at all the other slice positions. The MRPVM measurements were taken at five locations using transverse imaging slices (Figure 4.2):

1. 6.0 cm upstream from the orifice
2. At the orifice
3. 1.0 cm downstream from the orifice
4. 3.0 cm downstream from the orifice
5. 5.0 cm downstream from the orifice

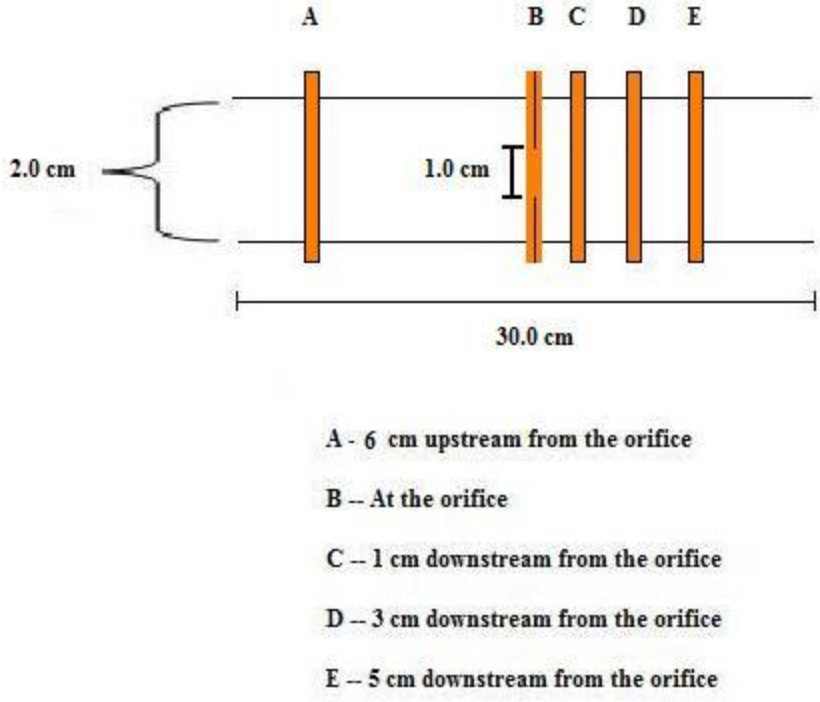

Figure 4.2: Schematic of the 75% Orifice model

94% Area Reduction Orifice Model:

Pyrex glass was the material used to make the model. It had an internal diameter (ID) of 2.0 cm both upstream and downstream from the orifice and it was 30.0 cm in length. The area of the orifice was 6.25 % the area of the unoccluded part, resulting in an orifice ID of 0.5 cm. Thus the cross-sectional area is 0.196 cm^2 at the throat of the orifice and 3.14 cm^2 at all the other slice positions. The MRPVM measurements were taken at five locations using transverse imaging slices (Figure 4.3):

1. 6.0 cm upstream from the orifice
2. At the orifice

3. 1.0 cm downstream from the orifice
4. 3.0 cm downstream from the orifice
5. 5.0 cm downstream from the orifice

Figure 4.4 represents a schematic of 94 % orifice model with imaging slice positions marked.

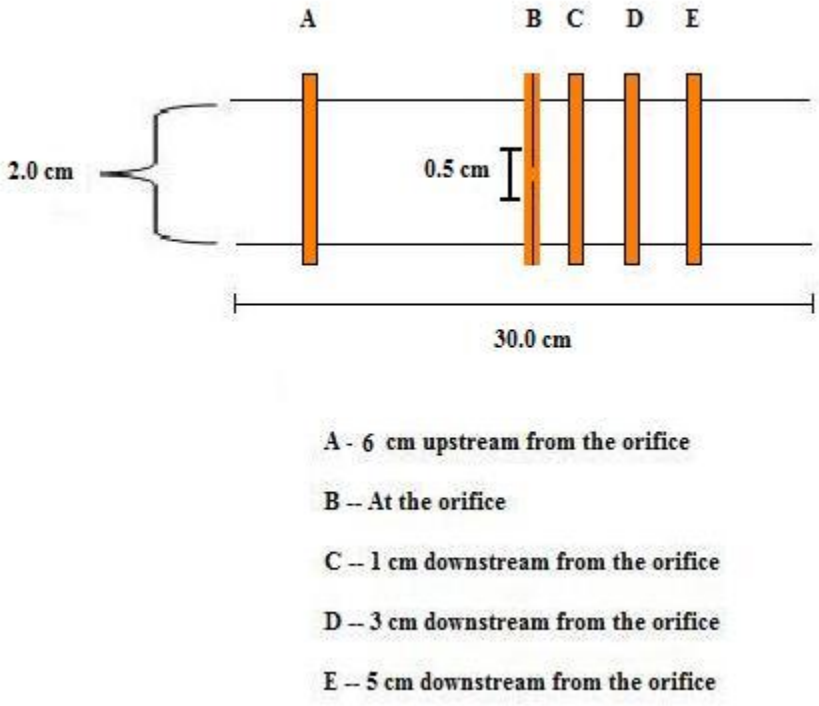

Figure 4.3: Schematic of the 94% Orifice model

4.3 Flow Conditions

Water was used as the working fluid throughout the experiments. The room temperature was approximately 20° centigrade and so a density of 998 kg/m^3 and viscosity of 0.001 kg/m-s for water were used in the calculation. A total of four Flow rates were used in the experiments: 1.2, 5.5 and 10.5 L/min in 75 % orifice case and 5.5 and 8.5 L/min in the 94 % orifice case experiments. Tables 4.1 and 4.2 summarize the Flow rates, cross-sectional average velocities and Reynolds numbers (Re) used in the case of the 75 % orifice model and in the case of the 94% orifice model, respectively.

Table 4.1: Flow rates, Average cross-sectional velocity values and Reynolds numbers in 75% orifice models

Flow Rate L/min	**Upstream cross-sectional velocity Cm/sec**	**Upstream Reynolds number**	**Orifice average Cross-sectional velocity Cm/sec**	**Orifice Reynolds number Re**
1.2	6.37	1271	25.48	2543
5.5	29.2	5827	116.77	11654
10.5	55.73	11124	222.93	22248

Table 4.2: Flow rates, Average cross-sectional velocity values and Reynolds numbers in 94% orifice models

Flow Rate L/min	**Upstream cross-sectional velocity Cm/sec**	**Upstream Reynolds number**	**Orifice average Cross-sectional velocity Cm/sec**	**Orifice Reynolds number Re**
5.5	29.2	5827	467.09	23308
8.5	45.12	9005	721.87	36021

4.4 Imaging Procedures and Parameters

The flow loop was constructed and inserted in the MRI scanner with the polycarbonate box positioned at the isocenter. The experiments were performed under steady flow conditions. So we had to wait till the flow was stabilized (at least 20 minutes before starting the image acquisition) and the flow loop was inspected in between the experiments to make sure that the flow rate was stable and no other issues occurred in the flow loop. MRPVM measurements were performed using gradient echo sequence with bipolar velocity encoding gradients. A variety of in-plane resolutions (0.9 x 0.9, 1.5 x 1.5 and 2.0 x 2.0 mm^2) and echo times (2.65, 3.5, 5, 7.5, 10 msec) were studied. A TR=130 msec was used in all the experiments. Venc values for the through plane velocity

measurements were selected based on the highest velocity at that slice position expected based on the flow condition. The flow rate stabilization and image acquisition for a single orifice model at one single flow rate took approximately 6-8 hours and so experiments were carried out on different days for different Flow rates. Tables 4.3-4.7 list the imaging parameters used in both orifice models.

Table 4.3: Imaging parameters used for the transverse MRPVM through-plane acquisitions in the 75% Orifice model - flow rate: 1.2 L/min.

Slice position	**ST Mm**	**FOV mm**	**Base resolution**	**Pixel size mm**	**TR ms**	**TE ms**	**VENC Cm/s**
Upstream	5.5	180	192	0.9	130	2.65 3.5 5.0 7.5 10.0	66
Upstream	5.5	280	192	1.5	130		66
Upstream	5.5	380	192	2.0	130		66
At the orifice	5.5	180	192	0.9	130		66
At the orifice	5.5	280	192	1.5	130		66
At the orifice	5.5	380	192	2.0	130		66
1 cm downstream	5.5	180	192	0.9	130		66
1 cm downstream	5.5	280	192	1.5	130		66
1 cm downstream	5.5	380	192	2.0	130		66
3 cm downstream	5.5	180	192	0.9	130		66
3 cm downstream	5.5	280	192	1.5	130		66
3 cm downstream	5.5	380	192	2.0	130		66
5 cm downstream	5.5	180	192	0.9	130		66
5 cm downstream	5.5	280	192	1.5	130		66
5 cm downstream	5.5	380	192	2.0	130		66

Table 4.4: Imaging parameters used for the transverse MRPVM through-plane acquisitions in the 75% Orifice model - flow rate: 5.5 L/min.

Slice position	**ST Mm**	**FOV mm**	**Base resolution**	**Pixel size mm**	**TR ms**	**TE ms**	**VENC Cm/s**
Upstream	5.5	180	192	0.9	130	2.65 3.5 5.0 7.5 10.0	66
Upstream	5.5	280	192	1.5	130		66
Upstream	5.5	380	192	2.0	130		66
At the orifice	5.5	180	192	0.9	130		150
At the orifice	5.5	280	192	1.5	130		150
At the orifice	5.5	380	192	2.0	130		150
1 cm downstream	5.5	180	192	0.9	130		200
1 cm downstream	5.5	280	192	1.5	130		200
1 cm downstream	5.5	380	192	2.0	130		200
3 cm downstream	5.5	180	192	0.9	130		200
3 cm downstream	5.5	280	192	1.5	130		200
3 cm downstream	5.5	380	192	2.0	130		200
5 cm downstream	5.5	180	192	0.9	130		150
5 cm downstream	5.5	280	192	1.5	130		150
5 cm downstream	5.5	380	192	2.0	130		150

Table 4.5: Imaging parameters used for the transverse MRPVM through-plane acquisitions in the 75% Orifice model - flow rate: 10.5 L/min.

Slice position	**ST Mm**	**FOV mm**	**Base resolution**	**Pixel size mm**	**TR ms**	**TE ms**	**VENC Cm/s**
Upstream	5.5	180	192	0.9	130	2.65 3.5 5.0 7.5 10.0	90
Upstream	5.5	280	192	1.5	130		90
Upstream	5.5	380	192	2.0	130		90
At the orifice	5.5	180	192	0.9	130		350
At the orifice	5.5	280	192	1.5	130		350
At the orifice	5.5	380	192	2.0	130		350
1 cm downstream	5.5	180	192	0.9	130		350
1 cm downstream	5.5	280	192	1.5	130		350
1 cm downstream	5.5	380	192	2.0	130		350
3 cm downstream	5.5	180	192	0.9	130		350
3 cm downstream	5.5	280	192	1.5	130		350
3 cm downstream	5.5	380	192	2.0	130		350
5 cm downstream	5.5	180	192	0.9	130		300
5 cm downstream	5.5	280	192	1.5	130		300
5 cm downstream	5.5	380	192	2.0	130		300

Table 4.6: Imaging parameters used for the transverse MRPVM through-plane acquisitions in the 94% Orifice model - flow rate: 5.5 L/min.

Slice position	**ST Mm**	**FOV mm**	**Base resolution**	**Pixel size mm**	**TR ms**	**TE ms**	**VENC Cm/s**
Upstream	5.5	180	192	0.9	130	2.65 3.5 5.0 7.5 10.0	66
Upstream	5.5	280	192	1.5	130		66
Upstream	5.5	380	192	2.0	130		66
At the orifice	5.5	180	192	0.9	130		700
At the orifice	5.5	280	192	1.5	130		700
At the orifice	5.5	380	192	2.0	130		700
1 cm downstream	5.5	180	192	0.9	130		700
1 cm downstream	5.5	280	192	1.5	130		700
1 cm downstream	5.5	380	192	2.0	130		700
3 cm downstream	5.5	180	192	0.9	130		700
3 cm downstream	5.5	280	192	1.5	130		700
3 cm downstream	5.5	380	192	2.0	130		700
5 cm downstream	5.5	180	192	0.9	130		600
5 cm downstream	5.5	280	192	1.5	130		600
5 cm downstream	5.5	380	192	2.0	130		600

Table 4.7: Imaging parameters used for the transverse MRPVM through-plane acquisitions in the 94% Orifice model - flow rate: 8.5 L/min.

Slice position	**ST mm**	**FOV mm**	**Base resolution**	**Pixel size mm**	**TR ms**	**TE ms**	**VENC Cm/s**
Upstream	5.5	180	192	0.9	130	2.65 3.5 5.0 7.5 10.0	90
Upstream	5.5	280	192	1.5	130		90
Upstream	5.5	380	192	2.0	130		90
At the orifice	5.5	180	192	0.9	130		999
At the orifice	5.5	280	192	1.5	130		999
At the orifice	5.5	380	192	2.0	130		999
1 cm downstream	5.5	180	192	0.9	130		999
1 cm downstream	5.5	280	192	1.5	130		999
1 cm downstream	5.5	380	192	2.0	130		999
3 cm downstream	5.5	180	192	0.9	130		999
3 cm downstream	5.5	280	192	1.5	130		999
3 cm downstream	5.5	380	192	2.0	130		999
5 cm downstream	5.5	180	192	0.9	130		999
5 cm downstream	5.5	280	192	1.5	130		999
5 cm downstream	5.5	380	192	2.0	130		999

Where,

ST = Slice Thickness

4.5 Image Data Analysis

Each acquisition produced two images; one phase image and one magnitude image. The acquired images were first analyzed at the Cleveland Clinic. Using the Argus software (Siemens Medical solutions, Erlangen, Germany), the measured Flow rates were calculated by selecting an ROI (tube lumen) in each image.

a) Magnitude image

b) Phase image

Figure 4.4: Sample Magnitude and Phase Images

The images were later transferred to a PC at CSU for further analysis, Transform (version 3.4, copyright 1990-1998, Fortner Software LLC and its Licensors) was used to correct any aliased velocity pixels and review the velocity data. Each phase image was imported into Transform and the phase values were converted into velocity values using the following equation

Velocity value= (Phasevalue-2048)*Venc/2048 (Eq: 4.1)

The aliased pixels were then corrected using the formula

New Pixel Velocity= Aliased pixel velocity + 2*Venc (Eq: 4.2)

CHAPTER V

RESULTS

In this chapter, the results from the MRPVM measurements in the two orifice models were presented.

In summary, the MRPVM measurements were made using five TEs (2.65, 3.5 5.0, 7.5, 10.5 msec) under 1.2, 5.5 and 10.5 L/min in the case of 75% orifice model and under 5.5 and 8.5 L/min in the case of 94% orifice model. The measured flow rates were then compared with the true flow rates known from the rotameter.

75% Area Reduction Orifice Model – True Flow Rate = 1.2 L/min

Tables 5.1-5.5 show the MRPVM measured flow rates at the five locations shown in Figure 4.2 for all TEs and in-plane spatial resolutions.

Table 5.1: Measured flow rates (L/min) at five TEs and three in-plane spatial resolutions; Slice location: 6.0 cm upstream from the orifice; True flow rate = 1.2 L/min; 75% orifice model

Spatial Resolution (mm^2)	**TE (ms)**	**Measured Flow rate (Lpm)**
0.9 x 0.9	2.65	1.04
	3.5	1.04
	5.0	1.12
	7.5	1.06
	10.0	1.16
1.5 x 1.5	2.65	1.06
	3.5	1.09
	5.0	1.09
	7.5	1.03
	10.0	1.15
2.0 x 2.0	2.65	1.02
	3.5	1.03
	5.0	1.05
	7.5	1.10
	10.0	1.09

Table 5.2: Measured flow rates (L/min) at five TEs and three in-plane spatial resolutions; Slice location: at the orifice; True flow rate = 1.2 L/min; 75% orifice model

Spatial Resolution (mm^2)	**TE (ms)**	**Measured Flow rate (Lpm)**
0.9 x 0.9	2.65	0.80
	3.5	0.84
	5.0	0.80
	7.5	0.78
	10.0	0.69
1.5 x 1.5	2.65	0.81
	3.5	0.79
	5.0	0.75
	7.5	0.78
	10.0	0.66
2.0 x 2.0	2.65	0.77
	3.5	0.74
	5.0	0.72
	7.5	0.68
	10.0	0.63

Table 5.3: Measured flow rates (L/min) at five TEs and three in-plane spatial resolutions; Slice location: 1.0 cm downstream from the orifice; True flow rate = 1.2 L/min; 75% orifice model

Spatial Resolution (mm^2)	**TE (ms)**	**Measured Flow rate (Lpm)**
0.9 x 0.9	2.65	1.08
	3.5	0.98
	5.0	0.89
	7.5	0.72
	10.0	0.85
1.5 x 1.5	2.65	1.03
	3.5	0.92
	5.0	0.91
	7.5	0.91
	10.0	0.78
2.0 x 2.0	2.65	1.04
	3.5	0.93
	5.0	0.87
	7.5	0.84
	10.0	0.75

Table 5.4: Measured flow rates (L/min) at five TEs and three in-plane spatial resolutions; Slice location: 3.0 cm downstream from the orifice; True flow rate = 1.2 L/min; 75% orifice model

Spatial Resolution (mm^2)	**TE (ms)**	**Measured Flow rate (Lpm)**
0.9 x 0.9	2.65	1.02
	3.5	0.98
	5.0	0.82
	7.5	0.76
	10.0	0.71
1.5 x 1.5	2.65	0.95
	3.5	0.85
	5.0	0.81
	7.5	0.72
	10.0	0.64
2.0 x 2.0	2.65	0.97
	3.5	0.93
	5.0	0.81
	7.5	0.67
	10.0	0.56

Table 5.5: Measured flow rates (L/min) at five TEs and three in-plane spatial resolutions; Slice location: 5.0 cm downstream from the orifice; True flow rate = 1.2 L/min; 75% orifice model

Spatial Resolution (mm^2)	**TE (ms)**	**Measured Flow rate (Lpm)**
0.9 x 0.9	2.65	0.94
	3.5	0.81
	5.0	0.67
	7.5	0.43
	10.0	0.31
1.5 x 1.5	2.65	0.95
	3.5	0.79
	5.0	0.66
	7.5	0.52
	10.0	0.30
2.0 x 2.0	2.65	0.89
	3.5	0.77
	5.0	0.65
	7.5	0.47
	10.0	0.30

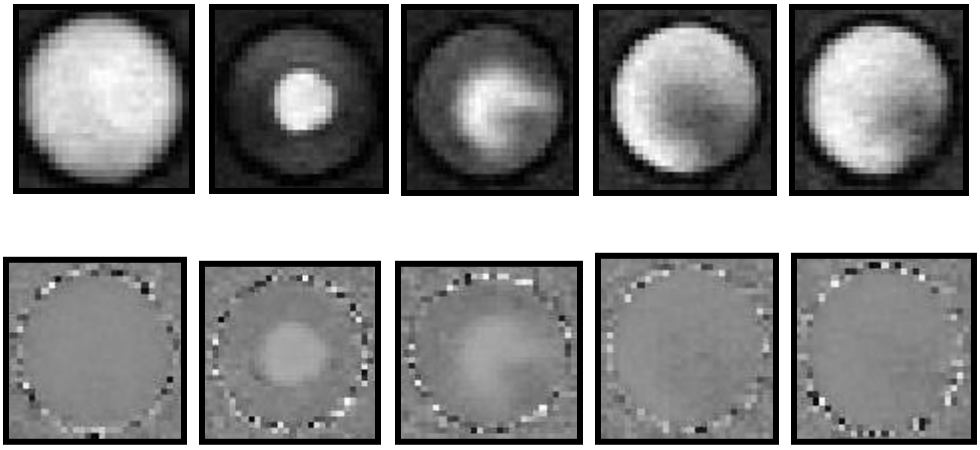

(a) (b) (c) (d) (e)

Figure 5.1: Magnitude and phase images of the 75 % orifice model at 1.2 L/min; in-plane resolution: 0.9 x 0.9 mm^2; TE = 2.65 msec. (a) 6.0 cm upstream from the orifice, (b) at the orifice, (c) 1.0 cm downstream from the orifice, (d) 3.0 cm downstream from the orifice, and (e) 5.0 cm downstream from the orifice.

Figures 5.2-5.4 show the % error in the measured flow rate (as % difference between measured and true flow rates) as a function of TE for each of the in-plane resolutions and slice positions in the case of the 75% orifice model. As seen, at 6.0 cm upstream from the orifice, the measured flow rates were well in agreement with the true flow rates with errors smaller than 15%. At the orifice, there was an underestimation of the flow rate which increased slightly with TE. At 1.0 cm, 3.0 cm, and 5.0 cm downstream from the orifice, there was an underestimation of the flow rate which again increased with TE with errors ranging from (10.0 % – 40.0 %), (15.0 % - 40.0 %) and (21.0 % - 75.0 %) respectively.

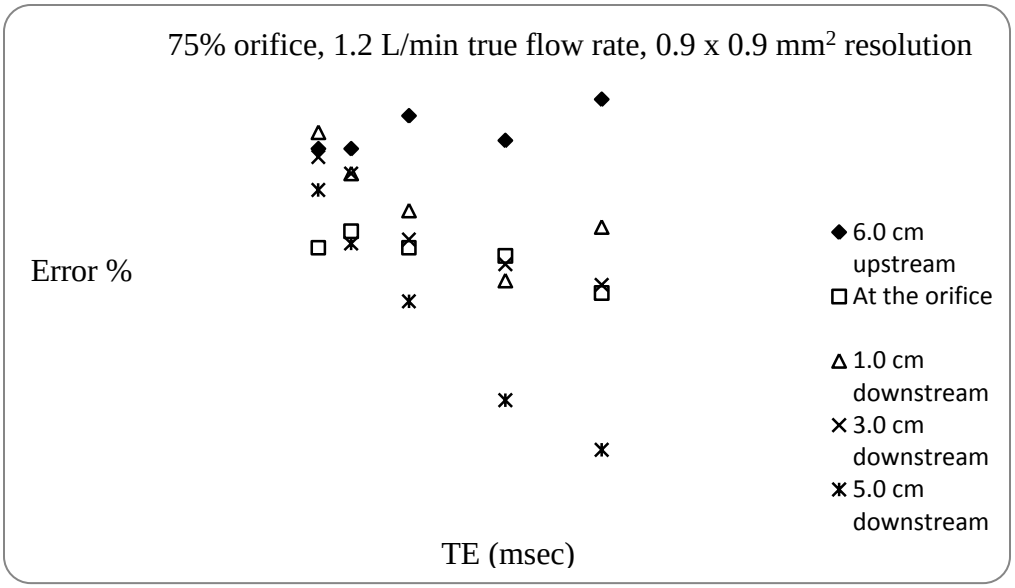

Figure 5.2: Percent error in flow rate measurement as a function of TE for the 75% orifice model, at each slice position for a true flow rate of 1.2 L/min; In-plane resolution: 0.9 x 0.9 mm^2.

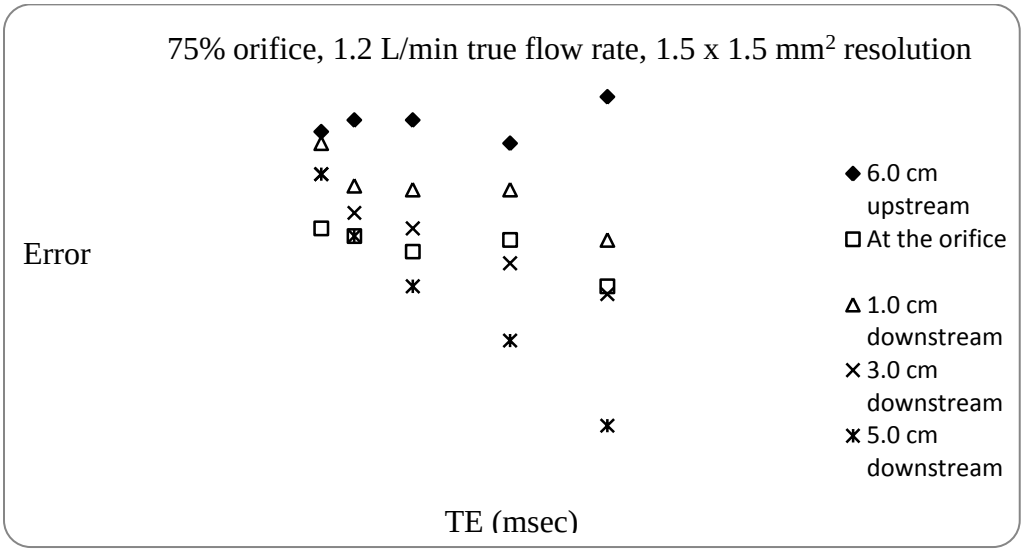

Figure 5.3: Percent error in flow rate measurement as a function of TE for the 75% orifice model, at each slice position for a true flow rate of 1.2 L/min; In-plane resolution: 1.5 x 1.5 mm^2.

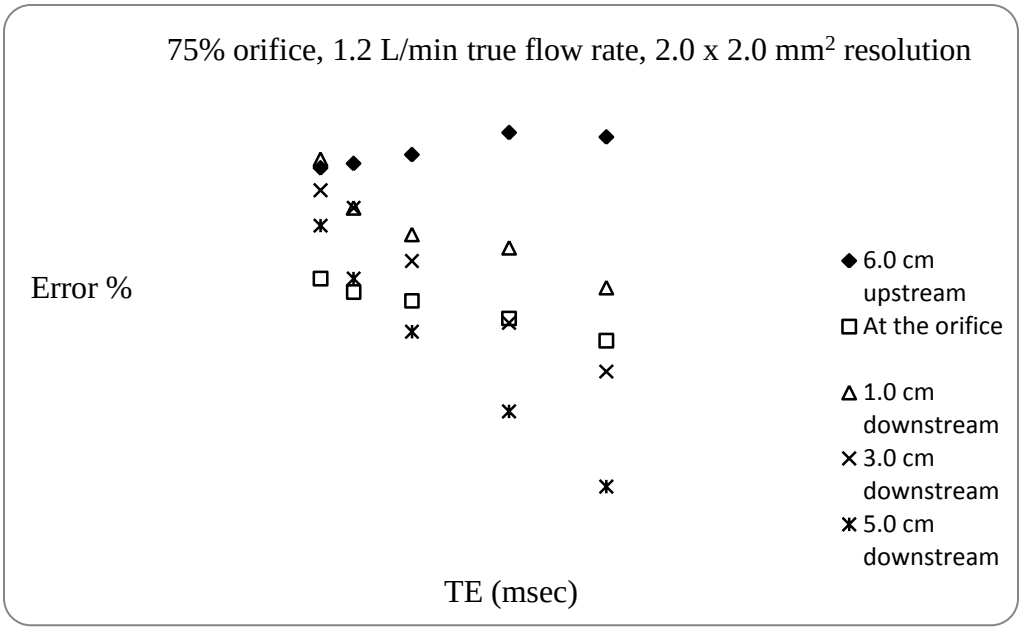

Figure 5.4: Percent error in flow rate measurement as a function of TE for the 75% orifice model, at each slice position for a true flow rate of 1.2 L/min; In-plane resolution: 2.0 x 2.0 mm^2.

Figures 5.5, 5.6 (and Figures A.1, A.2 and A.3 in Appendix A) show the % error in the measured flow rate (as % difference between measured and true flow rates) as a function of in-plane resolution for each TE and slice positions in the case of the 75% orifice model. As seen, the effect of in-plane resolution on the measured flow rates is negligible at all the five slice positions with a maximum of 10 % difference in the error between the highest and lowest resolutions.

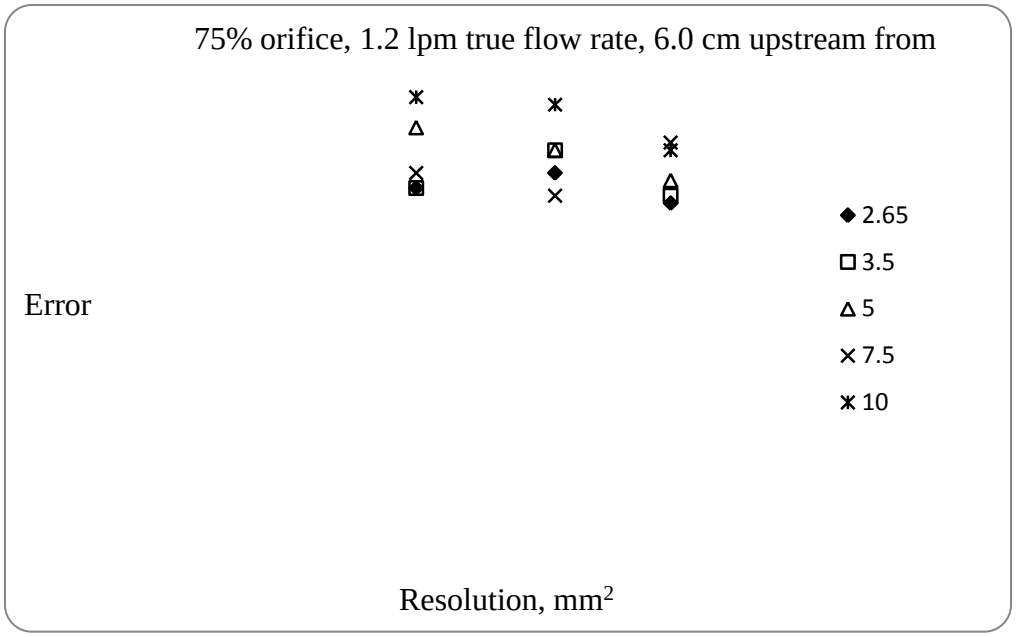

Figure 5.5: Percentage error in flow rate measurement as a function of in-plane resolution for the 75% orifice model; Slice position: 6.0 cm upstream; for a true flow rate of 1.2 L/min

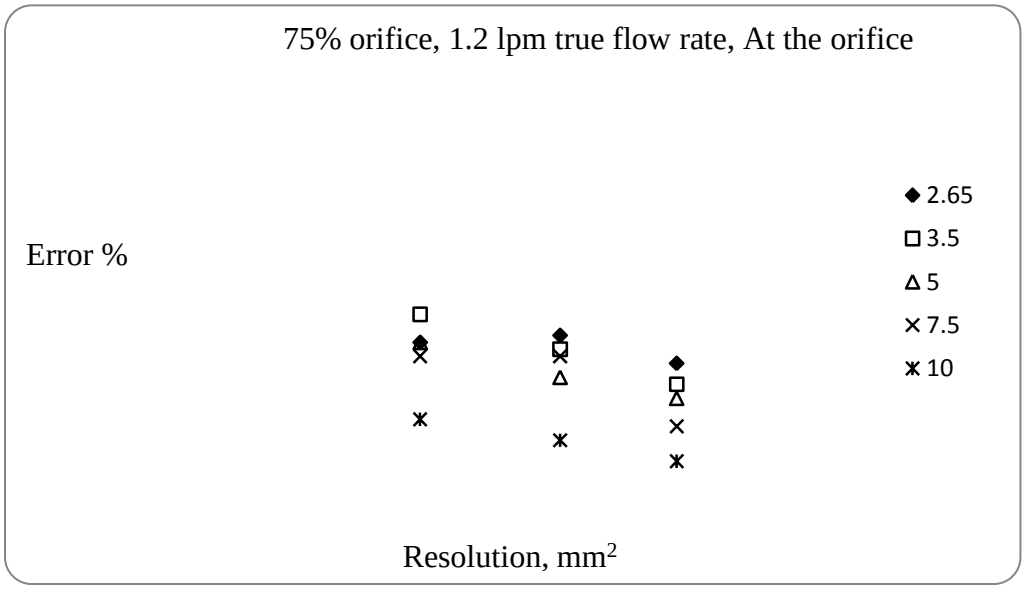

Figure 5.6: Percentage error in flow rate measurement as a function of in-plane resolution for the 75% orifice model; Slice position: at the orifice; for a true flow rate of 1.2 L/min

75% Area Reduction Orifice Model – True Flow Rate = 5.5 L/min

Tables 5.6-5.10 show the MRPVM measured flow rates at the five locations for all TEs and in-plane spatial resolutions.

Table 5.6: Measured flow rates (L/min) at five TEs and three in-plane spatial resolutions; Slice location: 6.0 cm upstream from the orifice; True Flow Rate =5.5 L/min; 75% orifice model

Spatial Resolution (mm^2)	**TE (ms)**	**Measured Flow rate (Lpm)**
0.9 x 0.9	2.65	5.49
	3.5	5.45
	5.0	5.42
	7.5	5.45
	10.0	5.42
1.5 x 1.5	2.65	5.47
	3.5	5.49
	5.0	5.40
	7.5	5.50
	10.0	5.41
2.0 x 2.0	2.65	5.47
	3.5	5.46
	5.0	5.44
	7.5	5.43
	10.0	5.38

Table 5.7: Measured flow rates (L/min) at five TEs and three in-plane spatial resolutions; Slice location: at the orifice; True Flow Rate =5.5 L/min; 75% orifice model

Spatial Resolution (mm^2)	**TE (ms)**	**Measured Flow rate (Lpm)**
0.9 x 0.9	2.65	4.59
	3.5	4.50
	5.0	4.93
	7.5	5.13
	10.0	4.95
1.5 x 1.5	2.65	4.13
	3.5	3.83
	5.0	4.90
	7.5	5.18
	10.0	5.06
2.0 x 2.0	2.65	4.29
	3.5	3.26
	5.0	4.74
	7.5	5.06
	10.0	5.22

Table 5.8: Measured flow rates (L/min) at five TEs and three in-plane spatial resolutions; Slice location: 1.0 cm downstream; True Flow Rate =5.5 L/min; 75% orifice model

Spatial Resolution (mm^2)	**TE (ms)**	**Measured Flow rate (Lpm)**
0.9 x 0.9	2.65	5.30
	3.5	5.23
	5.0	5.23
	7.5	4.81
	10.0	4.81
1.5 x 1.5	2.65	5.30
	3.5	5.29
	5.0	4.88
	7.5	4.72
	10.0	4.54
2.0 x 2.0	2.65	5.12
	3.5	5.10
	5.0	4.81
	7.5	4.57
	10.0	4.19

Table 5.9: Measured flow rates (L/min) at five TEs and three in-plane spatial resolutions; Slice location: 3.0 cm downstream; True Flow Rate = 5.5 L/min; 75% orifice model

Spatial Resolution (mm^2)	**TE (ms)**	**Measured Flow rate (Lpm)**
0.9 x 0.9	2.65	5.17
	3.5	5.09
	5.0	5.13
	7.5	5.05
	10.0	4.79
1.5 x 1.5	2.65	4.93
	3.5	4.73
	5.0	5.06
	7.5	4.72
	10.0	4.21
2.0 x 2.0	2.65	4.71
	3.5	4.54
	5.0	5.05
	7.5	4.61
	10.0	4.21

Table 5.10: Measured flow rates (L/min) at five TEs and three in-plane spatial resolution; Slice location: 5.0 cm downstream; True Flow Rate =5.5 L/min; 75% orifice model

Spatial Resolution (mm^2)	**TE (ms)**	**Measured Flow rate (Lpm)**
0.9 x 0.9	2.65	5.44
	3.5	5.29
	5.0	4.97
	7.5	4.80
	10.0	4.78
1.5 x 1.5	2.65	5.22
	3.5	4.98
	5.0	5.10
	7.5	4.97
	10.0	4.84
2.0 x 2.0	2.65	5.17
	3.5	5.13
	5.0	4.97
	7.5	5.11
	10.0	4.78

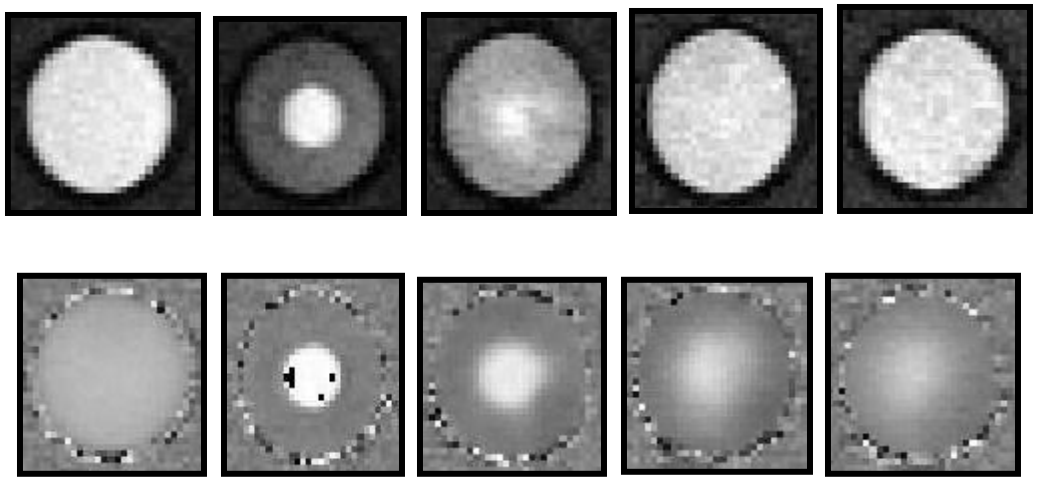

(a) (b) (c) (d) (e)

Figure 5.7: Magnitude and phase images of the 75% orifice model at 1.2 L/min; in-plane resolution: 0.9 x 0.9 mm^2; TE = 2.65 msec. (a) 6.0 cm upstream from the orifice, (b) at the orifice, (c) 1.0 cm downstream from the orifice, (d) 3.0 cm downstream from the orifice and (e) 5.0 cm downstream from the orifice.

Figures 5.8-5.10 show the % error as a function of TE for each in-plane resolution and slice position. In Figure 5.8, it seems that the measured flow rates were unaffected by TE at 6.0 cm upstream from the orifice with errors smaller than 1.5%. At the orifice, there was an underestimation of the flow rate which decreased as TE increased, except for a TE of 3.5 msec, with the highest error of 18.2%. Flow rates were underestimated at 1.0 cm, 3.0 cm, and 5.0 cm downstream from the orifice. At 1.0 cm downstream from the orifice, the measured flow rates exhibited an error of approximately 5% until a TE = 5.0 msec, after which they showed an error of 12.6%. At 3.0 cm downstream from the

orifice, the underestimation increased with the TE with errors smaller than 13%. Finally, at 5.0 cm downstream from the orifice, the measured flow rates were well in agreement with the true flow rates at TE = 2.65msec, with an error of 1.1%, whereas for higher TEs there was an underestimation which increased with the TE exhibiting errors up to 13%.

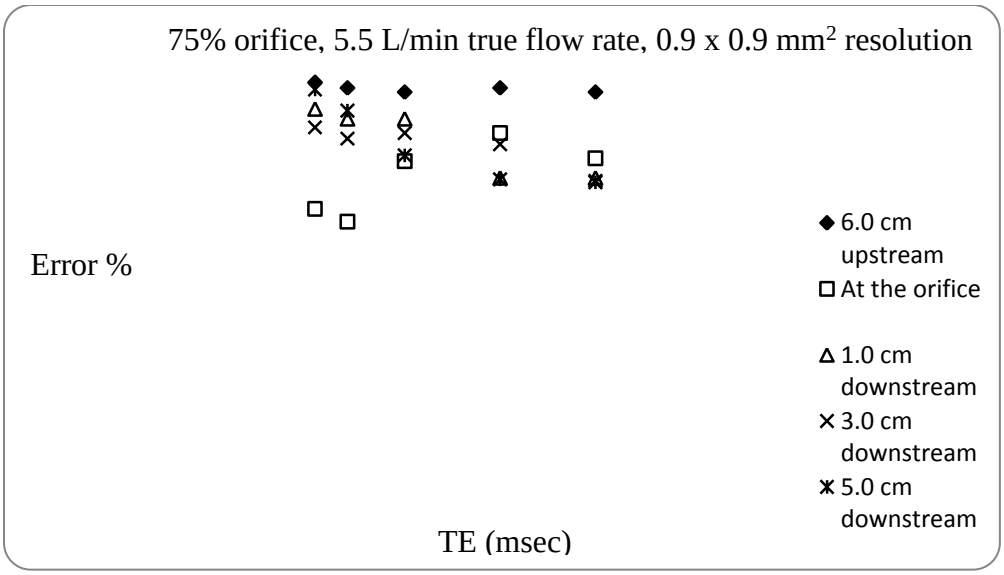

Figure 5.8: Percent error in flow rate measurement as a function of TE for the 75% orifice model, at each slice position for a true flow rate of 5.5 L/min; In-plane resolution: 0.9 x 0.9 mm^2.

Figure 5.9 shows that the measured flow rates were unaffected by the TE at 6.0 cm upstream from the orifice. At the orifice, there was an underestimation in the flow rate which decreased as the TE increased, except at TE = 3.5 msec. The flow rate was underestimated at 1.0 cm, 3.0 cm, and 5.0 cm downstream from the orifice. At 1.0 cm downstream from the orifice, the measured flow rates exhibited an error of 4% at low TE

values (2.65 msec and 3.5 msec), but the error increased with TE. At 3.0 cm and 5.0 cm downstream from the orifice, the error (from (10.0 % - 24.0 %) and (5.0 % - 12.0 %) respectively) increased with TE, except at TE=5.0 msec.

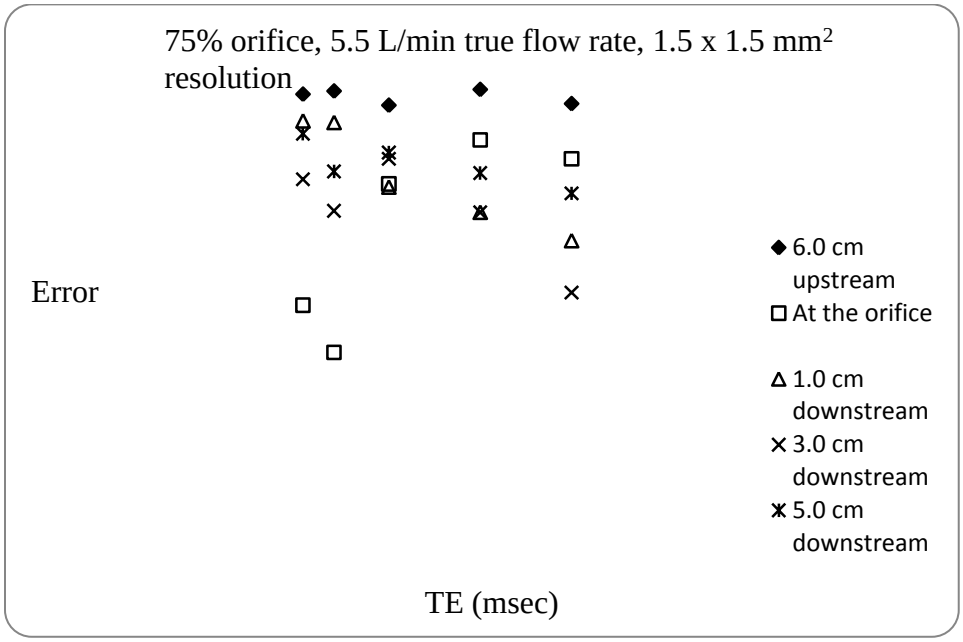

Figure 5.9: Percent error in flow rate measurement as a function of TE for the 75% orifice model, at each slice position for a true flow rate of 5.5 L/min; In-plane resolution: 1.5 x 1.5 mm^2.

Figure 5.10 indicates that the measured flow rates were well in agreement with the true flow rates at 6.0 cm upstream from the orifice with errors smaller than 2.5%. At the orifice, there was an underestimation with errors up to 40%. At 1.0 cm and 5.0 cm downstream from the orifice, there was an underestimation of the flow rate, which

increased with TE. At 3.0 cm downstream from the orifice, there was also an underestimation which increased with TE, except for a TE = 5.0 msec.

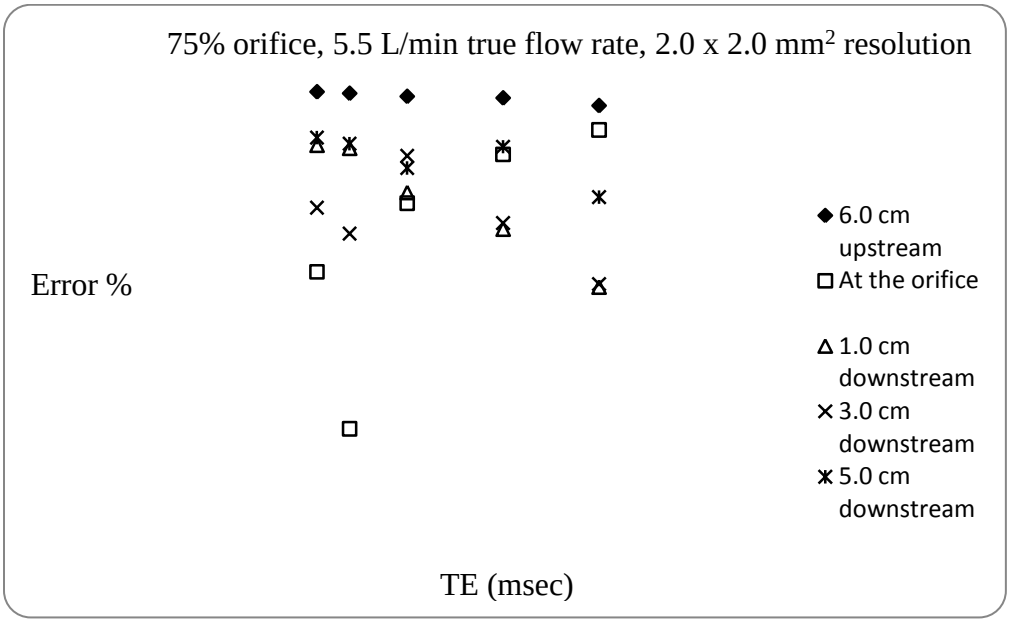

Figure 5.10: Percent error in flow rate measurement as a function of TE for the 75% orifice model, at each slice position for a true flow rate of 5.5 L/min; In-plane resolution: 2.0 x 2.0 mm^2.

Figures 5.11 - 5.13 (and figures A.4 and A.5 in Appendix A) display the % error of the measured flow rate as a function of the in-plane resolution for each of the TE values used and for each slice position. Figure 5.11 indicates that the measured flow rates were well in agreement with the true flow rates at all resolutions with errors smaller than 2.2%. Figure 5.12 shows that the measured flow rates were almost unaffected by the in-plane resolution, for all TE except that of 3.5 msec, where the measured flow rates exhibited

errors of 18.2%, 30.4%, and 40.7% at 0.9 x 0.9, 1.5 x 1.5 and 2.0 x 2.0 mm^2 in-plane resolutions, respectively. Finally, as seen from Figures 5.13, A.4 and A.5, the measured flow rates were almost unaffected by the resolution at all TEs with a maximum difference of 10.0 % between the errors at the highest and the lowest in-plane resolutions.

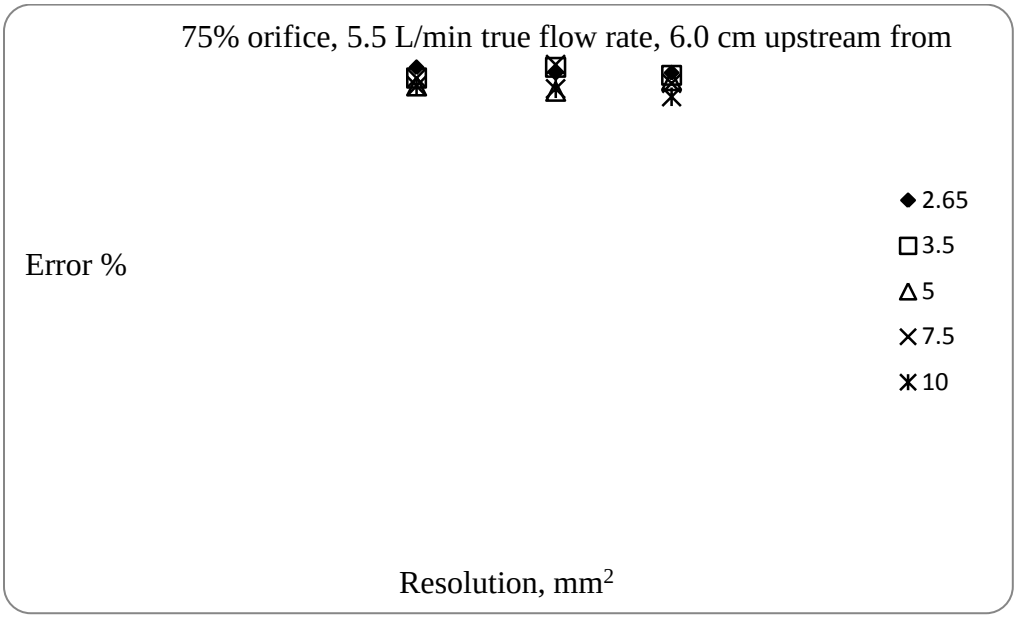

Figure 5.11: Percentage error in flow rate measurement as a function of in-plane resolution for the 75% orifice model; Slice position: 6.0 cm upstream; for a true flow rate of 5.5 L/min

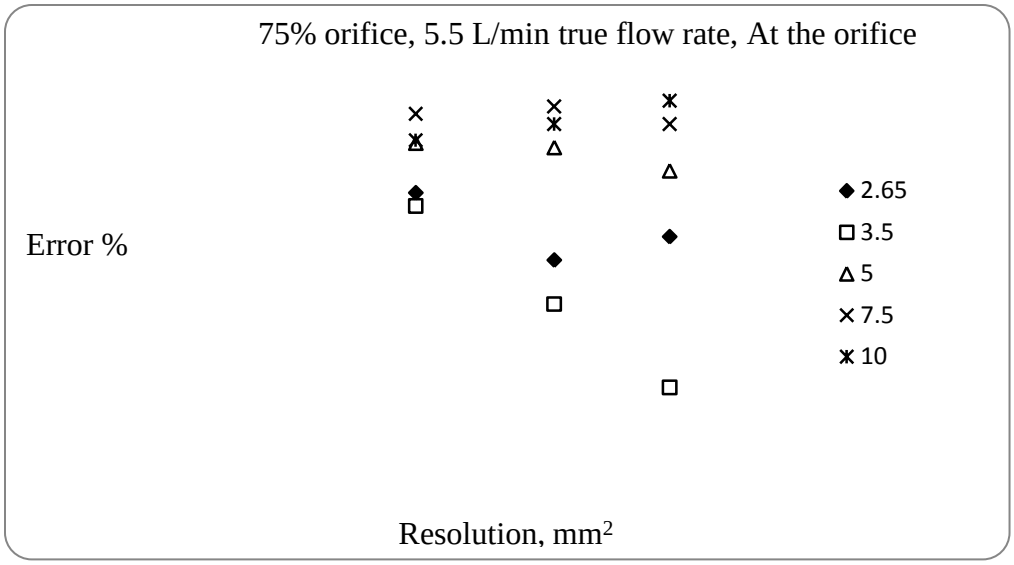

Figure 5.12: Percentage error in flow rate measurement as a function of in-plane resolution for the 75% orifice model; Slice position: at the orifice; for a true flow rate of 5.5 L/min

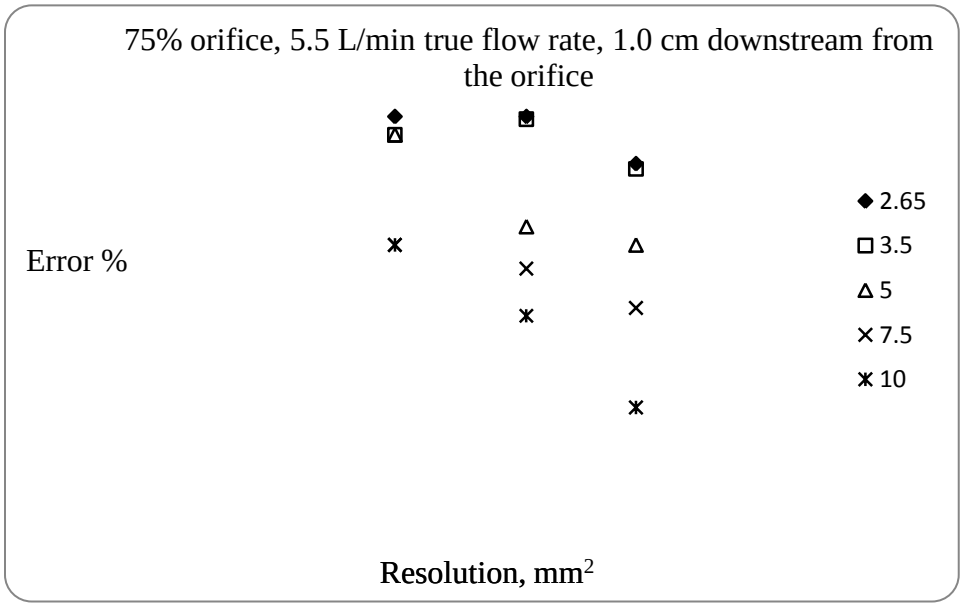

Figure 5.13: Percentage error in flow rate measurement as a function of in-plane resolution for the 75% orifice model; Slice position: 1.0 cm downstream; for a true flow rate of 5.5 L/min

75% Area Reduction Orifice Model – True Flow Rate = 10.5 L/min

Tables 5.11-5.15 show the MRPVM measured flow rates at the five locations for all TEs and in-plane spatial resolutions.

Table 5.11: Measured flow rates (L/min) at five TEs and three in-plane spatial resolutions; Slice location: 6.0 cm upstream from the orifice; True Flow Rate = 10.5 Lpm; 75% orifice model

Spatial Resolution (mm^2)	**TE (ms)**	**Measured Flow rate (Lpm)**
0.9 x 0.9	2.65	10.47
	3.5	10.44
	5.0	10.38
	7.5	10.10
	10.0	10.38
1.5 x 1.5	2.65	10.37
	3.5	10.49
	5.0	10.47
	7.5	9.98
	10.0	10.07
2.0 x 2.0	2.65	10.20
	3.5	10.37
	5.0	10.30
	7.5	10.27
	10.0	9.90

Table 5.12: Measured flow rates (L/min) at five TEs and three in-plane spatial resolutions; Slice location: at the orifice; True Flow Rate = 10.5 Lpm; 75% orifice model

Spatial Resolution (mm^2)	**TE (ms)**	**Measured Flow rate (Lpm)**
0.9 x 0.9	2.65	9.69
	3.5	9.02
	5.0	8.81
	7.5	8.72
	10.0	8.90
1.5 x 1.5	2.65	9.72
	3.5	9.00
	5.0	8.66
	7.5	8.69
	10.0	8.55
2.0 x 2.0	2.65	9.26
	3.5	8.90
	5.0	8.60
	7.5	8.37
	10.0	8.21

Table 5.13: Measured flow rates (L/min) at five TEs and three in-plane spatial resolutions; Slice location: 1.0 cm downstream; True Flow Rate = 10.5 Lpm; 75% orifice model

Spatial Resolution (mm^2)	**TE (ms)**	**Measured Flow rate (LPM)**
0.9 x 0.9	2.65	10.28
	3.5	9.36
	5.0	9.01
	7.5	9.34
	10.0	9.31
1.5 x 1.5	2.65	10.24
	3.5	9.09
	5.0	9.37
	7.5	8.56
	10.0	8.74
2.0 x 2.0	2.65	9.75
	3.5	9.01
	5.0	9.40
	7.5	8.46
	10.0	8.58

Table 5.14: Measured flow rates (L/min) at five TEs and three in-plane spatial resolutions; Slice location: 3.0 cm downstream from the orifice; True Flow Rate = 10.5 Lpm; 75% orifice model

Spatial Resolution (mm^2)	**TE (ms)**	**Measured Flow rate (LPM)**
0.9 x 0.9	2.65	10.15
	3.5	9.41
	5.0	9.05
	7.5	8.74
	10.0	8.54
1.5 x 1.5	2.65	9.43
	3.5	8.90
	5.0	8.43
	7.5	8.41
	10.0	8.16
2.0 x 2.0	2.65	8.42
	3.5	8.53
	5.0	8.51
	7.5	8.23
	10.0	7.46

Table 5.15: Measured flow rates (L/min) at five TEs and three in-plane spatial resolutions; Slice location: 5.0 cm downstream from the orifice; True Flow Rate = 10.5 Lpm; 75% orifice model

Spatial Resolution (mm^2)	**TE (ms)**	**Measured Flow rate (Lpm)**
0.9 x 0.9	2.65	10.35
	3.5	10.21
	5.0	9.52
	7.5	9.48
	10.0	9.14
1.5 x 1.5	2.65	10.20
	3.5	10.15
	5.0	10.02
	7.5	9.56
	10.0	8.32
2.0 x 2.0	2.65	9.95
	3.5	9.49
	5.0	9.62
	7.5	9.04
	10.0	8.42

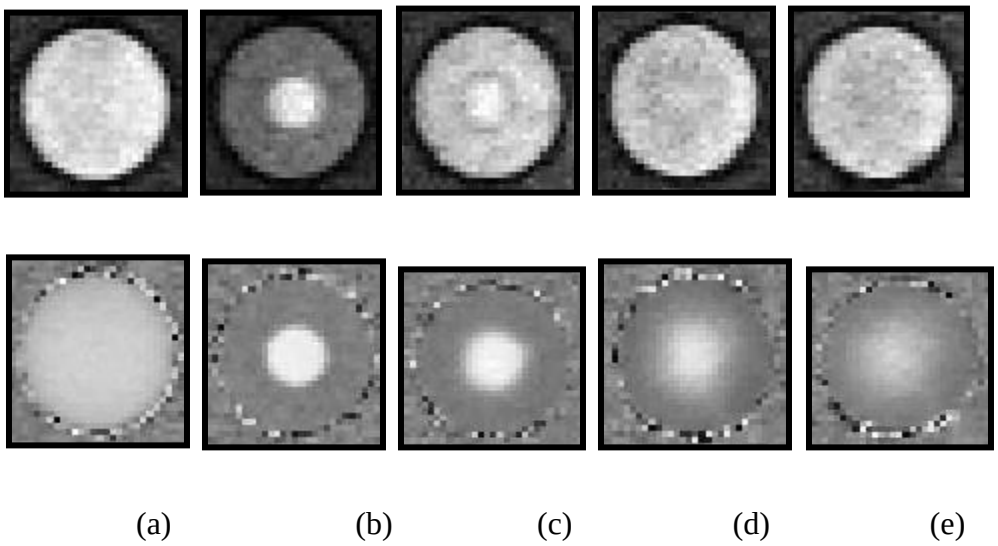

(a) (b) (c) (d) (e)

Figure 5.14: Magnitude and phase images of the 75% orifice model at 10.5 L/min; in-plane resolution: 0.9 x 0.9 mm^2; at TE = 2.65 msec. (a) 6.0 cm upstream from the orifice, (b) at the orifice, (c) 1.0 cm downstream from the orifice, (d) 3.0 cm downstream from the orifice and (e) 5.0 cm downstream from the orifice.

Figures 5.15-5.17 show the % error as a function of TE at each in-plane resolution and slice position. The measured flow rates were almost unaffected by TE at 6.0 cm upstream from the orifice with errors smaller than 2.0 % as seen in Figure 5.15. At the orifice, the flow rates were underestimated with the underestimation increasing with an increasing TE, except for a TE = 3.5 msec. At 1.0 cm, 3.0 cm, and 5.0 cm downstream from the orifice, there was again an underestimation which increased with TE.

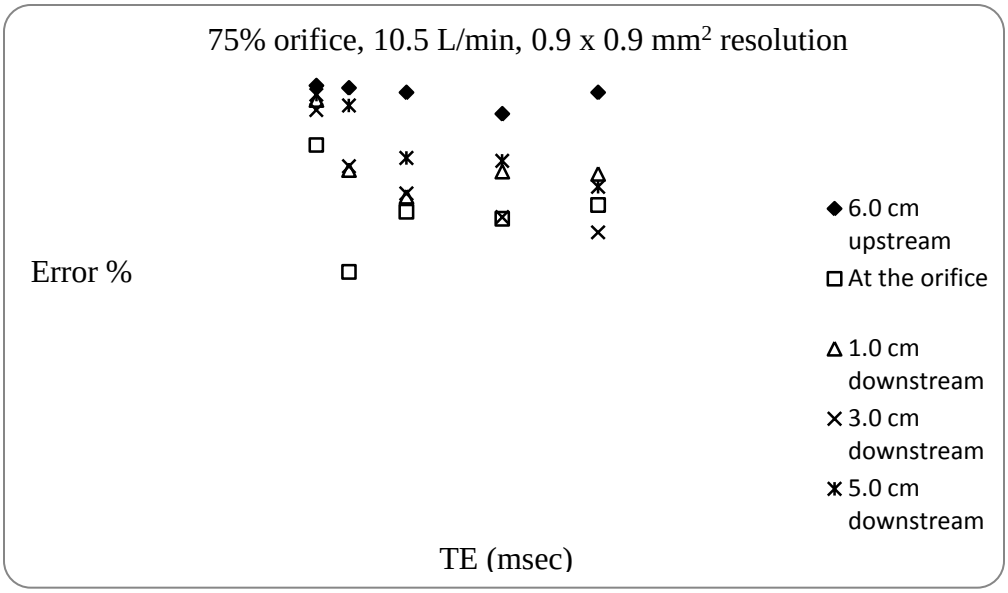

Figure 5.15: Percent error in flow rate measurement as a function of TE for 75% orifice model, at each slice position for a true flow rate of 10.5 L/min; In-plane resolution: 0.9 x 0.9 mm^2.

Figure 5.16 shows that the measured flow rates were well in agreement with the true flow rates for all TEs (TE≤5.0 msec) with errors smaller than 5.0 % at 6.0 cm upstream from the orifice. At the orifice, the flow rates were underestimated and the underestimation increased with TE exhibiting errors up to 19%. At 1.0 cm downstream from the orifice, there was an underestimation in the measured flow rates which increased with TE, except for TE=3.5msec. At 3.0 cm and 5.0 cm downstream from the orifice, the observed underestimation also increased with TE exhibiting errors up to 23%.

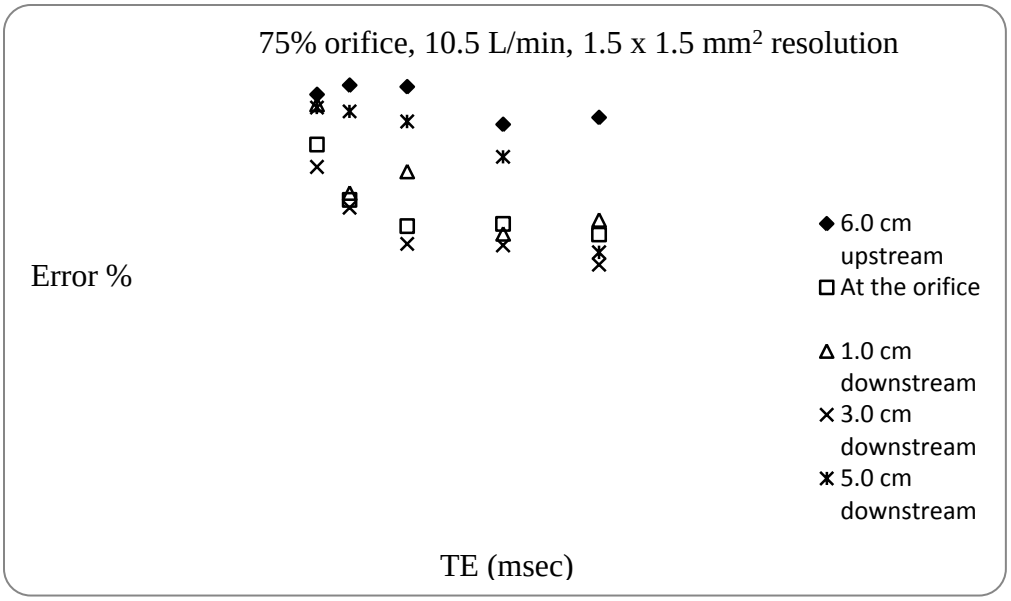

Figure 5.16: Percent error in flow rate measurement as a function of TE for 75% orifice model, at each slice position for a true flow rate of 10.5 L/min; In-plane resolution: 1.5 x 1.5 mm^2.

Figure 5.17 indicates that at 6.0 cm upstream from the orifice, the measured flow rates were well in agreement with the true flow rates at all TEs with errors smaller than 5.7%. At the orifice, the measured flow rates were underestimated and the underestimation increased with TE. At 1.0 cm downstream from the orifice, there was an underestimation in the measured flow rates which increased with TE, except for TE = 3.5 msec. At 3.0 cm and 5.0 cm downstream from the orifice, there was also an underestimation which increased with TE with errors lying between 19.0 % - 29.0 % and 5.0 % - 20.0 % respectively.

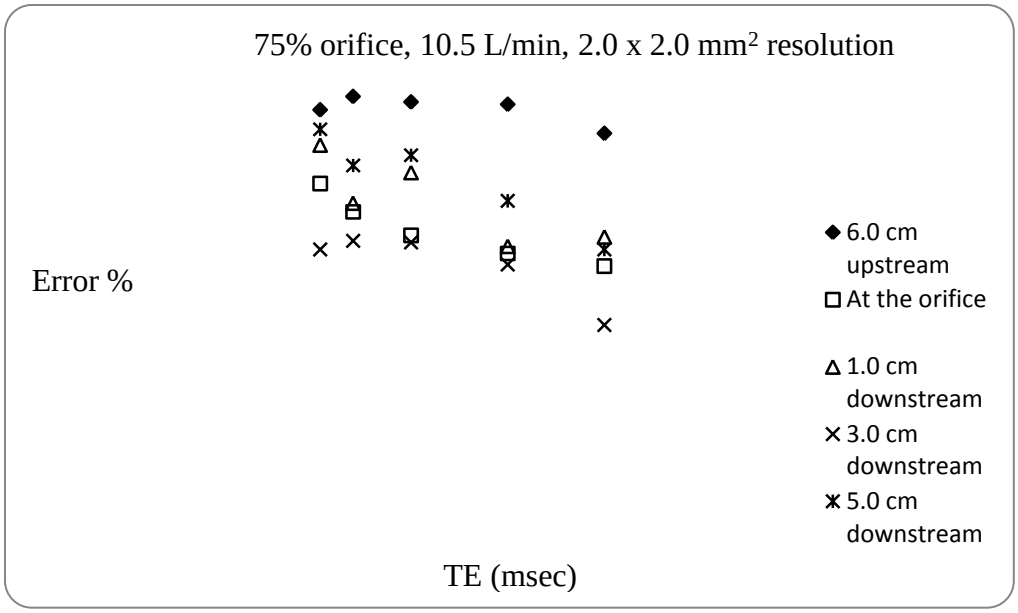

Figure 5.17: Percent error in flow rate measurement as a function of TE for 75% orifice model, at each slice position for a true flow rate of 10.5 L/min; In-plane resolution: 2.0 x 2.0 mm^2.

Figures 5.18, 5.19, 5.20 and (A.6 and A.7 in Appendix A) display the % error in the flow rate as a function of the in-plane resolution for each of the TEs and each slice position. Figure 5.18 shows that the measured flow rates were almost unaffected by the resolution at all TEs at 6.0 cm upstream from the orifice. At the orifice, as seen in Figure 5.19, the effect of the in-plane resolution on the flow rate measurements was negligible, except for TE = 3.5 msec, where the measured flow rate was highly underestimated at the highest resolution (0.9 x 0.9 mm^2) with an error of 23.6%. The error decreased with as the resolution decreased. As seen in the Figures 5.20, A.6 and A.7 the flow rate measurements were almost unaffected by resolution at all TEs.

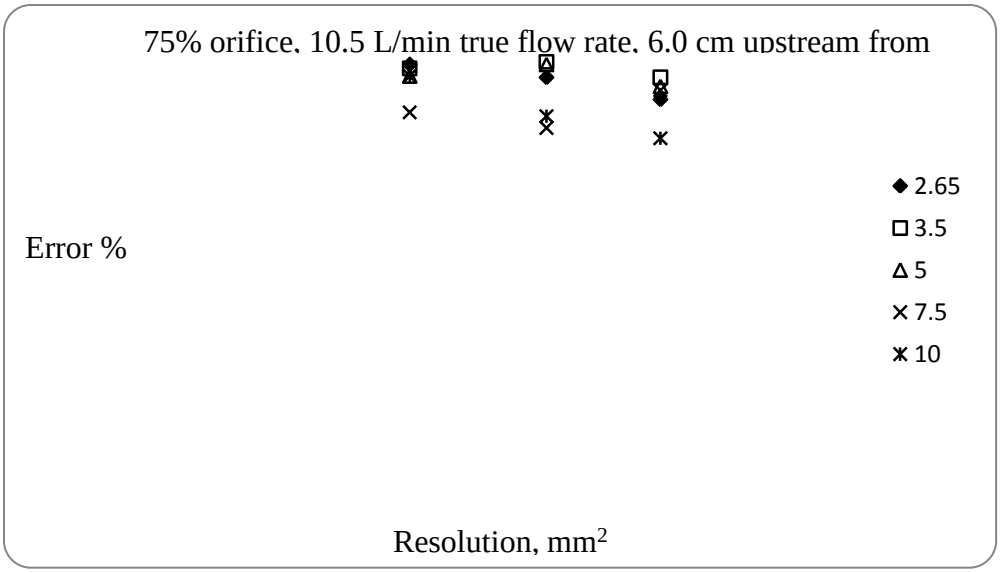

Figure 5.18: Percentage error in flow rate measurement as a function of in-plane resolution for the 75% orifice model; Slice position: 6.0 cm upstream; for a true flow rate of 10.5 L/min

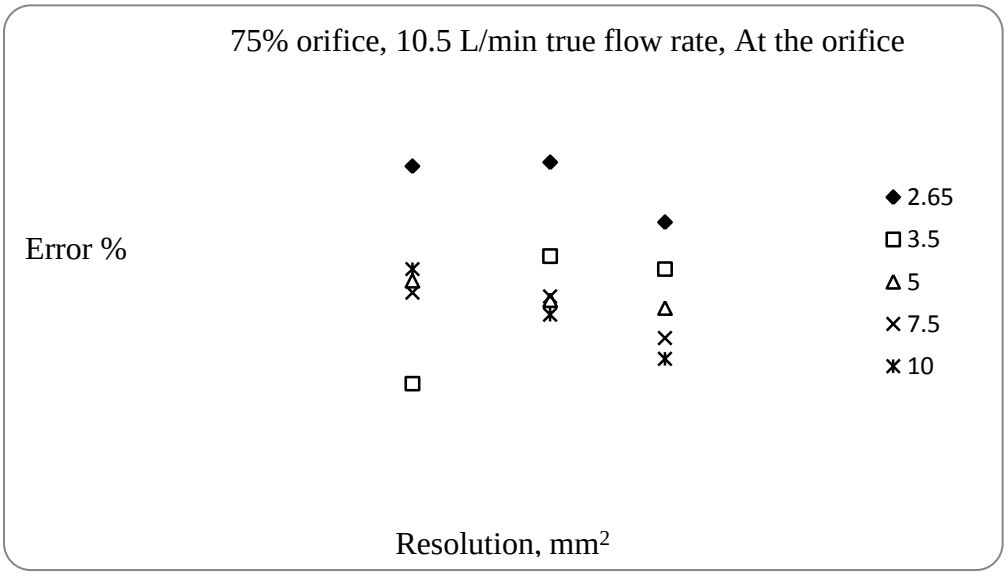

Figure 5.19: Percentage error in flow rate measurement as a function of in-plane resolution for the 75% orifice model; Slice position: at the orifice; for a true flow rate of 10.5 L/min

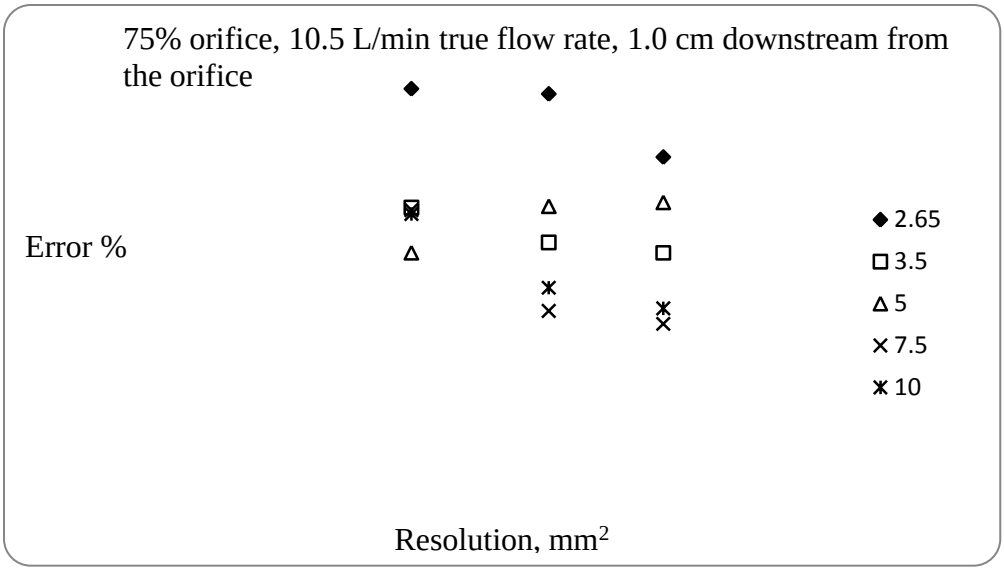

Figure 5.20: Percentage error in flow rate measurement as a function of in-plane resolution for the 75% orifice model; Slice position: 1.0 cm downstream; for a true flow rate of 10.5 L/min

94 % Area Reduction Orifice Model – True Flow Rate = 5.5 L/min

Tables 5.16-5.20 show the MRPVM measured flow rates at the five locations shown in Figure 4.3 for all TEs and in-plane spatial resolutions.

Table 5.16: Measured flow rates (L/min) at five TEs and three in-plane spatial resolutions; Slice location: 6.0 cm upstream from the orifice; True Flow Rate = 5.5 Lpm; 94% orifice model

Spatial Resolution (mm^2)	TE (ms)	Measured Flow rate (Lpm)
0.9 x 0.9	2.65	5.48
	3.5	5.48
	5.0	5.46
	7.5	5.50
	10.0	5.48
1.5 x 1.5	2.65	5.47
	3.5	5.45
	5.0	5.44
	7.5	5.45
	10.0	5.44
2.0 x 2.0	2.65	5.46
	3.5	5.43
	5.0	5.41
	7.5	5.43
	10.0	5.48

Table 5.17: Measured flow rates (L/min) at five TEs and three in-plane spatial resolutions; Slice location: At the orifice; True Flow Rate = 5.5 Lpm; 94% orifice model

Spatial Resolution (mm^2)	**TE (ms)**	**Measured Flow rate (LPM)**
0.9 x 0.9	2.65	4.74
	3.5	4.13
	5.0	3.24
	7.5	2.49
	10.0	1.51
1.5 x 1.5	2.65	4.68
	3.5	3.94
	5.0	2.94
	7.5	2.05
	10.0	1.19
2.0 x 2.0	2.65	4.25
	3.5	3.86
	5.0	2.77
	7.5	1.72
	10.0	1.30

Table 5.18: Measured flow rates (L/min) at five TEs and three in-plane spatial resolutions; Slice location: 1.0 cm downstream from the orifice; True Flow Rate = 5.5 Lpm; 94% orifice model

Spatial Resolution (mm^2)	**TE (ms)**	**Measured Flow rate (Lpm)**
0.9 x 0.9	2.65	5.39
	3.5	4.71
	5.0	4.42
	7.5	4.21
	10.0	3.61
1.5 x 1.5	2.65	5.23
	3.5	4.26
	5.0	3.89
	7.5	3.61
	10.0	2.94
2.0 x 2.0	2.65	4.97
	3.5	4.11
	5.0	3.52
	7.5	2.91
	10.0	2.34

Table 5.19: Measured flow rates (L/min) at five TEs and three in-plane spatial resolutions; Slice location: 3.0 cm downstream from the orifice; True flow rate = 5.5 L/min; 94% orifice model

Spatial Resolution (mm^2)	**TE (ms)**	**Measured Flow rate (Lpm)**
0.9 x 0.9	2.65	5.45
	3.5	5.42
	5.0	5.30
	7.5	5.28
	10.0	5.05
1.5 x 1.5	2.65	5.42
	3.5	5.41
	5.0	5.32
	7.5	5.11
	10.0	4.94
2.0 x 2.0	2.65	5.40
	3.5	5.31
	5.0	5.13
	7.5	4.42
	10.0	4.29

Table 5.20: Measured flow rates (L/min) at five TEs and three in-plane spatial resolutions; Slice location: 5.0 cm downstream from the orifice; True flow rate = 5.5 L/min; 94% orifice model

Spatial Resolution (mm^2)	**TE (ms)**	**Measured Flow rate (Lpm)**
0.9 x 0.9	2.65	5.42
	3.5	4.97
	5.0	4.93
	7.5	4.80
	10.0	4.88
1.5 x 1.5	2.65	5.40
	3.5	5.02
	5.0	4.91
	7.5	5.15
	10.0	4.81
2.0 x 2.0	2.65	5.28
	3.5	5.21
	5.0	4.97
	7.5	4.67
	10.0	4.21

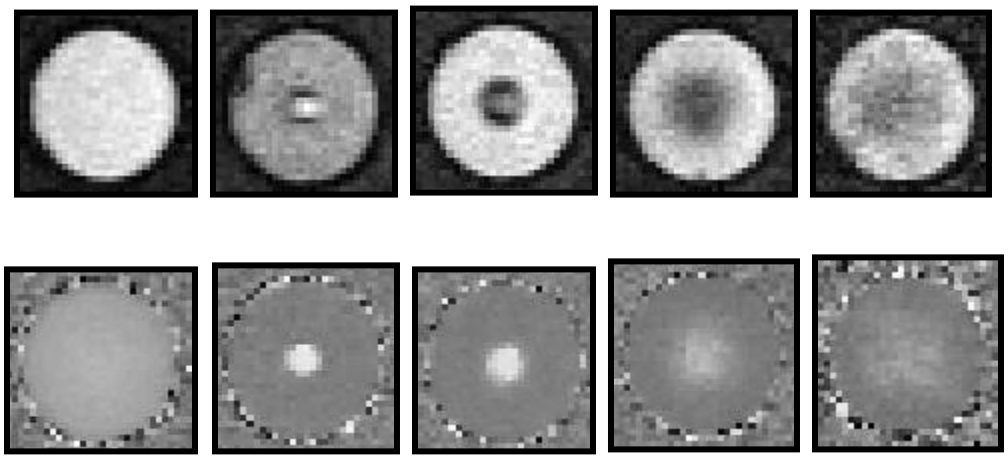

(a) (b) (c) (d) (e)

Figure 5.21: Magnitude and phase images of the 94 % orifice model at 5.5 L/min; in-plane resolution: 0.9 x 0.9 mm^2; TE = 2.65 msec. (a) 6.0 cm upstream from the orifice, (b) at the orifice, (c) 1.0 cm downstream from the orifice, (d) 3.0 cm downstream from the orifice and (e) 5.0 cm downstream from the orifice.

Figures 5.22 (A.8 and A.9 in Appendix A) shows the % error (% difference between the measured flow rates and true flow rates) as a function of TE for each in-plane resolution and slice position.

In Figures 5.22, A.8 and A.9, at 6.0 cm upstream from the orifice, the measured flow rates are well in agreement with true flow rates at all TEs. At the orifice and at 1.0 cm downstream from the orifice, the underestimation increased with TE. The underestimation of flow rates decreased as we move away from the orifice with an exception of 3.0 cm and 5.0 cm downstream from the orifice. The underestimation was

lesser at 3.0 cm downstream from the orifice when compared to 5.0 cm downstream from the orifice.

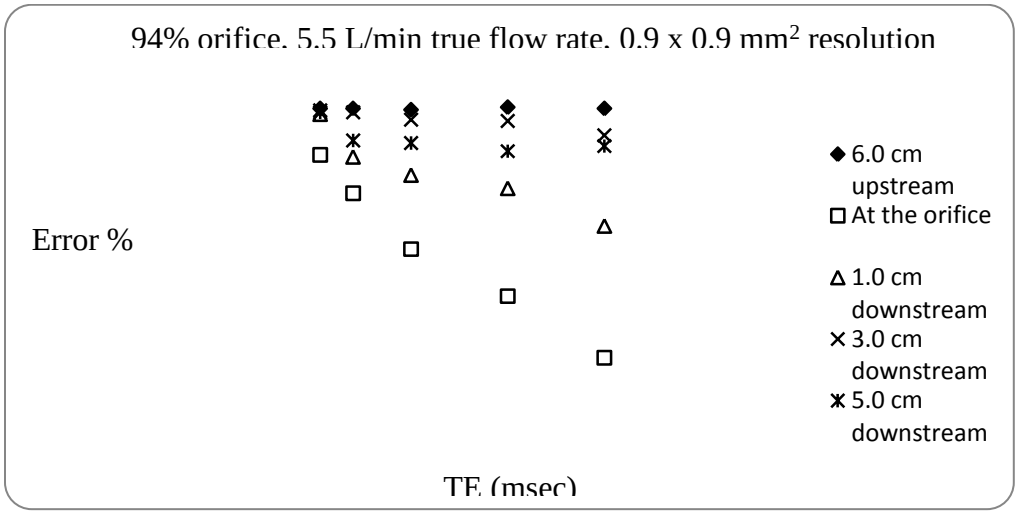

Figure 5.22: Percentage error in the flow rate measurement as a function of TE for 94% orifice model at each slice position for a true flow rate of 5.5 L/min; In-plane resolution: 0.9 x 0.9 mm^2

Figures 5.23, 5.24 (and Figures A.10, A.11 and A.12 in Appendix-A) shows the % error (% difference between the measured flow rates and true flow rates) as a function of in-plane resolution for each TE and slice position. In Figures A.10, A.11 and A.12 it seems that the measured flow rates were unaffected by resolution at all TEs and slice positions. In Figure 5.23, the error in the measured flow rates increased with a decrease in the resolution. In Figure 5.24, the measured flow rates were almost unaffected by resolution at TE = 2.65 msec and TE = 5.0 msec. The error in the measured flow rates decreased as the resolution decreased at TE = 3.5 msec and the error increased as the

resolution decreased at TE = 10.0 msec. At TE = 7.5 msec, the underestimation of flow rates is less at 1.5 x 1.5 mm^2 resolution when compared to other resolutions.

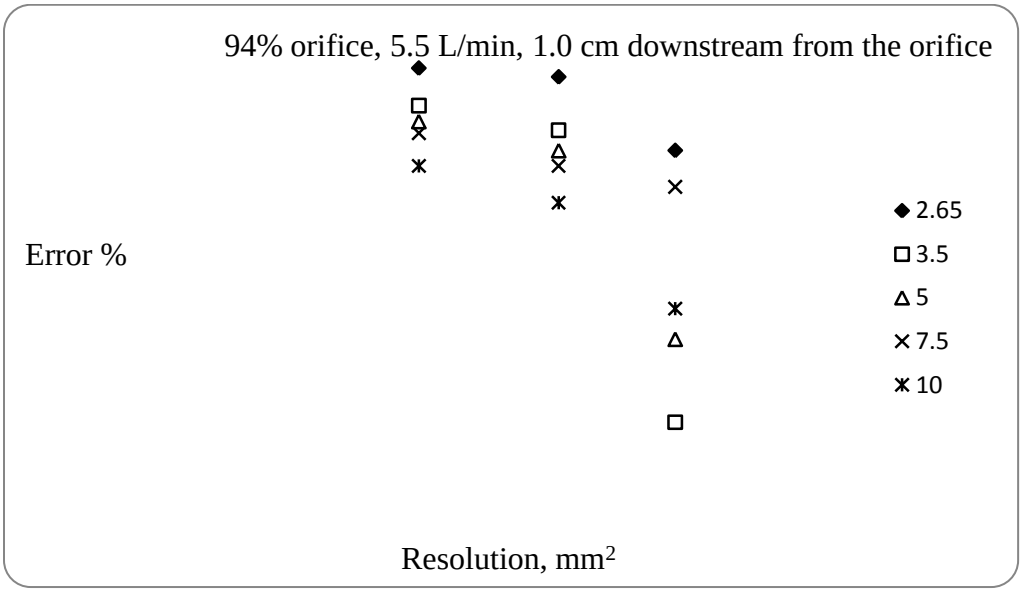

Figure 5.23: Percentage error in flow rate measurement as a function of in-plane resolution for the 94% orifice model; Slice position: 1.0 cm downstream; for a true flow rate of 5.5 L/min

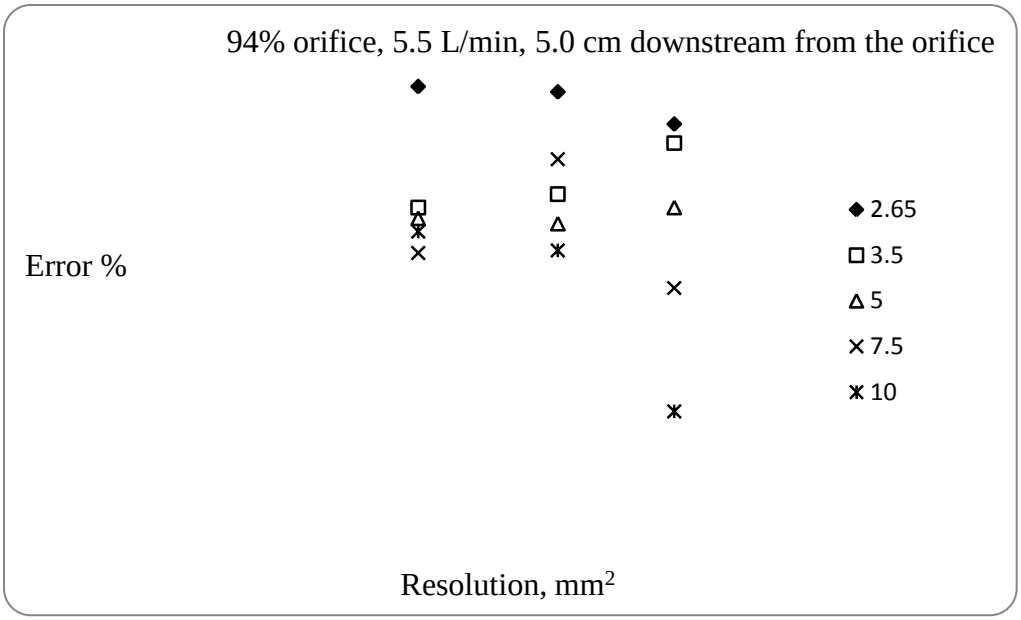

Figure 5.24: Percentage error in flow rate measurement as a function of in-plane resolution for the 94% orifice model; Slice position: 5.0 cm downstream; for a true flow rate of 5.5 L/min

94% Area Reduction Orifice Model – True Flow Rate = 8.5 lpm

Tables 5.21-5.25 show the MRPVM measured flow rates at the five locations shown in Figure 4.3 for all TEs and in-plane spatial resolutions.

Table 5.21: Measured flow rates (L/min) at five TEs and three in-plane spatial resolutions; Slice location: 6.0 cm upstream from the orifice; True flow rate = 8.5 L/min; 94% orifice model

Spatial Resolution (mm^2)	TE (ms)	Measured Flow rate (Lpm)
0.9 x 0.9	2.65	8.48
	3.5	8.47
	5.0	8.46
	7.5	8.46
	10.0	8.50
1.5 x 1.5	2.65	8.43
	3.5	8.45
	5.0	8.41
	7.5	8.42
	10.0	8.44
2.0 x 2.0	2.65	8.35
	3.5	8.43
	5.0	8.47
	7.5	8.47
	10.0	8.46

Table 5.22: Measured flow rates (L/min) at five TEs and three in-plane spatial resolutions; Slice location: At the orifice; True flow rate = 8.5 L/min; 94% orifice model

Spatial Resolution (mm^2)	**TE (ms)**	**Measured Flow rate (Lpm)**
0.9 x 0.9	2.65	5.32
	3.5	5.09
	5.0	4.36
	7.5	4.54
	10.0	4.20
1.5 x 1.5	2.65	5.15
	3.5	4.69
	5.0	3.51
	7.5	2.40
	10.0	2.69
2.0 x 2.0	2.65	3.89
	3.5	-1.06
	5.0	0.45
	7.5	3.23
	10.0	1.01

Table 5.23: Measured flow rates (L/min) at five TEs and three in-plane spatial resolutions; Slice location: 1.0 cm downstream from the orifice; True flow rate = 8.5 L/min; 94% orifice model

Spatial Resolution (mm^2)	**TE (ms)**	**Measured Flow rate (Lpm)**
0.9 x 0.9	2.65	-4.11
	3.5	-2.19
	5.0	0.27
	7.5	-3.87
	10.0	-5.22
1.5 x 1.5	2.65	-0.89
	3.5	0.88
	5.0	-2.15
	7.5	-1.88
	10.0	-3.80
2.0 x 2.0	2.65	0.94
	3.5	-0.57
	5.0	-2.08
	7.5	-4.69
	10.0	-3.70

Table 5.24: Measured flow rates (L/min) at five TEs and three in-plane spatial resolutions; Slice location: 3.0 cm downstream from the orifice; True flow rate = 8.5 L/min; 94% orifice model

Spatial Resolution (mm^2)	**TE (ms)**	**Measured Flow rate (Lpm)**
0.9 x 0.9	2.65	-4.30
	3.5	-6.34
	5.0	-3.39
	7.5	-3.74
	10.0	-1.88
1.5 x 1.5	2.65	5.32
	3.5	3.45
	5.0	1.37
	7.5	-1.67
	10.0	-2.57
2.0 x 2.0	2.65	4.25
	3.5	3.26
	5.0	0.77
	7.5	-1.70
	10.0	-2.48

Table 5.25: Measured flow rates (L/min) at five TEs and three in-plane spatial resolutions; Slice location: 5.0 cm downstream from the orifice; True flow rate = 8.5 L/min; 94% orifice model

Spatial Resolution (mm^2)	**TE (ms)**	**Measured Flow rate (Lpm)**
0.9 x 0.9	2.65	3.89
	3.5	3.20
	5.0	5.34
	7.5	2.89
	10.0	4.17
1.5 x 1.5	2.65	7.01
	3.5	6.11
	5.0	3.74
	7.5	5.24
	10.0	2.82
2.0 x 2.0	2.65	5.97
	3.5	4.62
	5.0	6.13
	7.5	4.32
	10.0	3.78

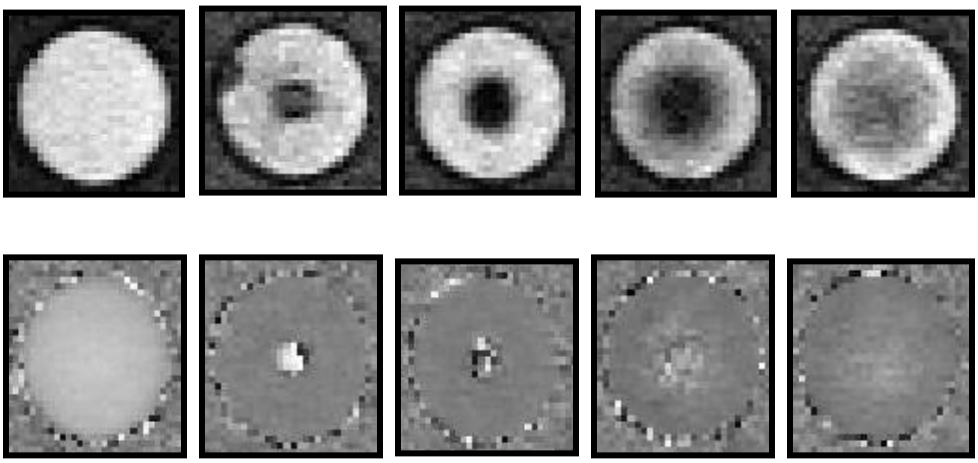

(a) (b) (c) (d) (e)

Figure 5.25: Magnitude and phase images of the 94% orifice model at 8.5 L/min; in-plane resolution: 0.9 x 0.9 mm^2; TE = 2.65 msec. (a) 6.0 cm upstream from the orifice, (b) at the orifice, (c) 1.0 cm downstream from the orifice, (d) 3.0 cm downstream from the orifice and (e) 5.0 cm downstream from the orifice.

Figures 5.26 (and Figures A.13 and A.14 in Appendix A) show the % error in the measured flow rate (as % difference between measured and true flow rates) as a function of TE for each of the in-plane resolutions and slice positions in the case of the 94% orifice model.

In Figures 5.26, A.13 and A.14, at 6 cm upstream from the orifice, the measured flow rates were well in agreement with true flow rates at all TEs. The behavior of the measured flow rates is highly inconsistent at the orifice, 1.0 cm downstream from the orifice, 3.0 cm downstream from the orifice and at 5.0 cm downstream from the orifice.

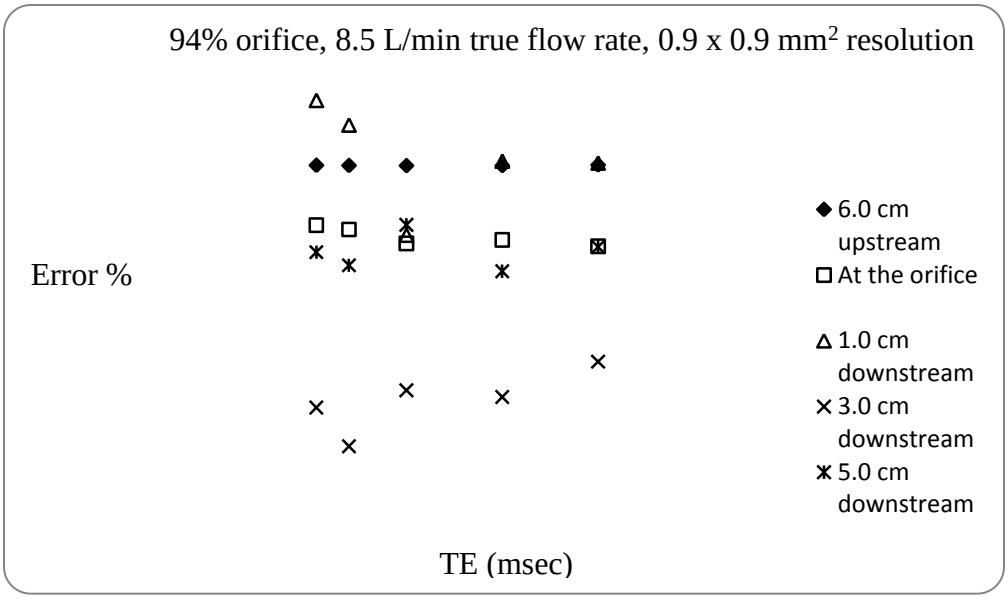

Figure 5.26: Percentage error in the flow rate measurement as a function of TE for 94% orifice model at each slice position for a true flow rate of 8.5 L/min; In-plane resolution: 0.9 x 0.9 mm^2

Figures 5.29-5.30 (and Figure A.18 in Appendix-A) show the % error in the measured flow rate (as % difference between measured and true flow rates) as a function of in-plane resolution for each TE and slice positions in the case of the 94% orifice model. In Figure A.18, at 6.0 cm upstream from the orifice, the measured flow rates were well in agreement with the true flow rates at all TEs and slice positions. In Figure 5.27, the error in measured flow rates increased as the resolution decreased at TE = 2.65, 5.0, 10.0 msec and exhibited an inconsistent behavior at TE = 3.5 msec and TE = 7.5 msec with a lowest error of 14.71% and 38.82% respectively at 2.0 x 2.0 mm^2. In Figure 5.28, there is an overestimation as well as underestimation of measured flow rates at different resolutions and TEs. In Figure 5.29, the measured flow rates were underestimated and the

underestimation was highest at lowest resolution at all TEs. In Figure 5.30, at TE = 2.65 msec and TE = 10 msec, the underestimation of flow rates is highest at 1.5 x 1.5 mm^2 resolution when compared to other two resolutions and vice-versa at all other TEs.

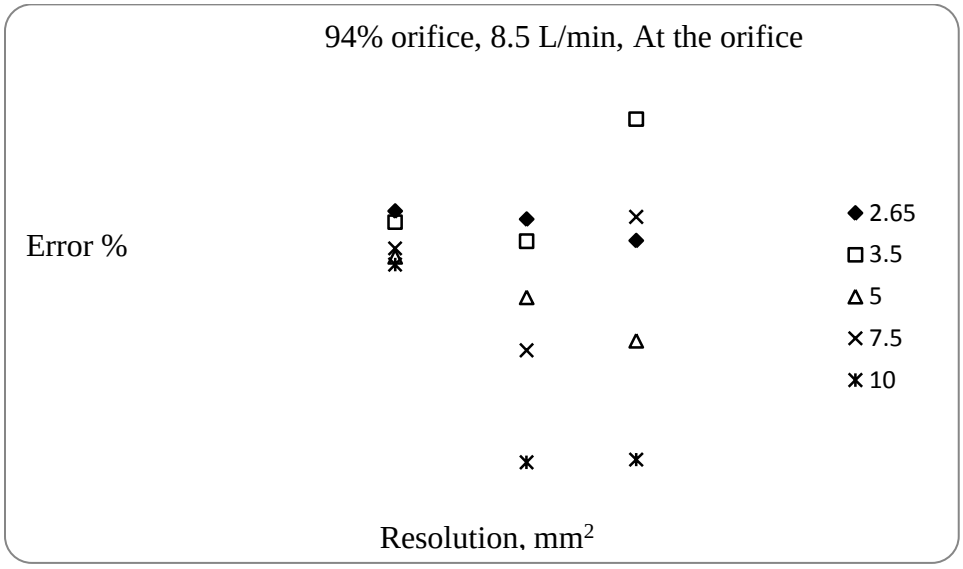

Figure 5.27: Percentage error in flow rate measurement as a function of in-plane resolution for the 94% orifice model; Slice position: at the orifice; for a true flow rate of 8.5 L/min

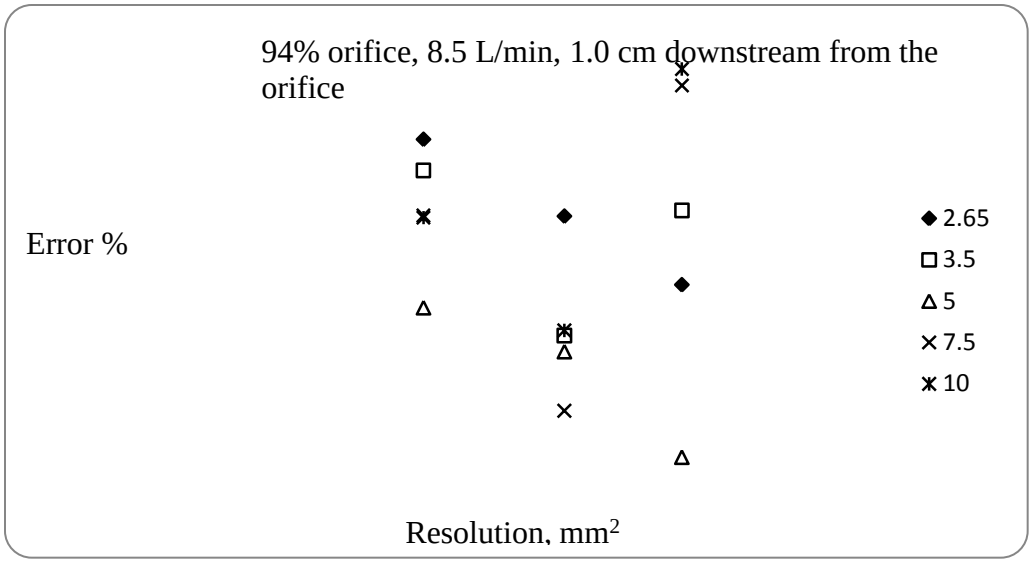

Figure 5.28: Percentage error in flow rate measurement as a function of in-plane resolution for the 94% orifice model; Slice position: 1.0 cm downstream; for a true flow rate of 8.5 L/min

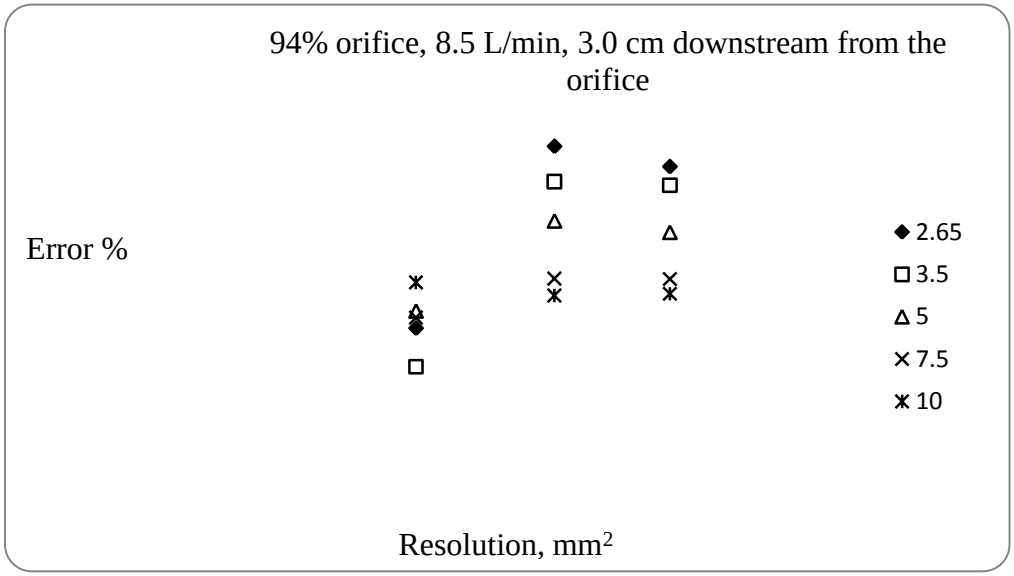

Figure 5.29: Percentage error in flow rate measurement as a function of in-plane resolution for the 94% orifice model; Slice position: 3.0 cm downstream; for a true flow rate of 8.5 L/min

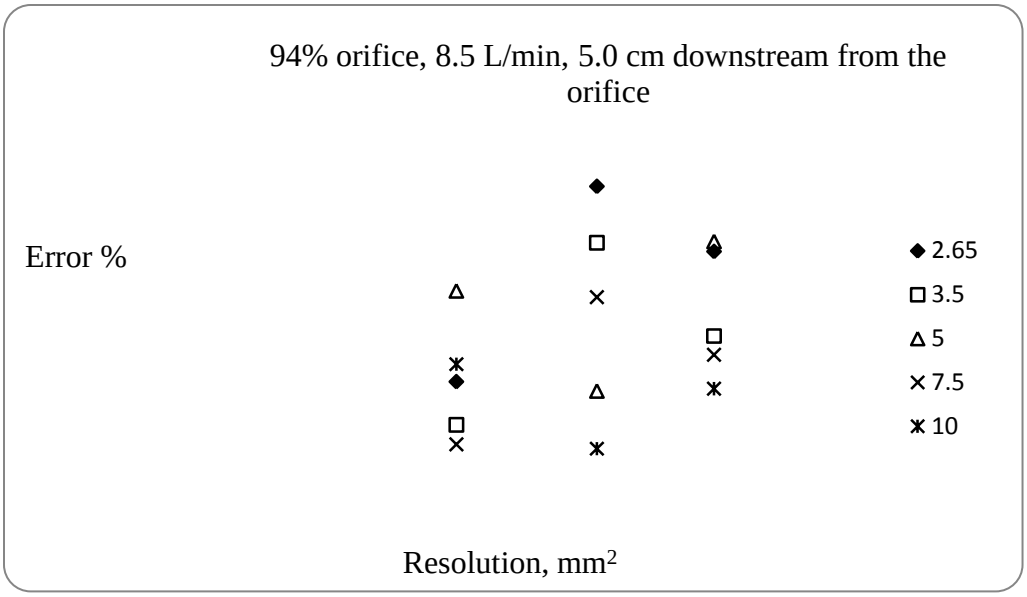

Figure 5.30: Percentage error in flow rate measurement as a function of in-plane resolution for the 94% orifice model; Slice position: 5.0 cm downstream; for a true flow rate of 8.5 L/min

To view the measurements from a different point of view, the following figures show selectively the measured flow rates plotted against the true flow rates.

Figures 5.31-5.35 show the relationship between the measured flow rates and true flow rates for an in-plane resolution of 0.9 x 0.9 mm^2 for all TEs and slice positions in the case of the 75% orifice model. From Figure 5.31 (as well as Figures B.1 and B.2 in Appendix B), it can be seen that the measured flow rates remained almost unaffected by the resolution and TE at 6.0 cm upstream from the orifice.

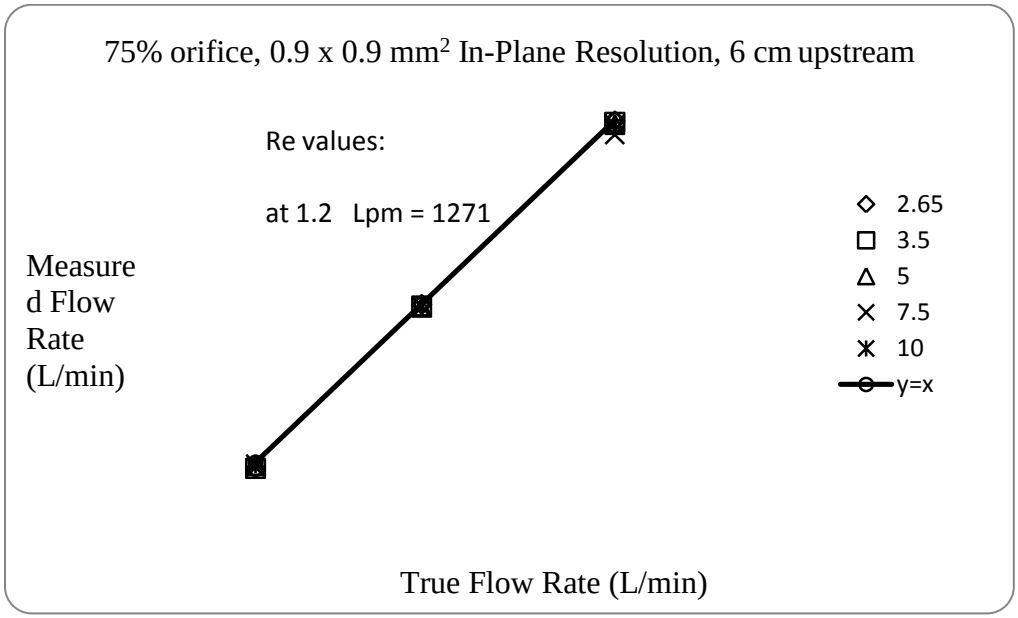

Figure 5.31: Relationship between the measured flow rate and the true flow rate for all TEs, at 6.0 cm upstream from the 75% orifice; In-plane resolution = 0.9 x 0.9 mm^2.

At the orifice, Figure 5.32 (and Figures B.3 and B.4 in Appendix B) shows that the percentage error in the underestimation of the measured flow rates was much higher for

the true flow rate of 1.2 L/min, when compared to that at higher flow rates, and increased with TE.

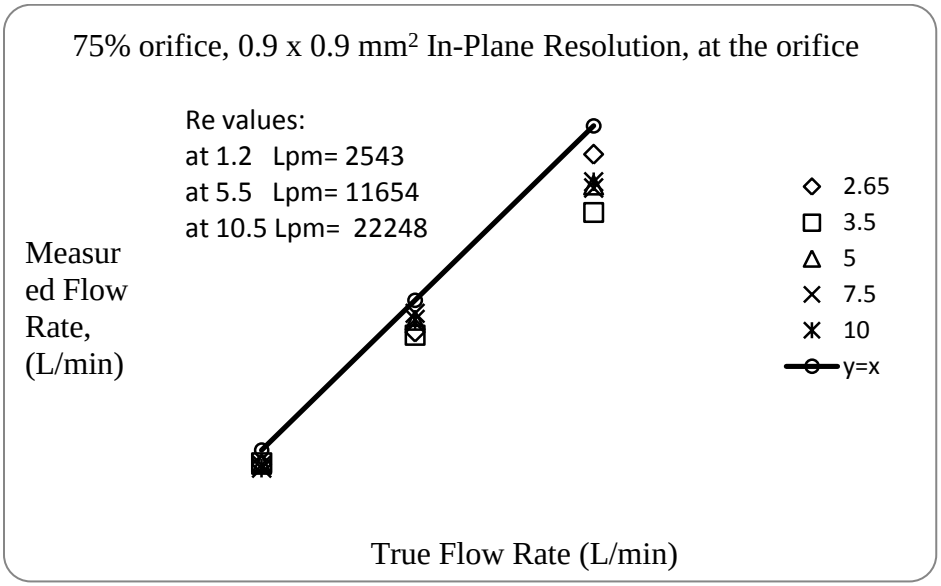

Figure 5.32: Relationship between the measured flow rate and the true flow rate for all TEs, at the Orifice, from the 75% orifice; In-plane resolution = 0.9 x 0.9 mm^2.

Similarly, at 1.0 cm downstream from the orifice, Figure 5.33 (and Figures B.5 and B.6 in Appendix B) shows that the percentage error in the underestimation of the measured flow rates was much higher for the true flow rate of 1.2 L/min, when compared to that at higher flow rates, and it also increased with in TE. The measured flow rates were much closer to the true flow rate in the case of 5.5 L/min.

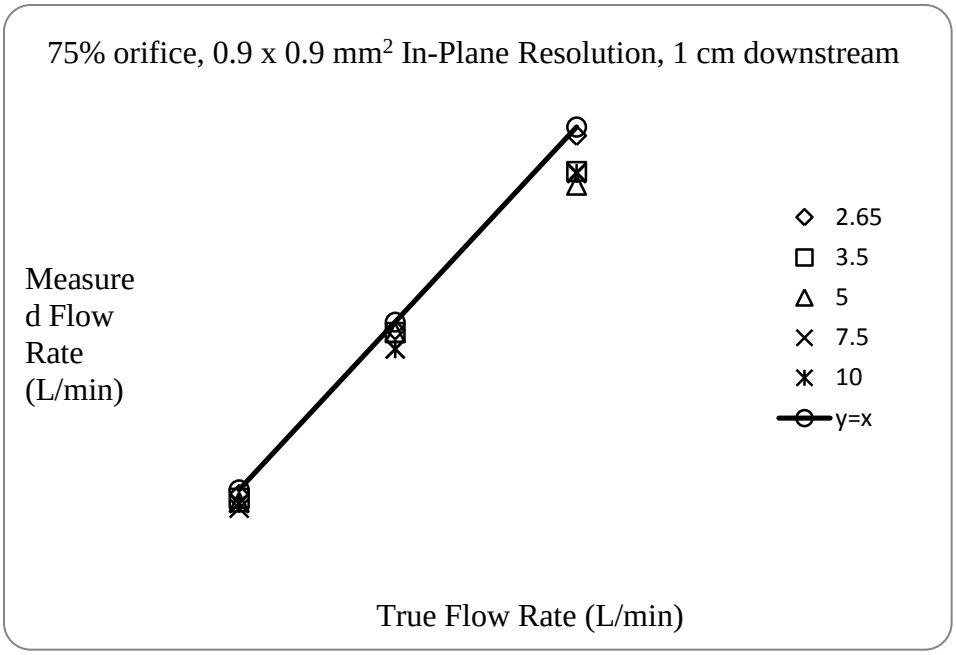

Figure 5.33: Relationship between the measured flow rate and the true flow rate for all TEs, at the 1 cm downstream from the 75% orifice; In-plane resolution = 0.9 x 0.9 mm^2.

In a similar way, Figure 5.34 (and Figures B.7 and B.8 in Appendix B) shows that the percentage error in the underestimation of the measured flow rates was much higher at 1.2 L/min when compared to that at higher flow rates. The percentage error in the underestimation was much lower at 5.5 L/min than at 10.5 L/min. The underestimation increased with an increase in TE.

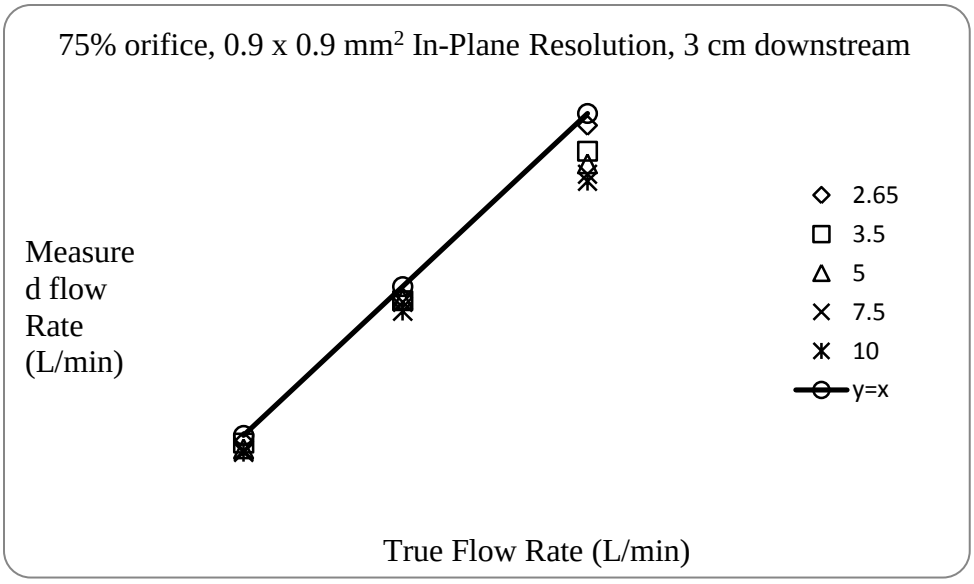

Figure 5.34: Relationship between the measured flow rate and the true flow rate for all TEs, at the 3 cm downstream from the 75% orifice; In-plane resolution = 0.9 x 0.9 mm^2.

Figure 5.35 (and Figures B.9 and B.10 in Appendix B) shows that the percentage error in the underestimation of measured flow rates was much higher at 1.2 L/min when compared to that at higher flow rates and it decreased as the flow rate increased. Also, the underestimation increased with TE.

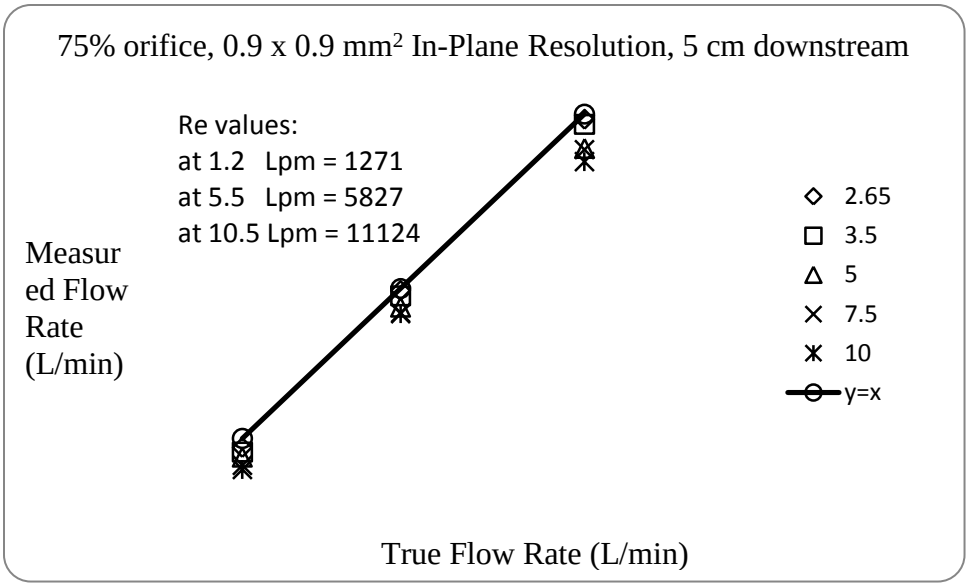

Figure 5.35: Relationship between the measured flow rate and the true flow rate for all TEs, at the 5 cm downstream from the 75% orifice; In-plane resolution = 0.9 x 0.9 mm^2.

Figures 5.36-5.40 show the relationship between the measured flow rates and true flow rates for an in-plane resolution of 0.9 x 0.9 mm^2 for all TEs and slice positions in the case of the 94% orifice model. From Figure 5.36 (as well as Figures B.11 and B.12 in Appendix B), it can be seen that the measured flow rates remained almost unaffected by the resolution and TE at 6.0 cm upstream from the orifice.

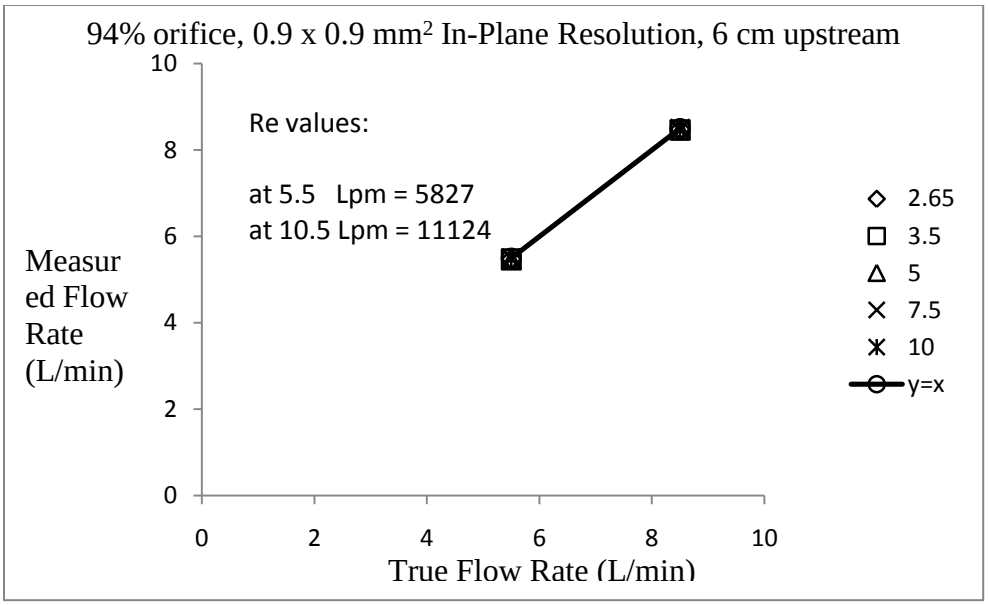

Figure 5.36: Relationship between the measured flow rate and the true flow rate for all TEs, at 6.0 cm upstream from the 94% orifice; In-plane resolution = 0.9 x 0.9 mm^2.

At the orifice, Figure 5.37 (and Figures B.13 and B.14 in Appendix B) shows that the measured flow rates were underestimated and the underestimation increased with an increase in the flow rate and with an increase in TE.

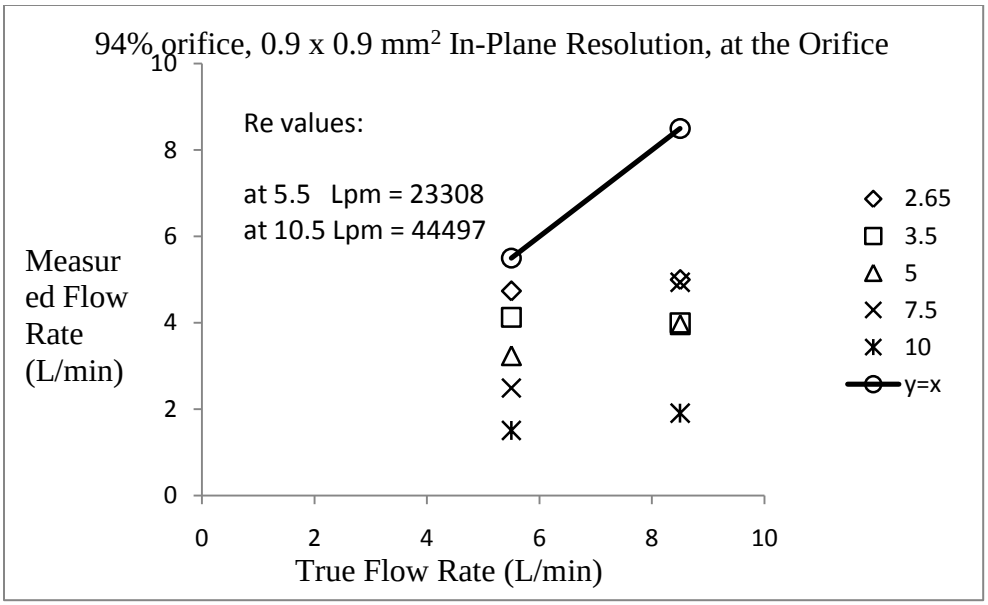

Figure 5.37: Relationship between the measured flow rate and the true flow rate for all TEs, at the Orifice, from the 94% orifice; In-plane resolution = 0.9 x 0.9 mm^2.

Similarly, at 1.0 cm downstream from the orifice, Figure 5.38 (and Figures B.15 and B.16 in Appendix B) shows that the measured flow rates were underestimated and the underestimation increased with an increase in the flow rate and with an increase in TE. At 8.5 L/min and at TE= 2.65 and 3.5 msec, flow rates were slightly overestimated.

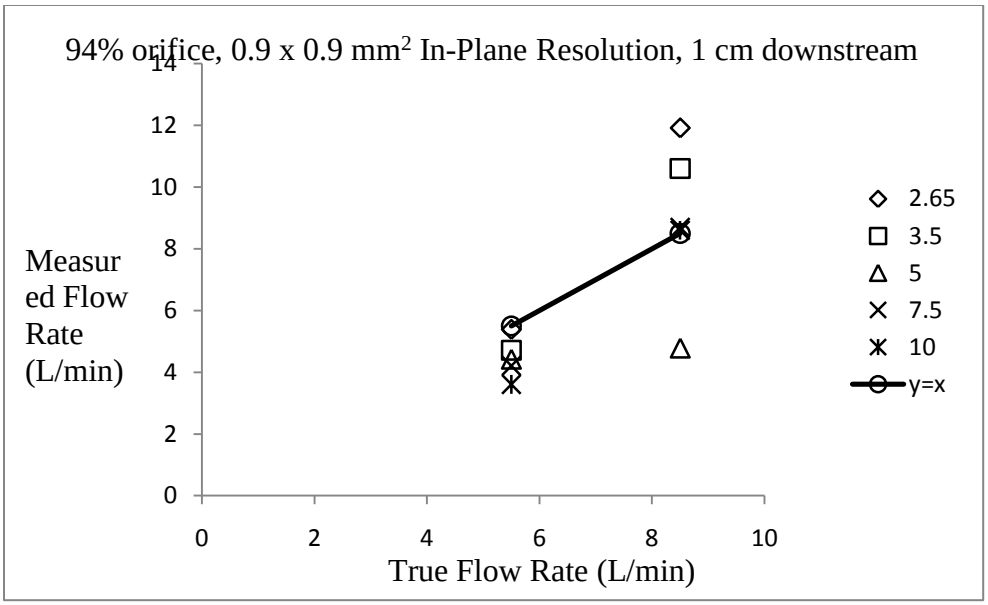

Figure 5.38: Relationship between the measured flow rate and the true flow rate for all TEs, at the 1 cm downstream from the 94% orifice; In-plane resolution = 0.9 x 0.9 mm^2.

In a similar way, Figure 5.39, 5.40 (and Figures B.17, B.18, B.19 and B.20 in Appendix B) shows that the measured flow rates were underestimated and the underestimation increased with an increase in the flow rate and with an increase in TE. The flow rates were highly underestimated at 8.5 L/min.

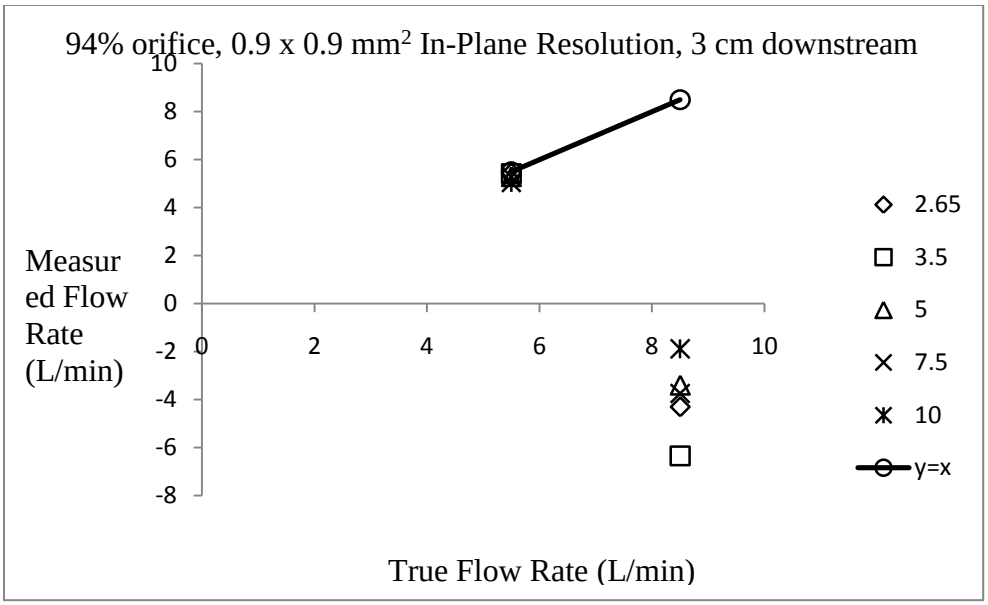

Figure 5.39: Relationship between the measured flow rate and the true flow rate for all TEs, at the 3 cm downstream from the 94% orifice; In-plane resolution = 0.9 x 0.9 mm^2.

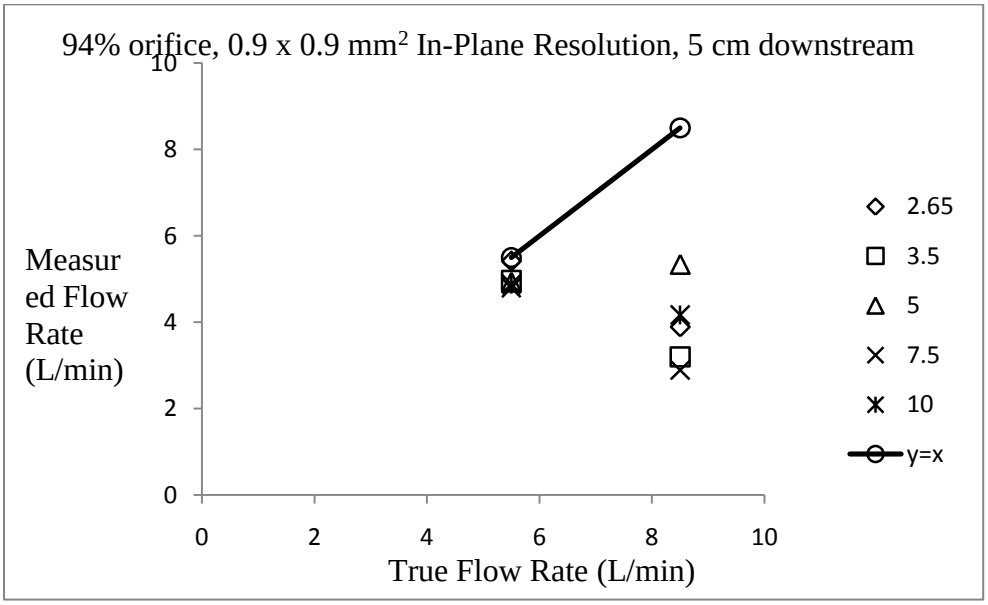

Figure 5.40: Relationship between the measured flow rate and the true flow rate for all TEs, at the 5 cm downstream from the 94% orifice; In-plane resolution = 0.9 x 0.9 mm^2.

In summary, the shorter the TE the better the measured flow rates and the in plane spatial resolution has a minimal effect on measured flow rates.

CHAPTER VI

DISCUSSION

The main aim of this study was to determine the ability of MRPVM to measure flow under turbulent flow conditions. In order to achieve this goal, two hypotheses were tested:

1. The lower the TE, the higher the accuracy of MRPVM under turbulent flow conditions
2. The higher the spatial resolution, the higher the accuracy of MRPVM under turbulent flow conditions

Axial MRPVM images were acquired for the two orifice models in a 1.5T Siemens MRI scanner under steady flow conditions. Images were acquired under various flow rates, imaging slice locations and imaging parameters as discussed in previous chapters.

Overall, the study indicated that lower TEs (2.65 msec and 3.5 msec) resulted in more accurate flow rates compared to higher TEs (5.0 msec, 7.5 msec, 10.0 msec).

Although the flow was turbulent (based on the Reynolds number), no signal loss was observed in the case of the 75% orifice model. Measurements showed an underestimation for a true flow rate of 1.2 L/min at 6.0 cm upstream from the orifice. In the case of 94% orifice model, slight signal loss was observed for a true flow rate of 5.5 L/min and significant signal loss was observed for 8.5 L/min.

The in-plane spatial resolution had a significant effect only in the 94% orifice model and at 5.5 L/min and 8.5 L/min true flow rates. The higher resolution (0.9 x 0.9 mm^2) resulted in more accurate measurements of the flow rate when compared to lower resolutions in most of the cases. The effect of in-plane resolution is negligible in all other cases.

Flow patterns in the arteries are governed by several important factors like blood viscosity, blood density, blood vessel diameter, elasticity of the muscular layer and smoothness of the vascular lumen. Laminar and turbulent are the basic types of blood flow patterns found in normal and diseased human arteries. Laminar flow is smooth flow in which all flow is in the same direction and is stable with streamline formations staying intact. It occurs at velocities up to a certain critical velocity and above this velocity, the flow is turbulent. In turbulence flow is characterized by multi-directional, multi-velocity streams. Vessel tortuosity and the collapse of high velocity jets to an arterial stenosis are the common reasons for turbulence. In clinical practice, this phenomenon is commonly seen downstream from the stenosis. The turbulence effects create excessive wall vibrations as well as multi velocity profiles flowing through the vessel in many different directions. The occurrence of turbulence also depends on the diameter of the vessel and

the viscosity of the blood. This is expressed by the ratio of inertial to viscous forces which is nothing but Re. In humans, the critical velocity is sometimes exceeded in the ascending aorta at the peak of systolic ejection, but mainly when there is an occlusion in an artery. Turbulent effects can be seen frequently in anemic cases because the viscosity of the blood is lower [65].

Presence of stenosis produces higher velocities. When the flow is in one direction, Doppler frequency spectrum shows elevated peak systolic velocities greater than 200 cm/sec and velocities greater than 140 cm/sec at end diastolic components. But downstream from the stenosis, there may be flow reversals and turbulence which increases the velocities to even higher values. Peak systolic values continue to increase with an increase in the degree of stenosis. Downstream from the stenosis, the Doppler signals indicate decreased velocities and absence of diastolic flow [65].

The Reynolds numbers used in the study vary between 1271 and 11124 at the upstream (ID = 2.0 cm) for both the models. Under normal conditions, the heart supplies about 5.5 L/min of blood to the body. But under abnormal conditions the flow rates can go upto five times the normal conditions [64]. The ID of the ascending aorta is approximately an inch which is close to the ID of the models used (2.0 cm). Also the models were similar in geometry with the aorta. At a flow rate of 5.5 L/min and the density and viscosity of blood being 1050 kg/m^3 and 0.0035 kg/m-sec, the Re number is approximately 1379 under healthy conditions. But as mentioned previously under abnormal conditions the flow rates can go upto five times resulting in Re = 6895. In our study a range of Re with the lowest being 1271 and highest being 11124 were studied.

Results indicate that at these Re values and lower, the lower TEs (2.65 msec and 3.5 msec) measured accurately when compared to higher TEs (5.0, 7.5, 10.0 msec) with error percentages below 10.0% in case of 75% area reduction. Also higher resolution (0.9 x 0.9 mm^2) measured accurately with errors lying within 10.0 % when compared to lower resolution (2.0 x 2.0 mm^2) where the errors were upto 40.0%. When compared to the physiological conditions, the flow rates can be accurately measured during early systole but at higher Re, the intensity of turbulence is very high that the imaging parameters do not play a role in determining the accuracy of MRPVM.

As the area of reduction increased further, the MRPVM is accurate upto flow rates of 5.5L/min and at lower TEs (2.65 and 3.5 msec) with errors lying within 25.0% when compared to higher TEs (5.0, 7.5 and 10.0 msec) where the errors reached up to 58.0%. But as the flow rate increased further at higher order Re, the behavior of the flow rates is undefined and the intensity of turbulence is very high that the flow rates did not have any particular trend at such high Re values.

In summary, the study indicates that MRPVM is accurate for an upstream Re values upto 5827 and area reduction of 94%, but at Re values higher than 5827, MRPVM can lead to errors in measurements due to signal loss.

Results are discussed in detail as follows:

The Effects of TE

Starting with the 75% orifice model, the measured flow rates upstream of the orifice were in close agreement with the true flow rates for all TEs used. This was true in all

flow rate cases except for 1.2 L/min in which case they were slightly underestimated, probably due to an experimental error, especially considering that it was more challenging to achieve a stabilized flow rate value in the lower flow rate cases (some vibration of the rotameter indicator was seen) than in the higher ones.

Figures 6.1 and 6.2 show no signal loss in the central region of the model, because the Reynolds number at the orifice and 1.0 cm downstream from the orifice was relatively low (Upstream Re = 1271, Orifice Re = 2543). However, some signal loss was observed between the central region and the wall of the model, especially at the "3 o'clock" and "9 o'clock" regions as seen in Figure 6.1. This was due to some flow disturbance secondary to small flow detachment immediately downstream of the orifice (which the imaging slice was covering) and flow recirculation causing a small intravoxel de-phasing. As a result, the flow rates were underestimated and the underestimation increased with an increase in TE. This is because as the echo time increases, the protons have more time between slice excitation and signal readout to move randomly in all directions (as a result of the turbulent velocity fluctuations) and thus cause voxel dephasing and errors in the velocity measurements. In fact, as the measurement location moved further downstream from the orifice, the underestimation increased as the turbulent jet diffused in the flow field causing more intense multi-directional flow patterns. The largest underestimation was observed was at 5.0 cm downstream from the orifice and for TE = 10.0 msec.

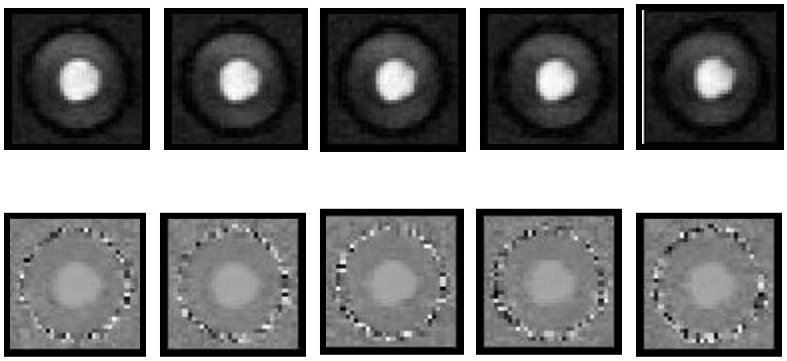

(a) (b) (c) (d) (e)

Figure 6.1: Set of magnitude images (top) and phase images (bottom) from the 75% orifice model; Slice location: at the orifice; Flow Rate = 1.2 L/min, Orifice Re = 2543; Spatial Resolution: 0.9x0.9 mm^2; TE: (a) 2.65, (b) 3.5, (c) 5.0, (d) 7.5, and (e) 10.0 msec.

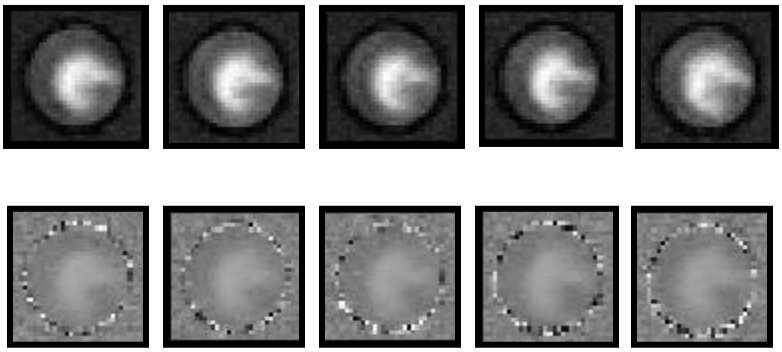

(a) (b) (c) (d) (e)

Figure 6.2: Set of magnitude images (top) and phase images (bottom) from the 75% orifice model; Slice location: 1.0 cm downstream from the orifice, Flow Rate = 1.2 L/min, Upstream Re = 1271; Spatial Resolution: 0.9x0.9 mm^2; TE: (a) 2.65, (b) 3.5, (c) 5.0, (d) 7.5 and (e) 10.0 msec.

In Figures 6.3 the underestimation of the flow rates was higher at the lower TEs (TE = 2.65 and TE = 3.5 msec) when compared to higher TEs. Although the flow through the model was turbulent with a Re = 11654 at the orifice and Upstream Re = 5827 downstream from the orifice, there was not much signal loss.

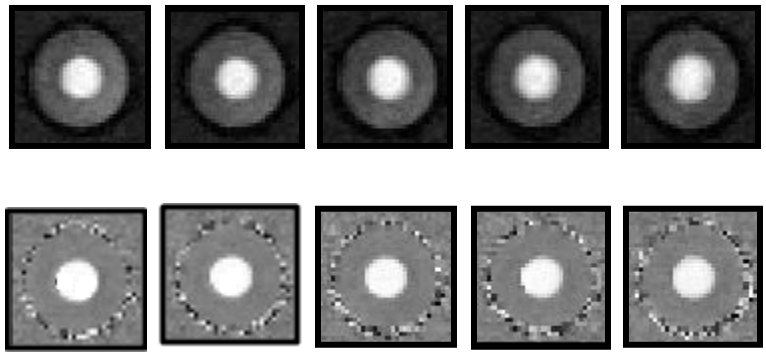

(a) **(b)** **(c)** **(d)** **(e)**

Figure 6.3: Set of magnitude images (top) and phase images (bottom) from the 75% orifice model; Slice location: at the orifice, Flow Rate = 5.5 L/min, Orifice Re = 11654; Spatial Resolution: 0.9x0.9 mm^2; TE: (a) 2.65, (b) 3.5, (c) 5.0, (d) 7.5 and (e) 10.0 msec.

Figure 6.4 shows that, the signal in the magnitude images improved with a decrease in TE. This is the result of the turbulent velocity fluctuations causing voxel dephasing and thus inducing errors in flow measurements

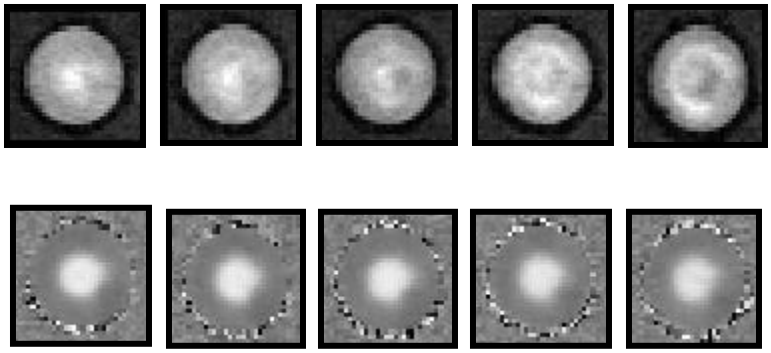

(a) **(b)** **(c)** **(d)** **(e)**

Figure 6.4: Set of magnitude images (top) and phase images (bottom) from the 75% orifice model; Slice location: 1.0 cm downstream from the orifice, Flow Rate = 5.5 L/min, Upstream Re = 5827; Spatial Resolution: 0.9x0.9 mm^2; TE: (a) 2.65, (b) 3.5, (c) 5.0, (d) 7.5 and (e) 10.0 msec.

Figures 6.5 and 6.6 show that the signal loss in the magnitude images and the noise in the phase images improved as the TE decreased. The flow through the model was highly turbulent with Re = 22248 at the orifice and Re = 11124 downstream from the orifice. As a result with an increase in TE, the protons have more time to move randomly in all directions and thus leading to intra voxel dephasing effects.

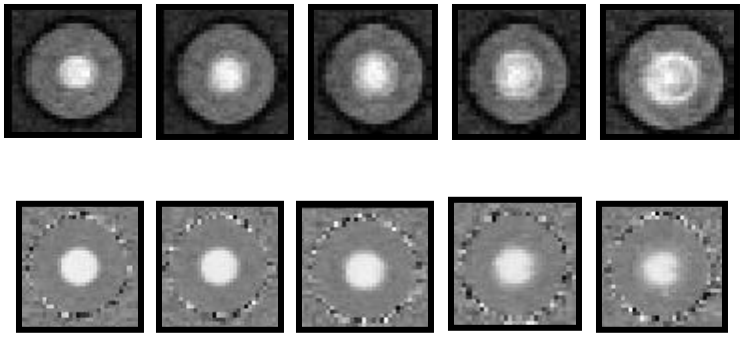

(a) (b) (c) (d) (e)

Figure 6.5: Set of magnitude images (top) and phase images (bottom) from the 75% orifice model; Slice location: at the orifice, Flow Rate = 10.5 L/min, Orifice Re = 22248; Spatial Resolution: 0.9x0.9 mm^2; TE: (a) 2.65, (b) 3.5, (c) 5.0, (d) 7.5 and (e) 10.0 msec.

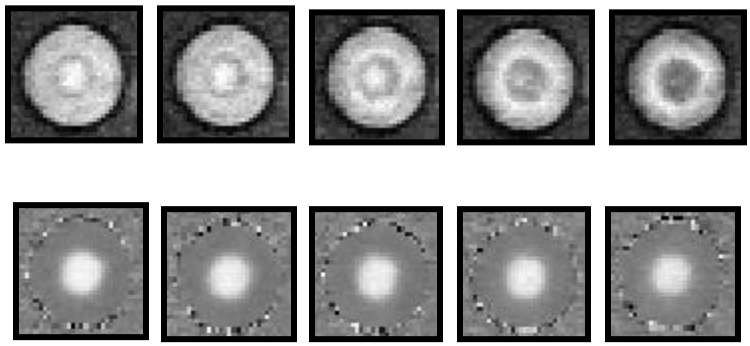

(a) (b) (c) (d) (e)

Figure 6.6: Set of magnitude images (top) and phase images (bottom) from the 75% orifice model; Slice location: 1.0 cm downstream from the orifice, Flow Rate = 10.5 L/min, Upstream Re = 11124; Spatial Resolution: 0.9x0.9 mm^2; TE: (a) 2.65, (b) 3.5, (c) 5.0, (d) 7.5 and (e) 10.0 msec.

Overall, although the flow was turbulent, not much signal loss was observed in the case of the 75 % orifice model. The signal loss in the magnitude images increased with an increase in TE.

In the 94% orifice model, the measured flow rates upstream of the orifice were in close agreement with the true flow rates for all TEs used.

Figures 6.7 – 6.10 show that the signal loss in the magnitude images and the noise in the phase images improved with a decrease in TE. Slight signal loss was observed at 1.0 cm downstream from the orifice and TE = 7.5 msec. Shorter TEs (2.65 and 3.5 msec) measured better at 5.5 L/min and the signal loss had an effect on the flow measurements leading to underestimation of the Flow rates at all TEs and slice locations. As the measurement location moved further downstream from the orifice, the underestimation increased as the turbulent jet caused more multi-directional flow patterns. This turbulence effect was more significant at 8.5 L/min.

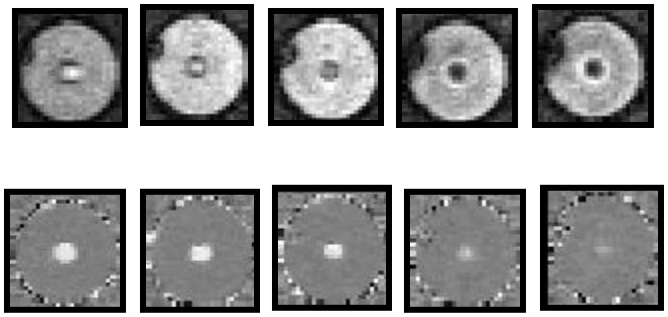

(a) (b) (c) (d) (e)

Figure 6.7: Set of magnitude images (top) and phase images (bottom) from the 94% orifice model; Slice location: At the orifice; Flow Rate = 5.5 L/min, Orifice Re = 23308; Spatial Resolution: 0.9x0.9 mm^2; TE: (a) 2.65, (b) 3.5, (c) 5.0, (d) 7.5 and (e) 10.0 msec.

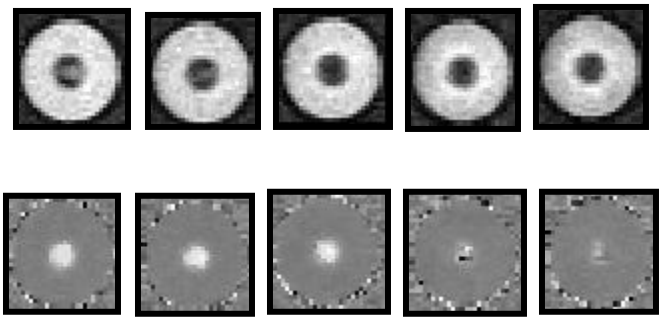

(a) (b) (c) (d) (e)

Figure 6.8: Set of magnitude images (top) and phase images (bottom) from the 94% orifice model; Slice location: 1.0 cm downstream from the orifice; Flow Rate = 5.5 L/min, Upstream Re = 5827; Spatial Resolution: 0.9x0.9 mm^2; TE: (a) 2.65, (b) 3.5, (c) 5.0, (d) 7.5 and (e) 10.0 msec.

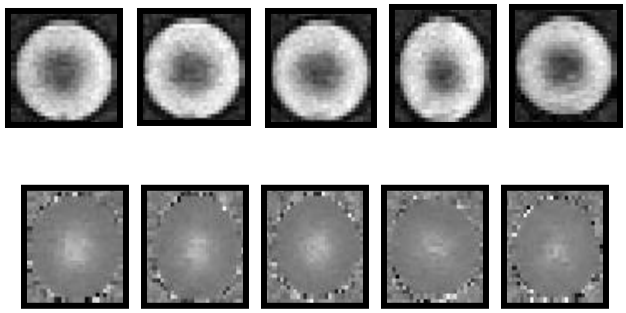

(a) (b) (c) (d) (e)

Figure 6.9: Set of magnitude images (top) and phase images (bottom) from the 94% orifice model; Slice location: 3.0 cm downstream from the orifice; Flow Rate = 5.5 L/min, Upstream Re = 5827; Spatial Resolution: 0.9x0.9 mm^2; TE: (a) 2.65, (b) 3.5, (c) 5.0, (d) 7.5 and (e) 10.0 msec.

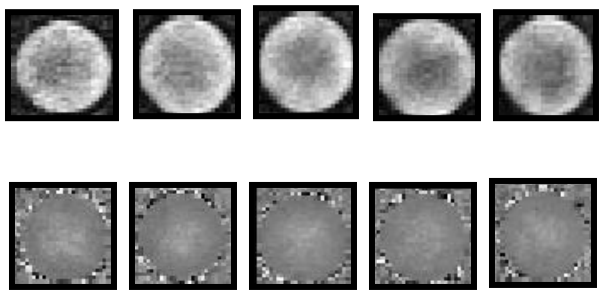

(a) (b) (c) (d) (e)

Figure 6.10: Set of magnitude images (top) and phase images (bottom) from the 94% orifice model; Slice location: 5.0 cm downstream from the orifice; Flow Rate = 5.5 L/min, Upstream Re = 5827; Spatial Resolution: 0.9x0.9 mm^2; TE: (a) 2.65, (b) 3.5, (c) 5.0, (d) 7.5 and (e) 10.0 msec.

Figure 6.11 shows that the signal loss in magnitude images and noise in phase images improved with a decrease in TE. The flow is highly turbulent with Re = 44496.

As the TE increased, the protons have more time to move randomly in all directions and thus causing voxel dephasing and errors in flow measurements.

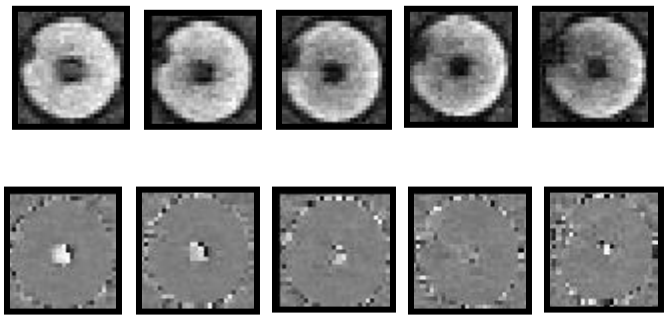

(a) (b) (c) (d) (e)

Figure 6.11: Set of magnitude images (top) and phase images (bottom) from the 94% orifice model; Slice location: At the orifice; Flow Rate = 8.5 L/min, Orifice Re = 44496; Spatial Resolution: 0.9x0.9 mm^2; TE: (a) 2.65, (b) 3.5, (c) 5.0, (d) 7.5 and (e) 10.0 msec.

Figures 6.12 – 6.14 show that TE did not have much effect on the signal loss in the magnitude images. The flow through the model is turbulent with Re = 11124. In the case of phase images, the noise improved with a decrease in TE, lower TEs (2.65 and 3.5 msec) measured better when compared to higher TEs because of lesser dephasing effects. Though there is signal loss observed at 1.0 cm downstream from the orifice, flow rates were overestimated at TE = 7.5 msec and TE = 10.0 msec. Signal loss was observed at TE = 3.5 msec at all the slice locations downstream from the orifice.

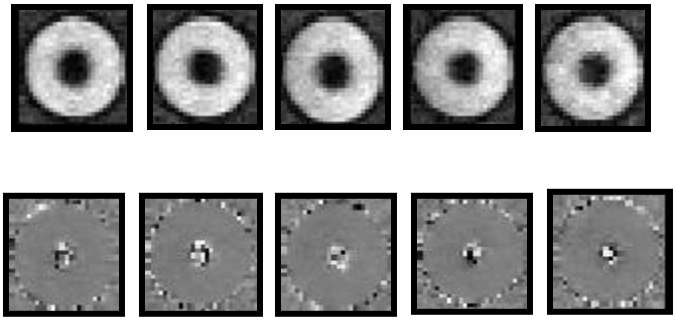

(a) (b) (c) (d) (e)

Figure 6.12: Set of magnitude images (top) and phase images (bottom) from the 94% orifice model; Slice location: 1.0 cm downstream from the orifice; Flow Rate = 8.5 L/min, Upstream Re = 11124; Spatial Resolution: 0.9x0.9 mm^2; TE: (a) 2.65, (b) 3.5, (c) 5.0, (d) 7.5 and (e) 10.0 msec.

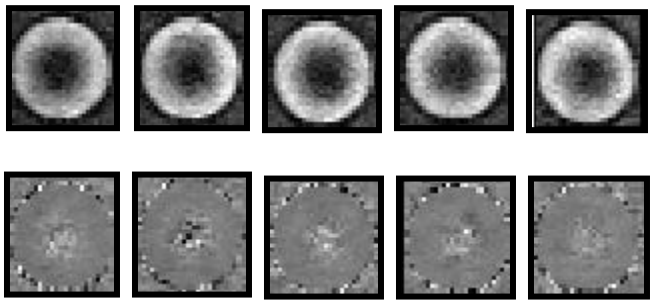

(a) (b) (c) (d) (e)

Figure 6.13: Set of magnitude (top) and phase images (bottom) from the 94% orifice model; Slice location: 3.0 cm downstream from the orifice; Flow Rate = 8.5 L/min, Re = 11124; Spatial Resolution: 0.9x0.9 mm^2; TE: (a) 2.65, (b) 3.5, (c) 5.0, (d) 7.5 and (e) 10.0 msec.

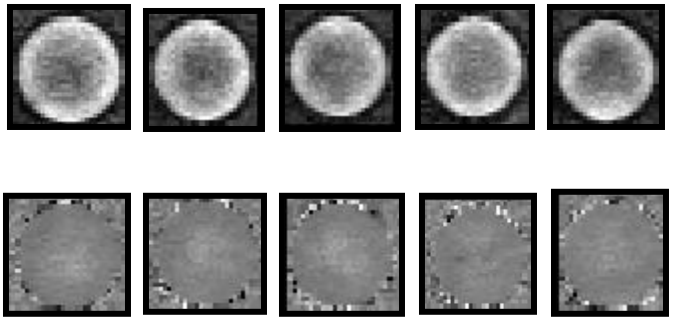

(a) (b) (c) (d) (e)

Figure 6.14: Set of magnitude (top) and phase images (bottom) from the 94% orifice model; Slice location: 5.0 cm downstream from the orifice; Flow Rate = 8.5 L/min, Re = 11124; Spatial Resolution: 0.9x0.9 mm^2; TE: (a) 2.65, (b) 3.5, (c) 5.0, (d) 7.5 and (e) 10.0 msec.

The Effects of In-plane Resolution

In the case of 75% orifice model, resolution had a minimal effect on the flow measurements. The effect can be seen at flow rates of 5.5 L/min and 10.5 L/min, at the orifice and at TE = 3.5 msec. At 5.5 L/min the measured flow rates exhibited errors of 18.2%, 30.4%, and 40.7% at 0.9 x 0.9, 1.5 x 1.5 and 2.0 x 2.0 mm^2 in-plane resolutions, respectively. Thus agreeing with the hypothesis of the higher the resolution the better the accuracy in the flow rate measurements. On the other hand, at 10.5 L/min, the measured flow rates followed a different trend with the highest resolution exhibiting the maximum error and the error decreased as the resolution decreased. This is an exception.

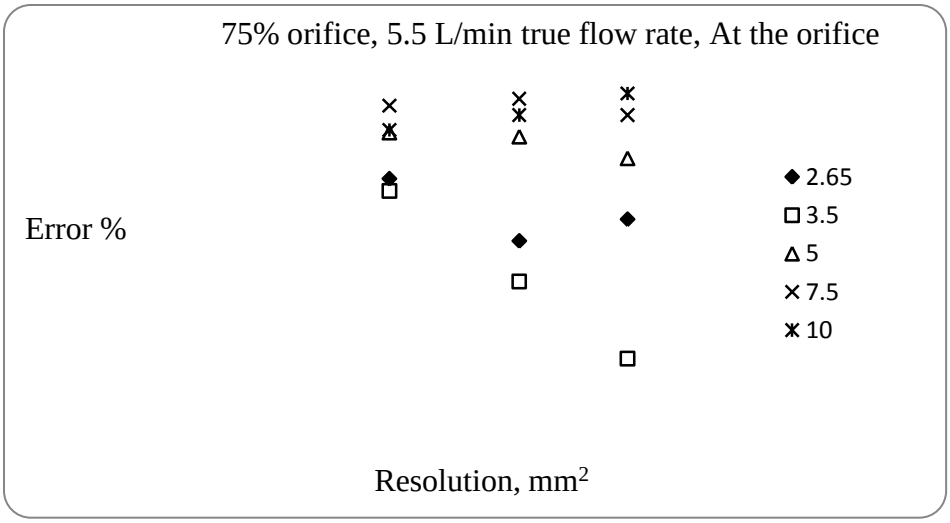

Figure 6.15: Percentage error in flow rate measurement as a function of in-plane resolution for the 75% orifice model; Slice position: at the orifice; for a true flow rate of 5.5 L/min

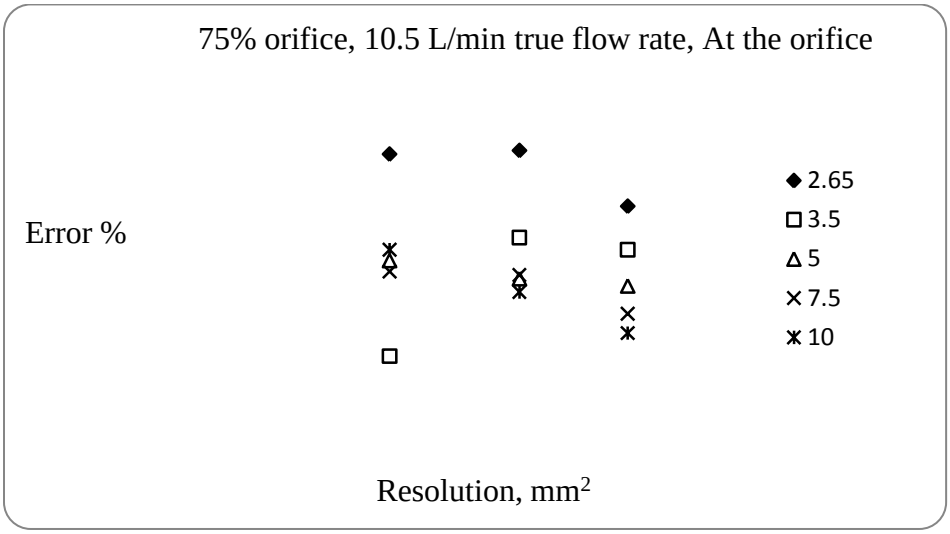

Figure 6.16: Percentage error in flow rate measurement as a function of in-plane resolution for the 75% orifice model; Slice position: at the orifice; for a true flow rate of 10.5 L/min

In the case of 94% orifice model, resolution played a significant role in the flow measurements. At 5.5 L/min, the in-plane resolution did not play a significant role in affecting the flow rate measurements with a few exceptions. At 1.0 cm downstream from the orifice the error in the measured flow rates increased with a decrease in the resolution, thus the results were in agreement with our hypothesis. But at 5.0 cm downstream from the orifice and TE = 7.5 msec, the measured flow rates were more accurate at 1.5 x 1.5 mm^2 resolution when compared to the other 2 resolutions (0.9 x 0.9 mm^2 and 2.0 x 2.0 mm^2).

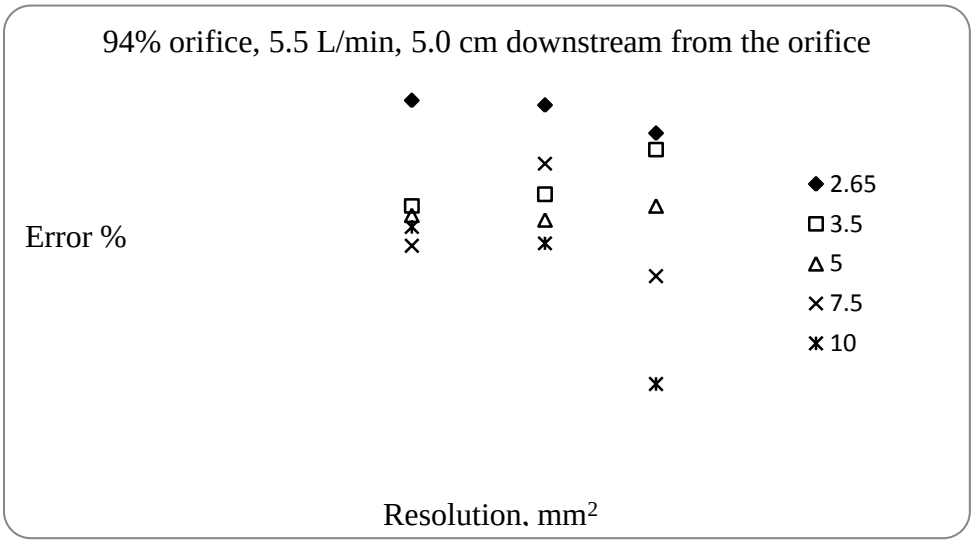

Figure 6.17: Percentage error in flow rate measurement as a function of in-plane resolution for the 94% orifice model; Slice position: 5.0 cm downstream; for a true flow rate of 5.5 L/min

At 8.5 L/min, the in-plane resolution had a significant effect on the flow measurements at all the slice locations except for the 6.0 cm upstream. At the orifice, the error in the flow measurements increased with a decrease in the resolution, thus proving that the higher the resolution the accurate the measurements except at TE = 3.5 and 7.5 msec, where the behavior is inconsistent which might be due to the signal loss effect. At 1.0 cm downstream from the orifice, though signal loss was observed, the some of the measured flow rates were overestimated, thus the signal loss did not show an effect on the measurements. Surprisingly, at 3.0 and 5.0 cm downstream from the orifice, the lower resolution (2.0 x 2.0 mm^2) resulted in accurate flow measurements compared to the highest resolution (0.9 x0.9 mm^2). It is clear that the high turbulence and signal loss had an effect on the measurements at 8.5 L/min and at slice locations downstream of the stenosis.

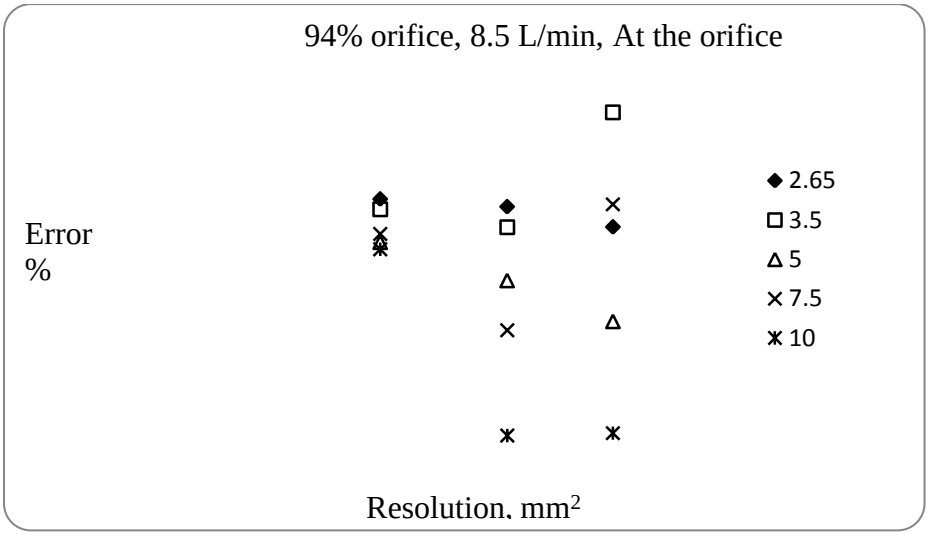

Figure 6.18: Percentage error in flow rate measurement as a function of in-plane resolution for the 94% orifice model; Slice position: at the orifice; for a true flow rate of 8.5 L/min

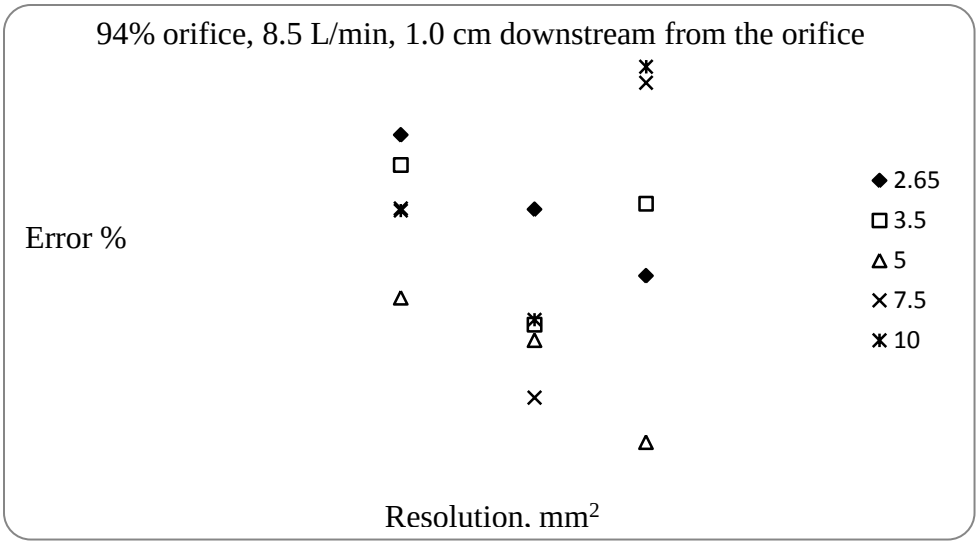

Figure 6.19: Percentage error in flow rate measurement as a function of in-plane resolution for the 94% orifice model; Slice position: 1.0 cm downstream; for a true flow rate of 8.5 L/min

Effect of Imaging Parameters and Geometry on MRPVM Flow Measurements

One of the hypotheses of the study was that lower TEs provide more accurate flow measurements. In order to avoid signal loss, appropriate Venc values were chosen in all flow rate cases. In the study, major signal loss was observed in the 94% orifice model and for a true flow rate of 8.5 L/min. A slight signal loss was observed for the 5.5 L/min true flow rate case as well. This has affected the flow measurements at those particular flow rates. Approximately, for the same Re = 23000, no signal loss was observed in case of 75% orifice model, but signal loss was observed in case of 94% orifice model. Also, the

results indicate that lower TEs (2.65 msec and 3.5 msec) produced more accurate flow rate measurements compared to higher TEs. In general, the results of this study are in agreement with previous similar studies [62]**.** Measurements were slightly underestimated at 1.2 L/min and at 6.0 cm upstream from the orifice. This possibly is due to experimental errors.

In-plane spatial resolution had a significant effect only in the 94% orifice model and at 5.5 L/min and 8.5 L/min flow rates. The higher resolution (0.9 x 0.9 mm^2) measured accurately when compared to the lower resolutions in most of the cases. The effect of in-plane resolution is negligible in other cases.

The effect of geometry can also be clearly seen. For the same Reynolds number, the signal was observed in case of 94 % orifice model but not in 75 % orifice model. Also, the effect of turbulence can be clearly seen from the signal loss in the flow compensated magnitude images and noise in the phase images.

As the Reynolds number increased, the effect of TE on the flow rate measurements increased, as a result we can see more scattering of the results at higher Reynolds numbers (i.e. at 8.5 L/min).

CHAPTER VII

LIMITATIONS AND FUTURE RECOMMENDATIONS

There were several limitations in the study conducted. First and foremost, water was used as the working fluid, whose viscosity differs from that of the blood. Secondly, the orifice models used have stationary walls whereas the tissue walls contract and expand during the blood flow in the human body.

All the experiments were carried out under steady flow conditions whereas pulsatile flow conditions prevail in-vivo. The results need to be validated. Finally only two degrees of area reduction orifice model were tested. Another limitation was the experiments were carried out only once, no repetitions were performed.

Experiments need to be conducted to compare the steady flow results with the pulsatile flow results. Also, in our experiments studies were conducted only on two orifice models, further study on more degrees of area reduction orifice models would be useful in evaluating the accuracy of MRPVM in measuring Flow rates.

Comparing these results with CFD simulated results might provide valuable information for clinical valuation. Also studying more number of TEs in a short range at lower TE values might provide us information in choosing better TEs in clinical studies.

CHAPTER VIII

CONCLUSIONS

The main of this study was to investigate the effect of vessel geometry and imaging parameters (echo times and in-plane spatial resolution) on the quality of acquired MRPVM data in turbulent flow conditions. Two glass models with different percentage of area reductions were used in the experiments. The experiments were carried out using five different TE values: 2.65, 3.5, 5.0, 7.5 and 10.0 msec and three different in plane spatial resolutions: 0.9 x 0.9 mm^2, 1.5 x1.5 mm^2, 2.0 x 2.0 mm^2 and at four different Flow rates: 1.2, 5.5, 8.5 and 10.5 L/min. Axial MRPVM acquisitions were acquired at five different slice positions: 6 cm upstream from the orifice, at the orifice, 1 cm downstream from the orifice, 3 cm downstream from the orifice and 5 cm downstream from the orifice. Flow rates were obtained from the acquired phase images and then compared with the true Flow rates measured via rotameter to see the accuracy.

The results prove that MRPVM is very accurate under laminar flow conditions but leads to underestimation of Flow rates under turbulent flow conditions. Turbulence and signal loss were the main reasons for the underestimation of the Flow rates. This underestimation increased with an increase in the flow rate and with an increase in the percentage of area reduction in the orifice. Resolution had a negligible effect on the measurements but when it comes to echo times, lower TEs measured accurately compared to higher TEs.

From our experiments we conclude that MRPVM can be used for flow measurements under laminar flow conditions, but more in vivo studies and CFD simulations needs to be carried out to see its efficiency under turbulent flow conditions.

REFERENCES

1. www.americanheart.org
2. E.J.Armstrong, J.Bischoff. Heart valve development: endothelial cell signaling and differentiation. Circ Res. (2004) 459-70.
3. Richard E. Klabunde, PhD. Cardiovascular physiology concepts. Lippincott Williams & Wilkins, (2005).
4. P.R.Moran, A flow velocity zeumatographic interlace for NMR imaging in human, Magnetic Resonance Imaging (1982) 197-203.
5. Y Suguru, N Masanori, W Shigeo., I Haruo, T Hiroyasu, Y Takami. Quantitative measurement on the on the human ascending aortic flow using 2D cine phase-contrast MRI. JSME International Journal (2005) 459-467.
6. A.F.Bolger, N.L.Eigler, G.Maurer. Quantifying valvular regurgitation: limitations and inherent assumptions of Doppler techniques. Circulation (1988) 1316-1318.
7. I.Simpson, D.Sahn. Quantification of valvular regurgitation by Doppler echocardiography. Circulation (1991) 188-192.
8. B.A.Carabello, F.A.Crawford. Valvular heart disease. N Engl J Med (1997) 1362-1367.
9. P.J.Currie, J.B.Seward, G.S.Reeder, R.E.Vlietstra, D.R.Bresnahan, J.F.Bresnahan, H.C.Smith, D.J.Hagler, A.J.Tajik. Continuous wave Doppler echocardiographic assessment of the severity of calcific aortic stenosis: a simultaneous Doppler-catheter correlative study in 100 adult patients. Circulation (1985) 1162-1169.
10. J.A.Kisslo, D.B.Adams. Doppler Evaluation Of Valvular Stenosis. RDCS.

11. C.M.Otto. The Practice of Clinical Echocardiography, 895.
12. M.Cheitlin. Valvular heart disease: management and intervention. Circulation (1991) 259-264.
13. K.K.Stout, C.M.Otto. Quantification of Valvular Aortic Stenosis. Division of Cardiology, Department of Medicine, University of Washington, Seattle, Washington. (2003).
14. S.Globits, C.B.Higgins. Assessment of valvular heart disease by magnetic resonance imaging. Am Heart. J (1995) 369-381.
15. A.J.Duerinckx, C.B.Higgins. Valvular heart disease. Radiol Clin North Am. (1994) 613-630.
16. C.B.Higgins, H.Sakuma. Heart disease: functional evaluation with MR imaging. Radiology (1996) 307-315.
17. G.H.Mostbeck, G.R.Caputo, C.B.Higgins. MR measurements of blood flow in the cardiovascular system. AJR Am J Roentgenol (1992) 453-461.
18. S.A.Rebergen, E.E.Van der Wall EE, J.Doornbos, A.De Roos. Magnetic resonance measurements of velocity and flow: technique, validation and cardiovascular applications. Am Heart J (1993) 1439-1456.
19. D.Bluestein, S.Einav. The effect of varying degrees of stenosis on the characteristics of turbulent pulsatile flow through heart valves. Department of Mechanical Engineering, Florida International University, Miami, USA. J Biomech. (1995) 915-24.

20. S.D. Caruthers, S.J. Lin, M.P. Watkins, T. Williams, P.A. Brown, K.A. Lehr, G.M. Lanza and S.A. Wickline. Using Velocity-Encoded MRI and The Velocity-Time Integral Approach To Analyze the Aortic Valve in Patients with Aortic Stenosis: A Reproducibility Study 'Cardiovascular MR Laboratories, Washington University, St. Louis, MO, USA. Philips Medical Systems, Netherlands.
21. K.R.O'Brien, B.R.Cowan, M.Jain., R.A.H. Stewart, A.J.Kerr., A.A.Young. MRI phase contrast velocity and flow errors in turbulent stenotic jets. JMRI (2008) 210-218.
22. Perry Sprawls, Jr. Physical Principles Of Medical Imaging. An Aspen Publication, (1987).
23. R.H Hashemi., W.G Bradley., C.J Lisanti. MRI: The Basics. 2nd Ed., Lippincott Williams & Wilkins, Philadelphia, (2003).
24. H.G.Boegren, M.H.Buonocore. Blood flow measurements in the aorta and major arteries with MR velocity mapping. JMRI (1994) 119-30.
25. L.R.Pelc, N.J.Pelc, S.C.Rayhill, L.J.Castro, G.H.Glover, R.J.Herfkens . Arterial and venous blood flow: Noninvasive quantitation with MR imaging Radiology (1992) 809-12.
26. G.P.Chatzimavroudis, P.G.Walker, J.N.Oshinski, R.H.Franch, R.I.Pettigrew, A.P.Yoganathan. Slice location dependence of aortic regurgitation measurements with MR phase velocity mapping. Magnetic Resonance Med (1997) 545-51.
27. N.J.Pelc, M.A.Bernstein, A.Shimakawa, G.H.Glover. Encoding strategies for three direction phase-contrast MR imaging of flow. JMRI (1991) 405-413.

28. N.J.Pelc, R.J.Herfkens, A.Shimakawa, D.R.Enzmann. Phase contrast cine magnetic resonance imaging. Magn Reson Q. (1991) 229-254.
29. H.Zhang., S.S.Halliburton., J.R.Moore., O.P.Simeonetti., P.R.Schvartzman., R.D.White., G.P.Chatzimavroudis. Accurate quantification of steady and pulsatile flow with segmented k-space magnetic resonance velocimetry. Experiments in Fluids (2002) 458-463.
30. V.S.lee, M.Helmers. Cardiovascular MRI: Physical principles to practical protocols. Lippincott Williams & Wilkins, New York, (2005).
31. M.Frank. White.Fluid Mechanics. 5th edition, New York, (2003).
32. M.G.Friedrich, J.Schulz-Menger, T.Poetsch, B.Pilz, F.Uhlich, R.Dietz. Quantification of valvular aortic stenosis by magnetic resonance imaging. Am Heart J (2002) 329-334.
33. S.E.Maiser, D.Meier, P.Boesiger, U.T.Moser, A.Vieli. Human abdominal aorta: comparative measurements of blood flow with MR imaging and multigated Doppler US. Radiology (1989) 487-492.
34. F.Bloch, W.W.Hansen and M.Packard. Nuclear induction. Phys. Rev. 69 (1946), 127.
35. E.Purcell, H.Torrey and R.Pound. Resonance absorption by nuclear magnetic moments in a solid. Phys. Rev. 69 (1946) 37.
36. F.Stahlberg, A.Ericsson, B.Nordell, C.Thomsen, O.Henriksen, B.R.R.Persson. MR Imaging, Flow and Motion, Review article, (1992).

37. P.Van Dijk. Direct cardiac NMR imaging of the heart wall and blood flow velocity. J Computer Assisted Tomography (1983) 429-436.
38. T.Matsuda, K.Shimizu, T.Sakurai, A. Fujita, S. Okamura, S. Hashimoto and H. Ohara. Measurement of aortic blood flow with MR imaging: comparative study with Doppler US. Radiology (1987) 857-861.
39. M.J.Podolak, L.W.Hedlund, A.J.Evans, R.J.Herfkens. Evaluation of flow through simulated vascular stenosis with gradient echo magnetic resonance imaging. Invest Radiol (1989) 184-189.
40. P.E.Valk, J.D.Hale, L.E.Crooks, L.Kaufman, M.S.Roos, D.A.Ortendahl, C.B.Higgins. MRI of blood flow: correlation of image appearance with spin-echo phase shift and signal intensity. AJR Am J Roentgenol (1986) 931-939.
41. S.E.Rittgers, D.Y.Fei, K.A.Kraft, P.P.Fatouros. Velocity profiles in stenosed models using magnetic resonance imaging. Monogr Atheroscler (1990) 43-53
42. C.A.Hamilton, P.R.Moran, P.Santago, S.A.Rajala. Effects of intravoxel velocity distributions on the accuracy of the phase-mapping method in phase contrast MR angiography. JMRI (1994) 752-755.
43. M.A.Bernstein, K.F.King, X.J.Zhou. Handbook of MRI pulse sequences. Amsterdam: Elsevier Academic Press; (2004).
44. J.H.Gao, J.O.Gore. Turbulent flow effects on NMR imaging: measurement of turbulent intensity. Med Phys (1991) 1045-1051.

45. R.P.Spielmann, O.Schneider, F.Thiele, M.Heller, E.Bucheler. Appearance of poststenostic jets in MRI: dependence on flow velocity and on imaging parameters. Magnetic Resonance Imaging (1991) 67-72.
46. A.J.Evans, L.W.Hedlund, R.J.Herfkensl. J.A.Utz, E.K. Fram and R.A.Blinder. Evaluation of steady and pulsatile flow with dynamic MRI using limited flip angles and gradient refocused echoes. Magnetics Resonance Imaging (1987) 475-482.
47. W.G.Bradley, V.Waluch. Blood flow: magnetic resonance imaging. Radiology (1985) 443-450.
48. A.J.Evans, R.A.Blinder, R.J.Herfkens, C.E.Spritzer, D.O.Kuethe, E.K.Fram, L.W.Hedlund. Effects of turbulence on signal intensity in gradient echo images. Invest Radiol (1988) 512-518.
49. P.D.Gatehouse, D.N.Firmin, S.Collins, D.B.Longmore. Real time blood flow imaging by spiral scan phase velocity mapping. MRM (1994) 504-512.
50. W.G.Bradley, V.Waluch, K.S.Lai, E.J.Fernandez, C.Spalter. The appearance of rapidly flowing blood on magnetic resonance images. AJR (1984) 1167-1174.
51. B.Allgayer, D.Liepsch, P.Lukas, M.Deimling, N.Rupp, M.Reiser. The effects of fluid mechanical factors on MR imaging in the arterial model. Eur J Radiol (1985) 231-235.
52. J.P.Grant, C.Back. NMR rheotomography: feasibility and clinical potential. Med Phys (1982) 188-193.

53. C.R.George, G.Jacobs, W.J.MacIntyre, R.J.Lorig, R.T.Go, Y.Nose, T.F.Meaney. Magnetics resonance signal intensity patterns obtained from continuous and pulsatile flow models. Radiology (1984) 421-428.
54. G.K.Von Schulthess, C.B.Higgins. Blood flow imaging with MR: spin-phase phenomena. Radiology (1985) 687-695.
55. F.Stalhberg, L.Sondergaard, C.Thomsen, O.Henriksen. Qunatification of complex flow using MR phase imaging- a study of parameters influencing the phase/velocity relation. Magnetic Resonance Imaging (1992) 13-23.
56. L.Sondergaard, F.Stahlberg, C.Thomsen, A.Stensgaard, K.Lindvig, O.Henriksen . Accuracy and precision of MR velocity mapping in measurement of stenotic cross-sectional area, flow rate and pressure gradient. JMRI (1993) 433-437.
57. L.C.Man, M.P.John, G.Dwight, Nishimura, A.Macovski. Nonsubtractive spiral phase contrast velocity imaging. Magn Reson Med (1999) 704-713.
58. K.W.Moser, E.C.Kutter, J.G.Georgiadis, R.O.Buckius, H.D.Morris, J.R.Torczynski. Velocity measurements of a flow through a step stenosis using magnetic resonance imaging. Experiments in fluids (2000) 438-447.
59. H.Zhang, S.S.Halliburton, R.D.White, G.P.Chatzimavroudis. Fast measurements of flow through mitral regurgitant orifices with magnetic resonance phase velocity mapping. Annals of Biomedical Engineering (2004) 1618-1627.
60. J.N.Oshinski, D.N.Ku, R.I.Pettigrew. Turbulent fluctuation velocity: The most significant determinant of signal loss in stenotic vessels. Magn Reson med (1995) 193-199.

61. A.J.Sederman, M.D.Mantle, C.Buckley, L.F.Gladden. MRI technique for measurement of velocity vectors, acceleration and autocorrelation functions in turbulent flow. JMR (2004) 182-189.
62. K.R.O'Brien, B.R.Cowan and A.A.Young. Auckland MRI Research Group, University of Auckland, New Zealand.
63. P.J.Kilner, D.N.Firmin, R.S.O.Rees, J.Martinez, D.J.Pennell, R.H.Mohiaddin, S.R.Underwood, D.B.Longmore. Magnetic resonance jet velocity mapping for assessment of valve and great vessel stenosis. Radiology (1991) 229-235.
64. J.Fay, N.A.Sonwalker. Fluid Mechanics hypercourse. Cambridge, MA, MIT Press (1996).
65. Arterial anatomy and Hemodynamics. Professional Ultrasound Services, San Francisco, CA (2006).
66. N.S.Lakkadi. Flow measurements in turbulent flow fields with magnetic resonance phase velocity mapping. Thesis book. Cleveland State University. (2009).

APPENDIX

Appendix A

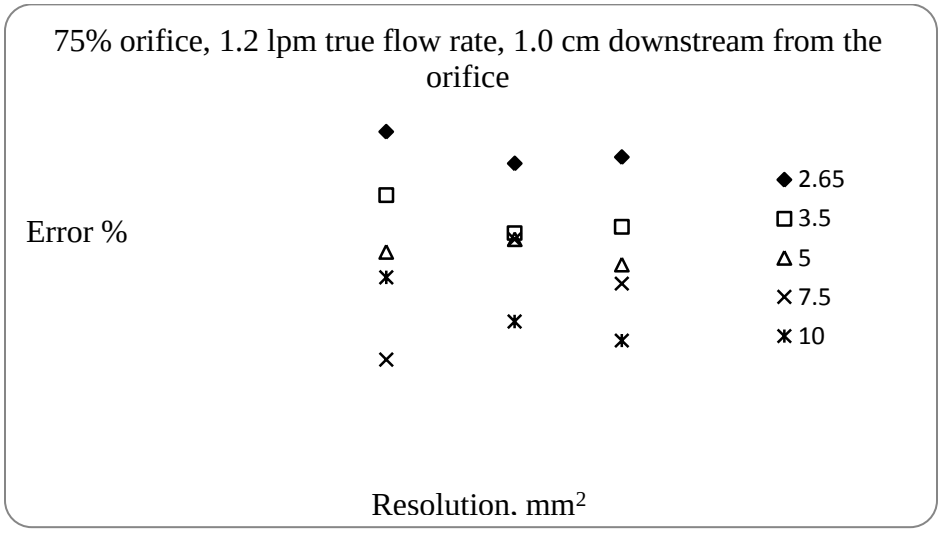

Figure A.1: Percentage error in flow rate measurement as a function of in-plane resolution for the 75% orifice model; Slice position: 1.0 cm downstream; for a true flow rate of 1.2 L/min

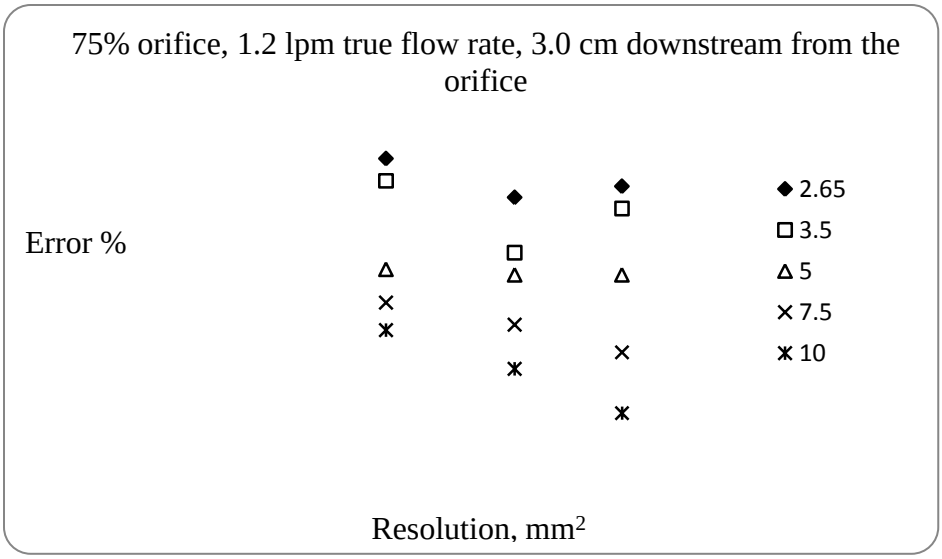

Figure A.2: Percentage error in flow rate measurement as a function of in-plane resolution for the 75% orifice model; Slice position: 3.0 cm downstream; for a true flow rate of 1.2 L/min

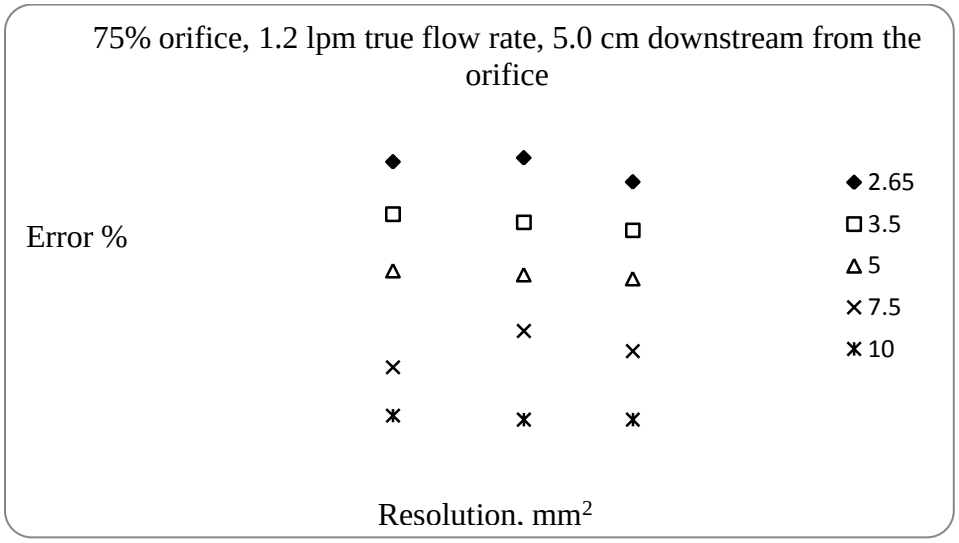

Figure A.3: Percentage error in flow rate measurement as a function of in-plane resolution for the 75% orifice model; Slice position: 5.0 cm downstream; for a true flow rate of 1.2 L/min

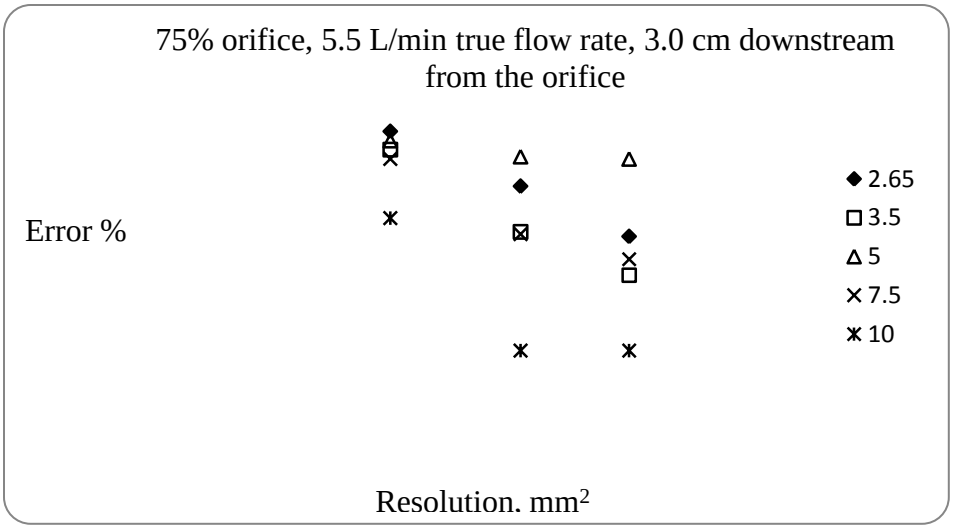

Figure A.4: Percentage error in flow rate measurement as a function of in-plane resolution for the 75% orifice model; Slice position: 3.0 cm downstream; for a true flow rate of 5.5 L/min

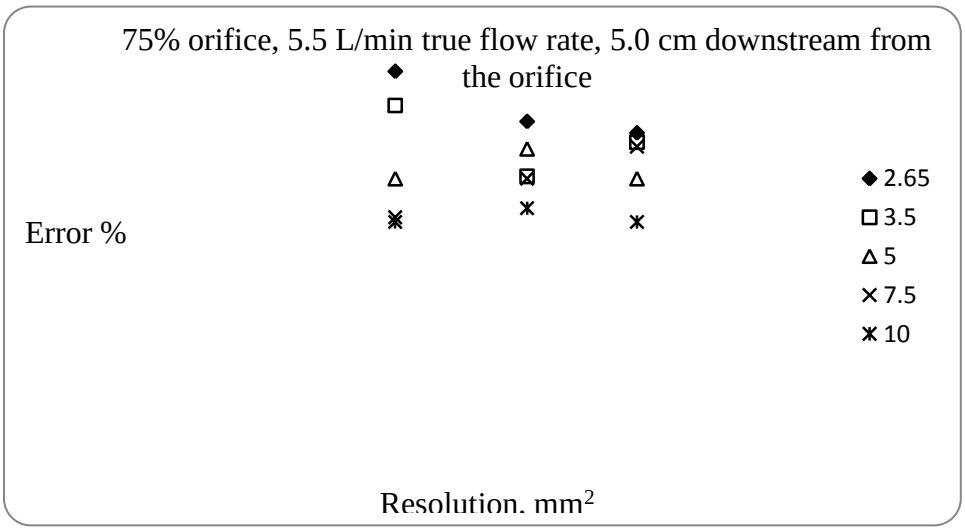

Figure A.5: Percentage error in flow rate measurement as a function of in-plane resolution for the 75% orifice model; Slice position: 5.0 cm downstream; for a true flow rate of 5.5 L/min

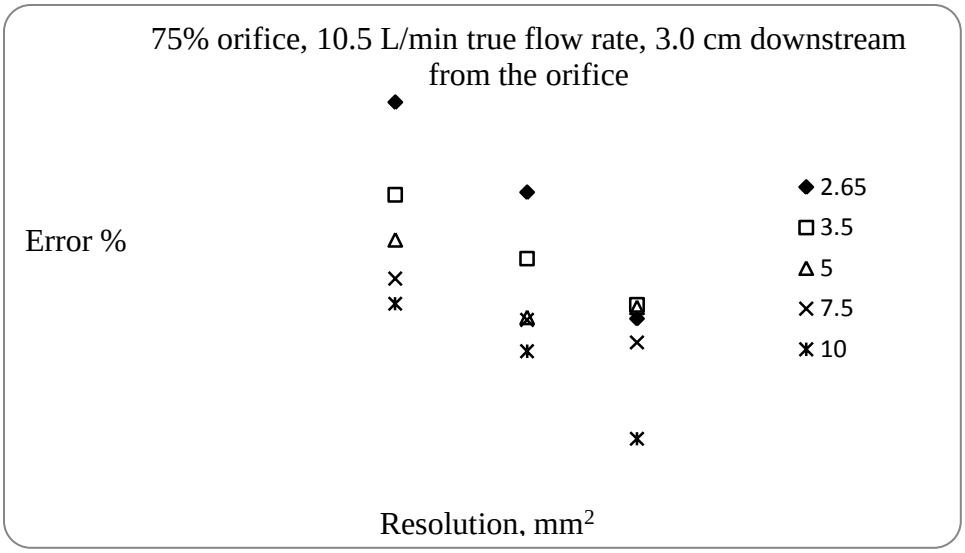

Figure A.6: Percentage error in flow rate measurement as a function of in-plane resolution for the 75% orifice model; Slice position: 3.0 cm downstream; for a true flow rate of 10.5 L/min

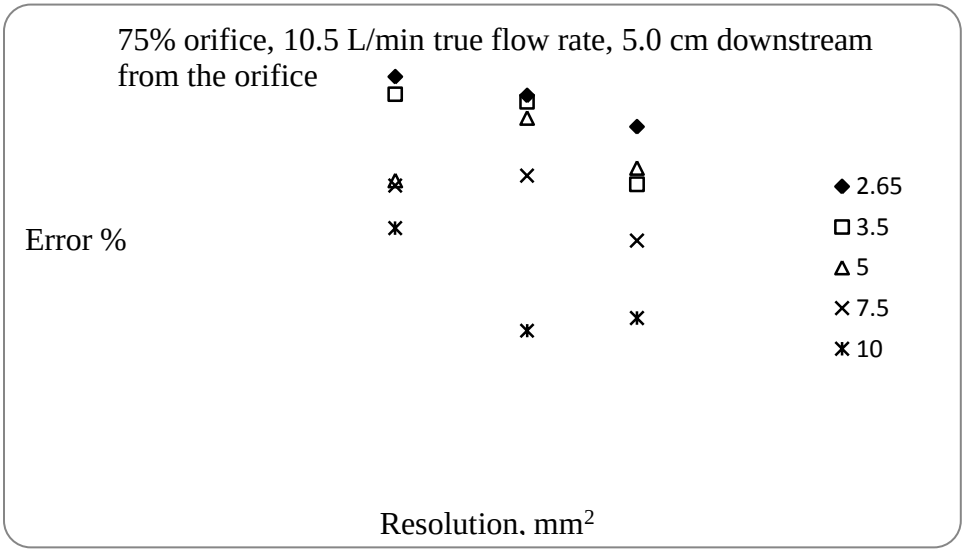

Figure A.7: Percentage error in flow rate measurement as a function of in-plane resolution for the 75% orifice model; Slice position: 5.0 cm downstream; for a true flow rate of 10.5 L/min

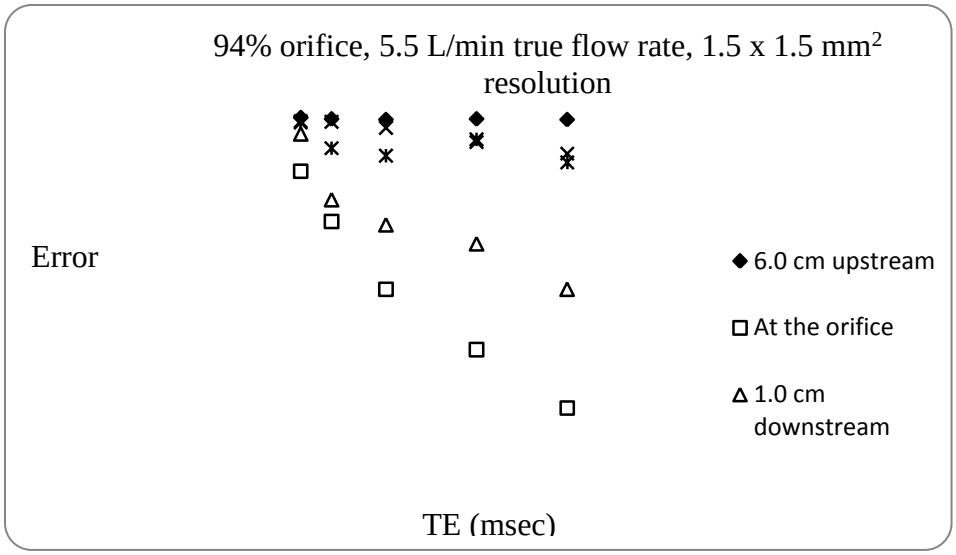

Figure A.8: Percentage error in the flow rate measurement as a function of TE for 94% orifice model at each slice position for a true flow rate of 5.5 L/min; In-plane resolution: 1.5 x 1.5 mm^2

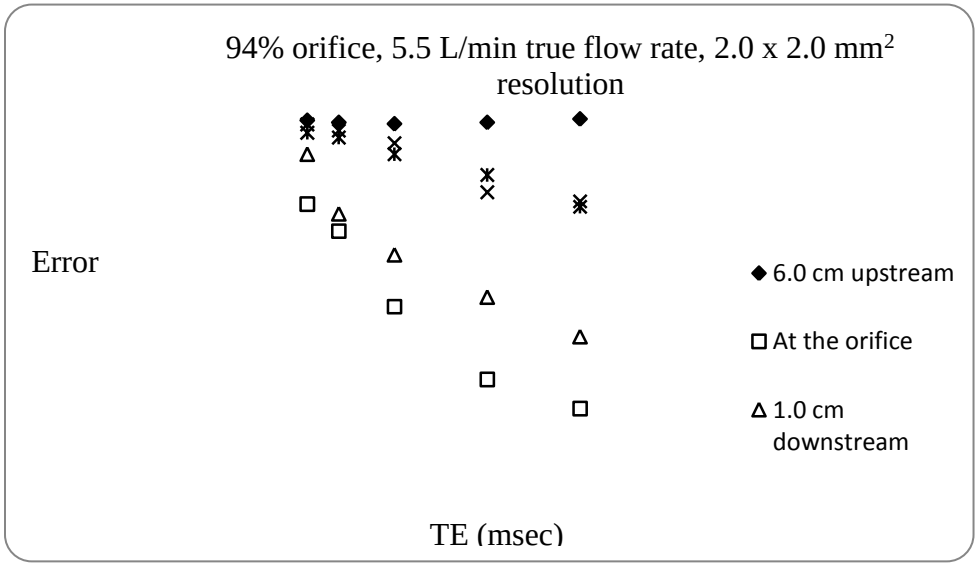

Figure A.9: Percentage error in the flow rate measurement as a function of TE for 94% orifice model at each slice position for a true flow rate of 5.5 L/min; In-plane resolution: 2.0 x 2.0 mm^2

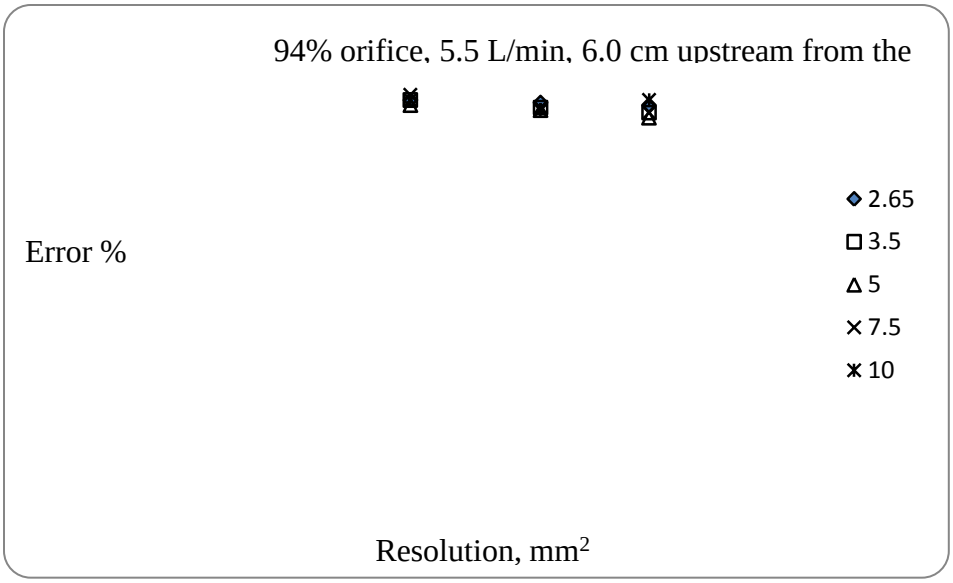

Figure A.10: Percentage error in flow rate measurement as a function of in-plane resolution for the 94% orifice model; Slice position: 6.0 cm upstream; for a true flow rate of 5.5 L/min

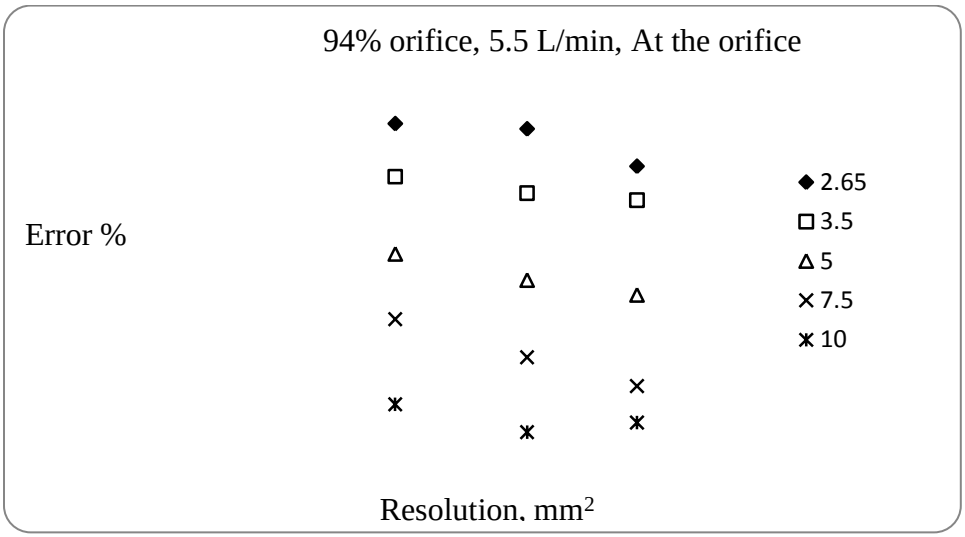

Figure A.11: Percentage error in flow rate measurement as a function of in-plane resolution for the 94% orifice model; Slice position: At the orifice; for a true flow rate of 5.5 L/min

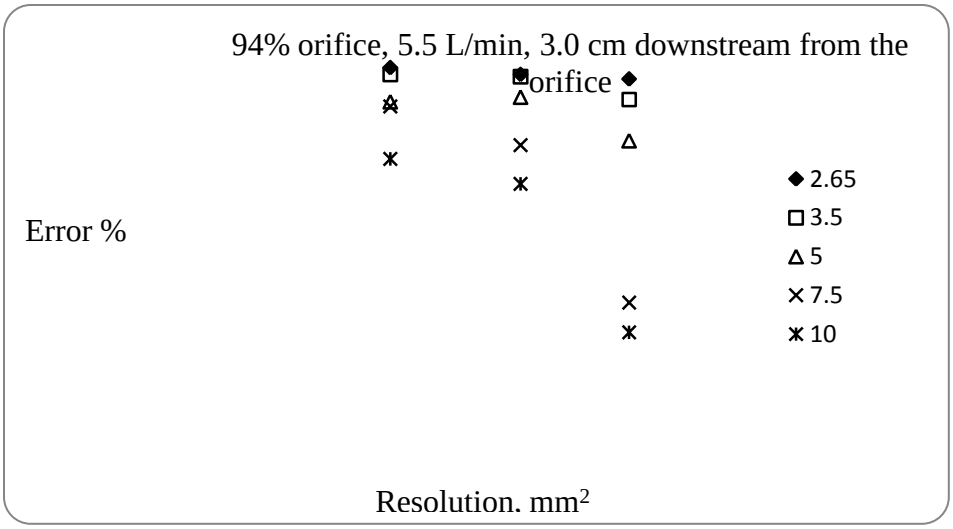

Figure A.12: Percentage error in flow rate measurement as a function of in-plane resolution for the 94% orifice model; Slice position: 3.0 cm downstream; for a true flow rate of 5.5 L/min

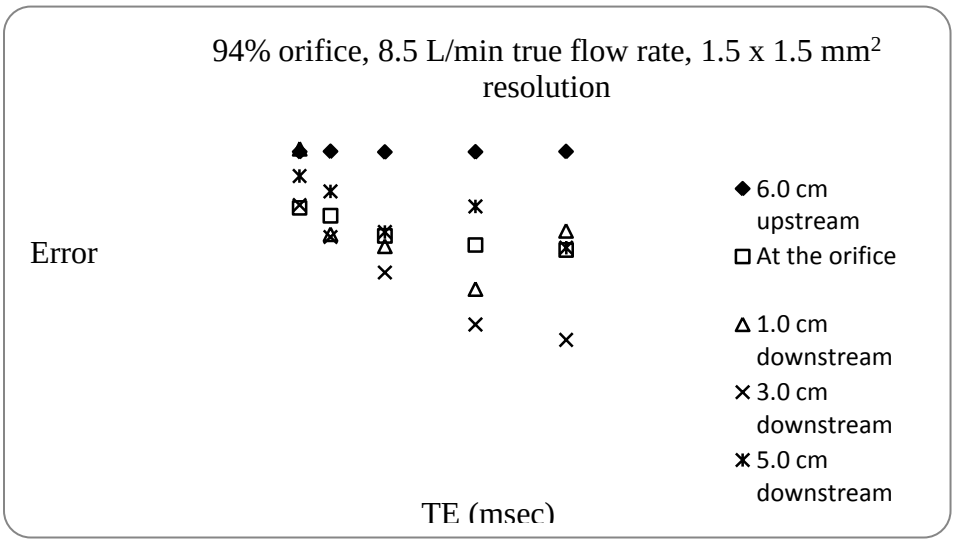

Figure A.13: Percentage error in the flow rate measurement as a function of TE for 94% orifice model at each slice position for a true flow rate of 8.5 L/min; In-plane resolution: 1.5 x 1.5 mm^2

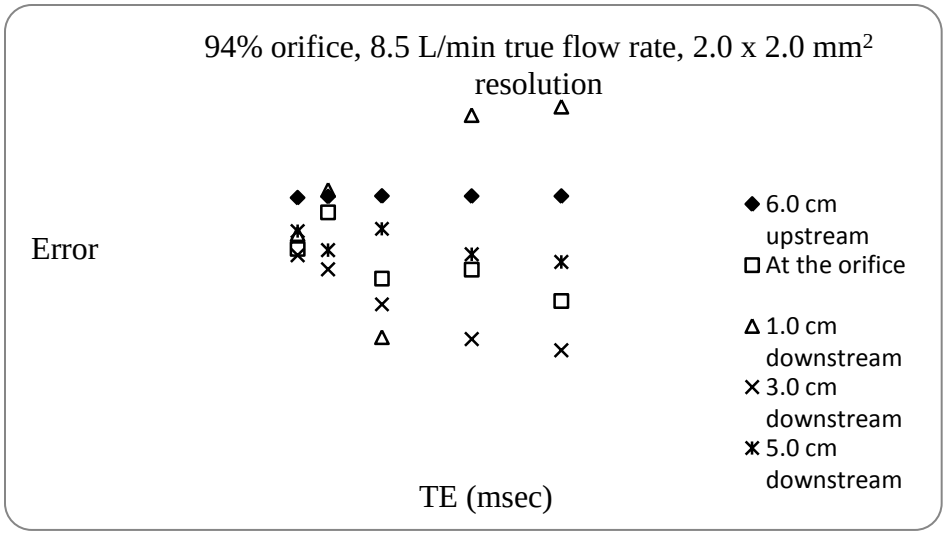

Figure A.14: Percentage error in the flow rate measurement as a function of TE for 94% orifice model at each slice position for a true flow rate of 8.5 L/min; In-plane resolution: 1.5 x 1.5 mm^2

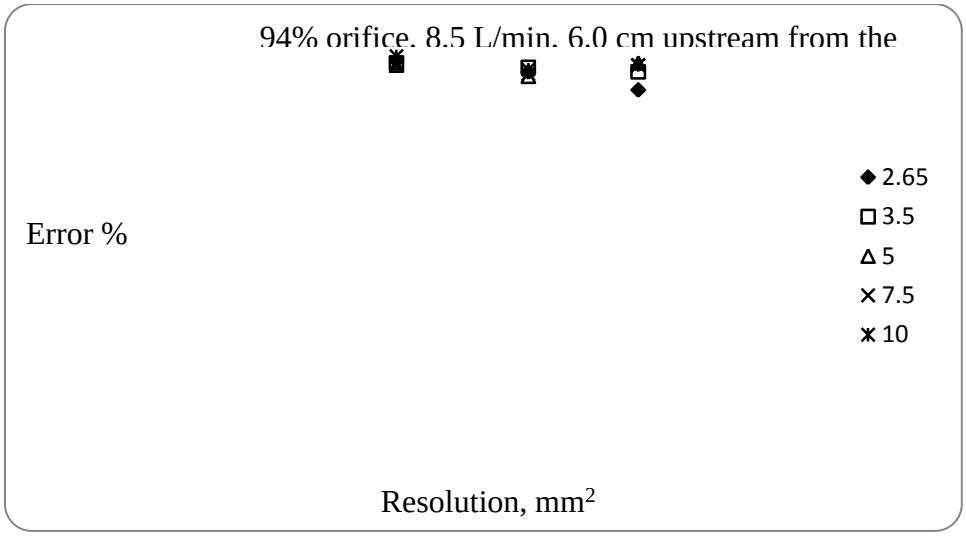

Figure A.15: Percentage error in flow rate measurement as a function of in-plane resolution for the 94% orifice model; Slice position: 6.0 cm upstream; for a true flow rate of 8.5 L/min

Appendix B

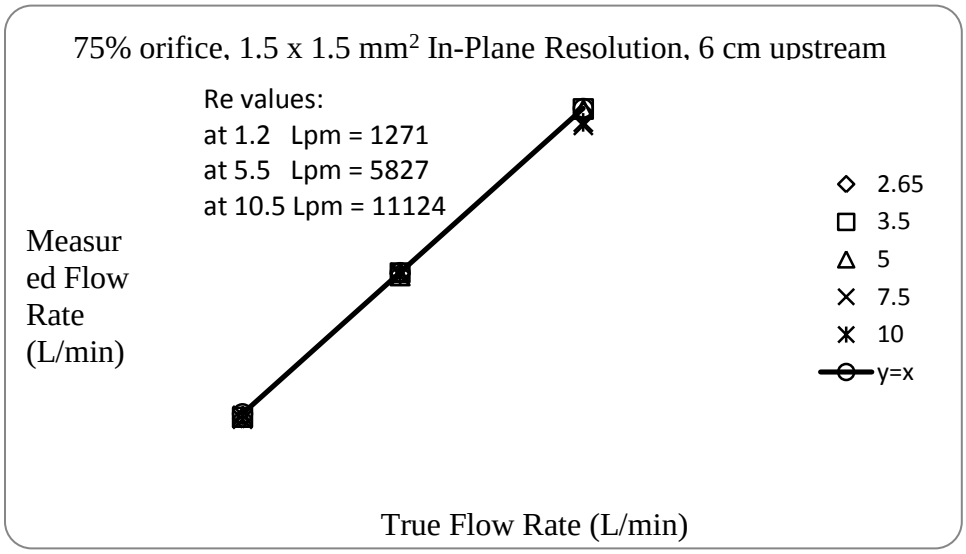

Figure B.1: Relationship between the measured flow rate and the true flow rate for all TEs, at 6.0 cm upstream from the 75% orifice; In-plane resolution = 1.5 x 1.5 mm^2.

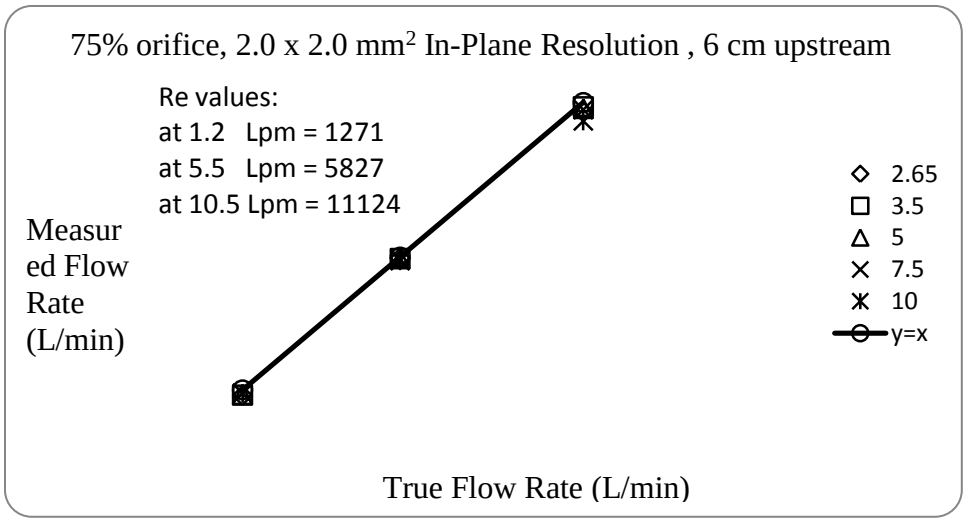

Figure B.2: Relationship between the measured flow rate and the true flow rate for all TEs, at 6.0 cm upstream from the 75% orifice; In-plane resolution = 2.0 x 2.0 mm^2.

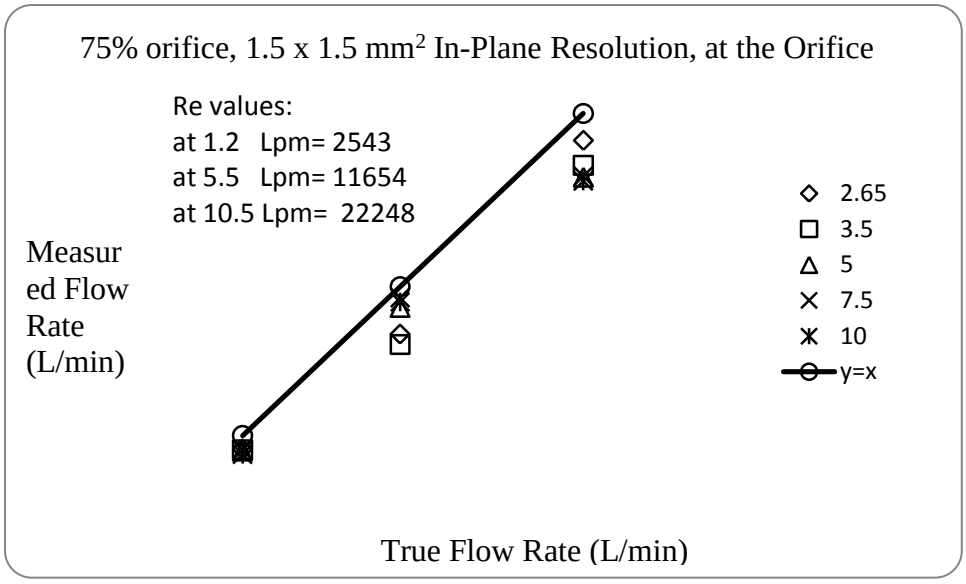

Figure B.3: Relationship between the measured flow rate and the true flow rate for all TEs, at the orifice, from the 75% orifice; In-plane resolution = 1.5 x 1.5 mm^2.

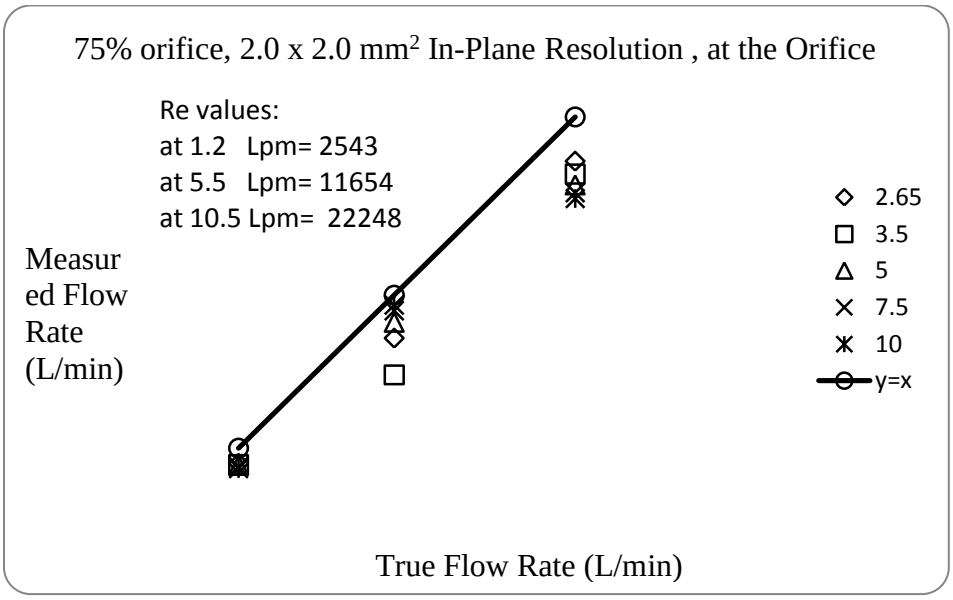

Figure B.4: Relationship between the measured flow rate and the true flow rate for all TEs, at the orifice, from the 75% orifice; In-plane resolution = 2.0 x 2.0 mm^2.

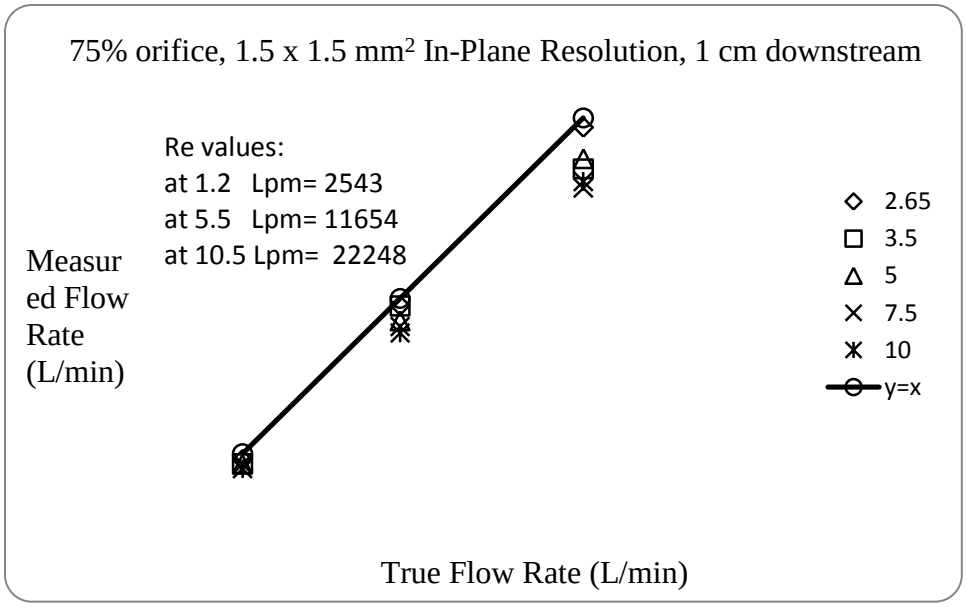

Figure B.5: Relationship between the measured flow rate and the true flow rate for all TEs, at 1.0 cm downstream from the 75% orifice; In-plane resolution = 1.5 x 1.5 mm^2.

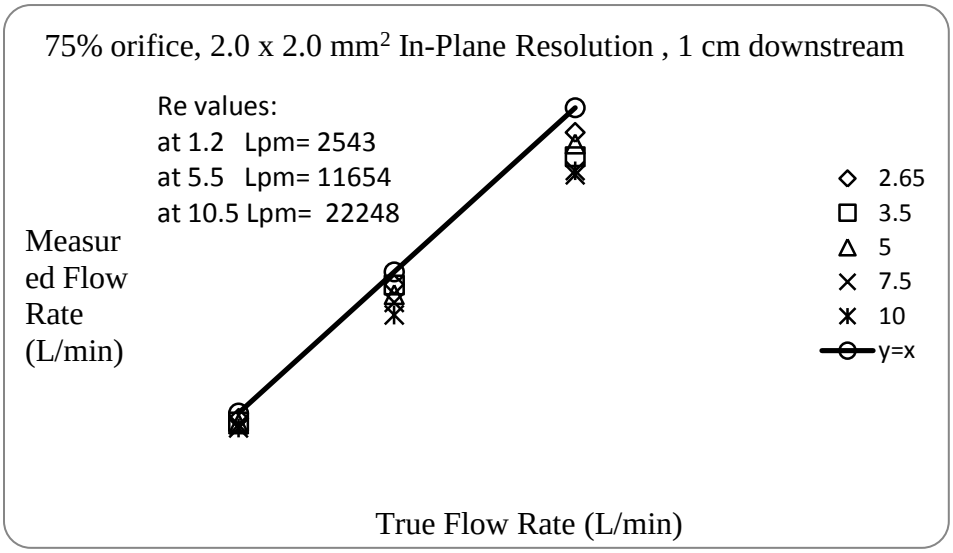

Figure B.6: Relationship between the measured flow rate and the true flow rate for all TEs, at 1.0 cm downstream from the 75% orifice; In-plane resolution = 2.0 x 2.0 mm^2.

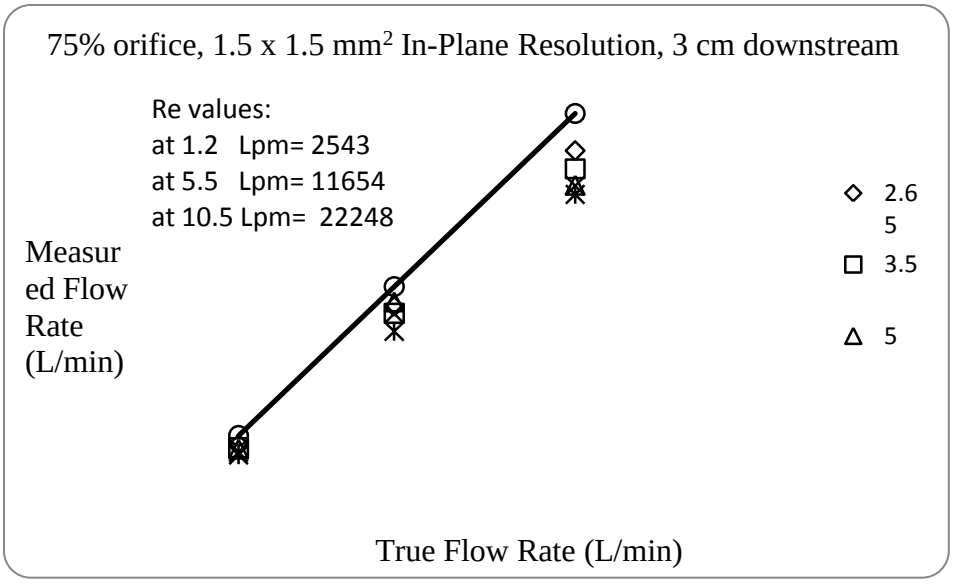

Figure B.7: Relationship between the measured flow rate and the true flow rate for all TEs, at 3.0 cm downstream from the 75% orifice; In-plane resolution = 1.5 x 1.5 mm^2.

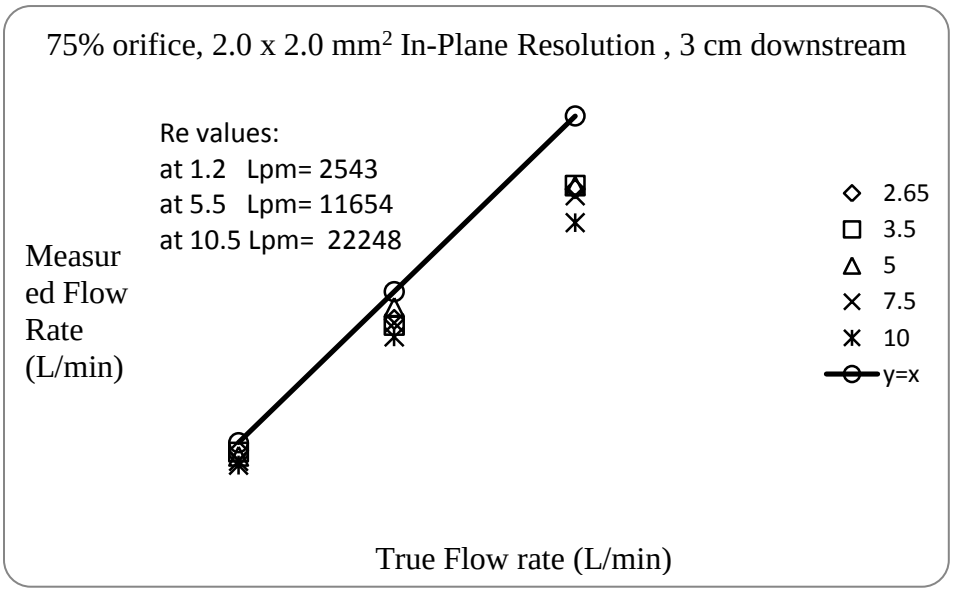

Figure B.8: Relationship between the measured flow rate and the true flow rate for all TEs, at 3.0 cm downstream from the 75% orifice; In-plane resolution = 2.0 x 2.0 mm^2.

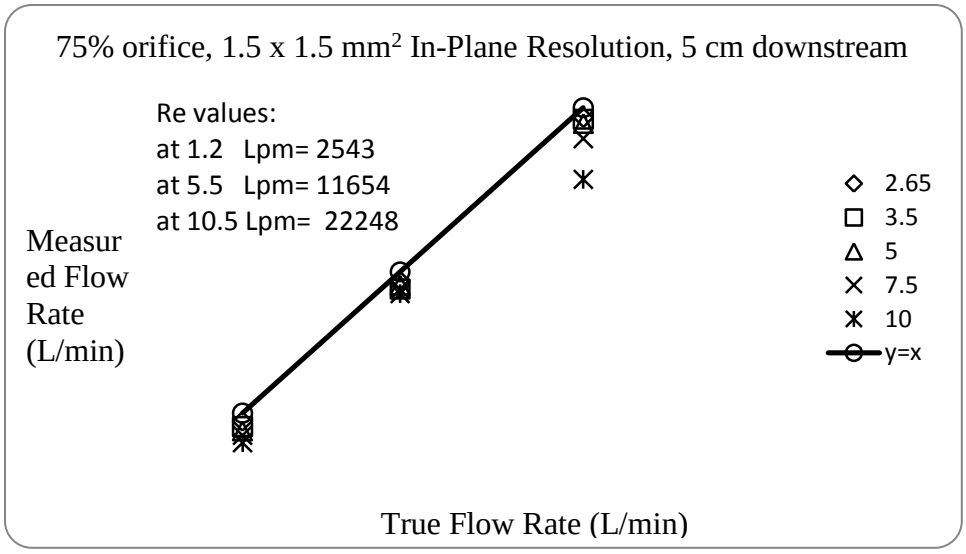

Figure B.9: Relationship between the measured flow rate and the true flow rate for all TEs, at 5.0 cm downstream from the 75% orifice; In-plane resolution = 1.5 x 1.5 mm^2.

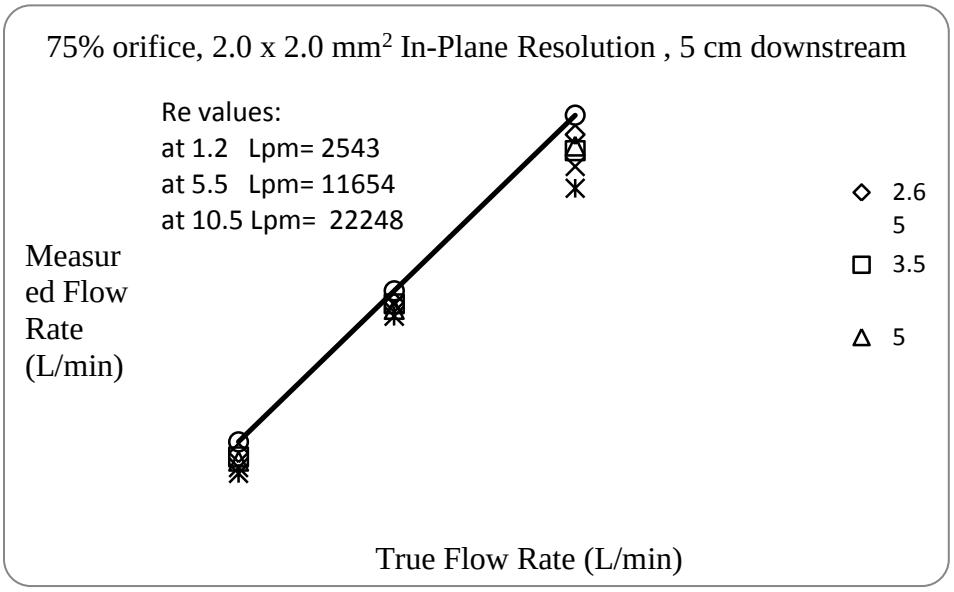

Figure B.10: Relationship between the measured flow rate and the true flow rate for all TEs, at 5.0 cm downstream from the 75% orifice; In-plane resolution = 2.0 x 2.0 mm^2.

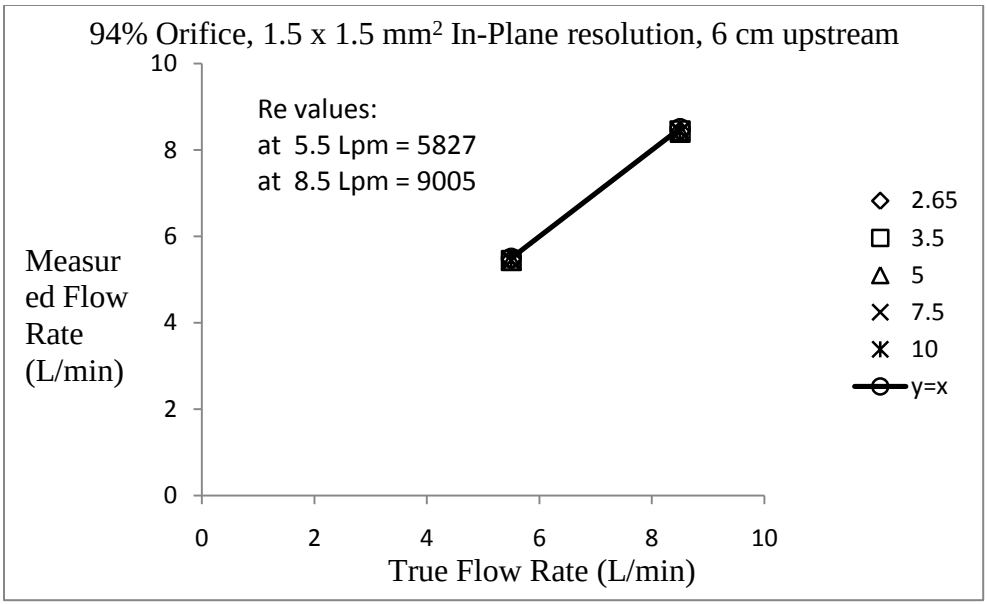

Figure B.11: Relationship between the measured flow rate and the true flow rate for all TEs, at 6.0 cm upstream from the 94% orifice; In-plane resolution = 1.5 x 1.5 mm^2.

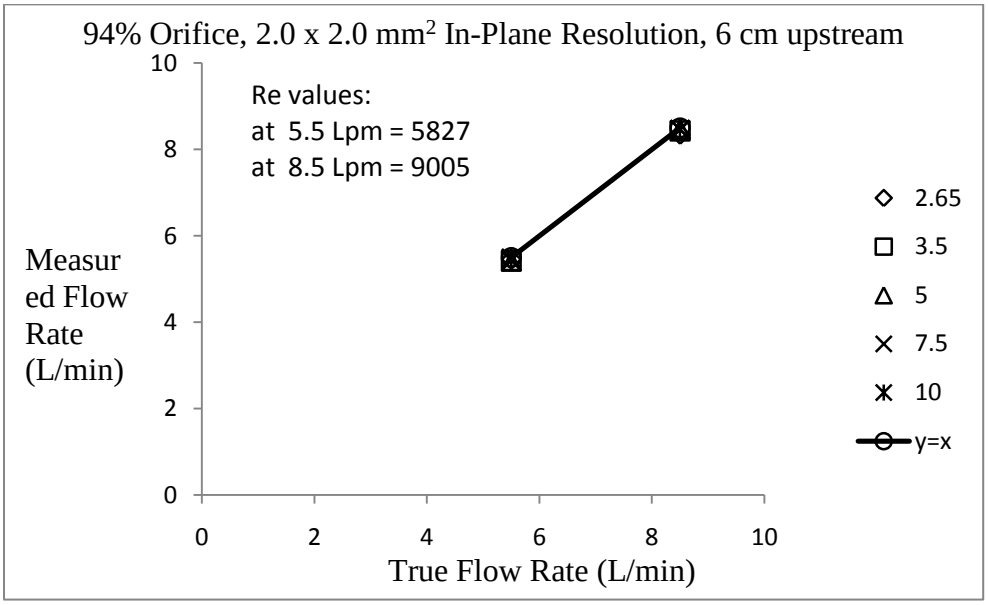

Figure B.12: Relationship between the measured flow rate and the true flow rate for all TEs, at 6.0 cm upstream from the 94% orifice; In-plane resolution = 2.0 x 2.0 mm^2.

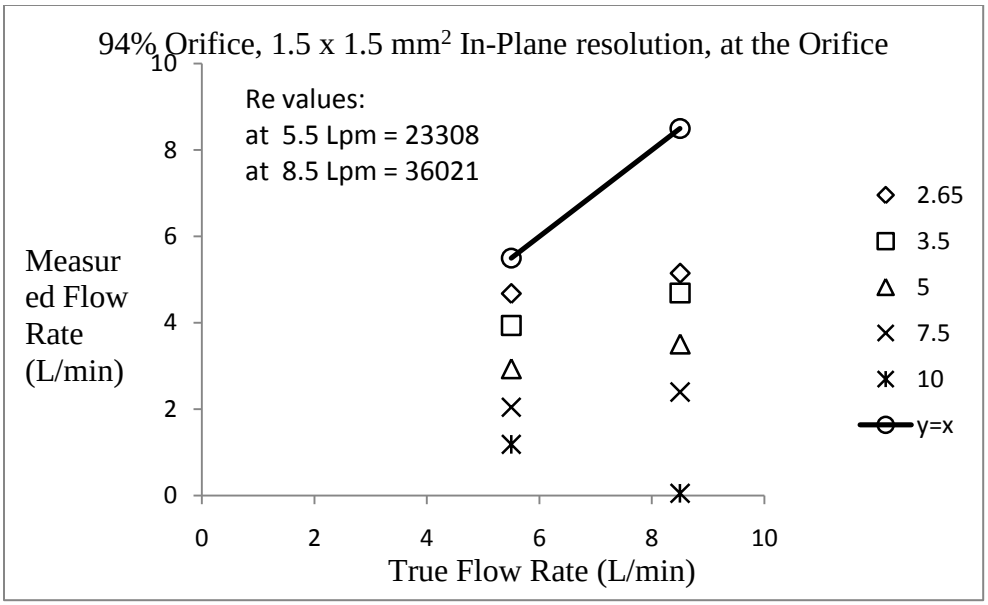

Figure B.13: Relationship between the measured flow rate and the true flow rate for all TEs, at the orifice, from the 94% orifice; In-plane resolution = 1.5 x 1.5 mm^2.

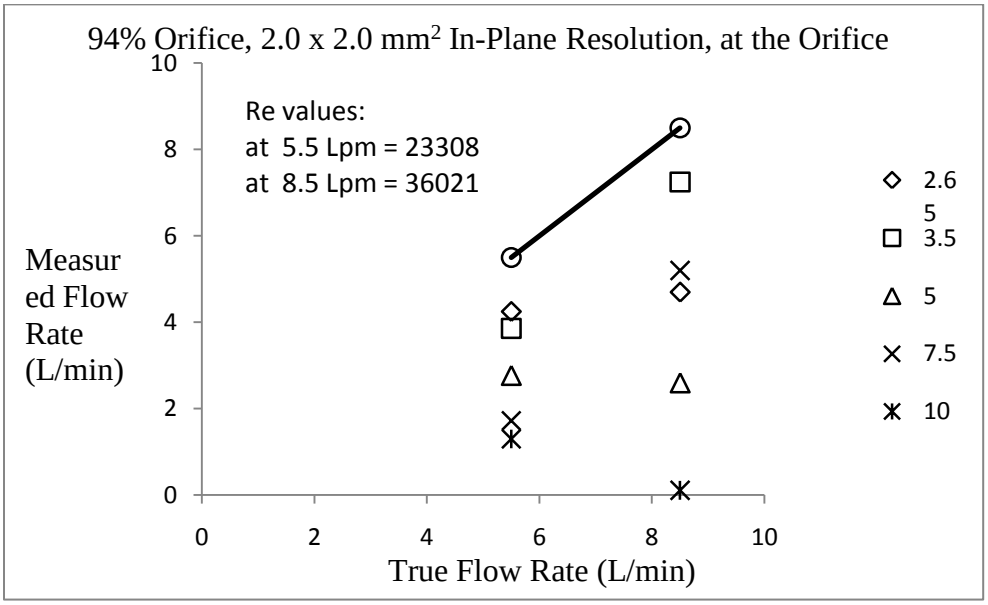

Figure B.14: Relationship between the measured flow rate and the true flow rate for all TEs, at the orifice, from the 94% orifice; In-plane resolution = 2.0 x 2.0 mm^2.

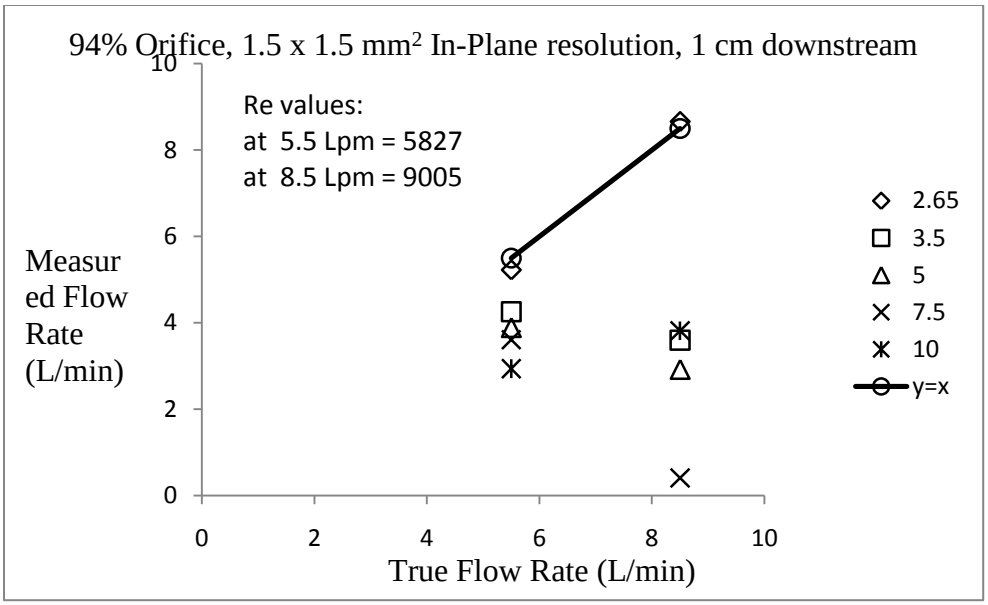

Figure B.15: Relationship between the measured flow rate and the true flow rate for all TEs, at 1.0 cm from the 94% orifice; In-plane resolution = 1.5 x 1.5 mm^2.

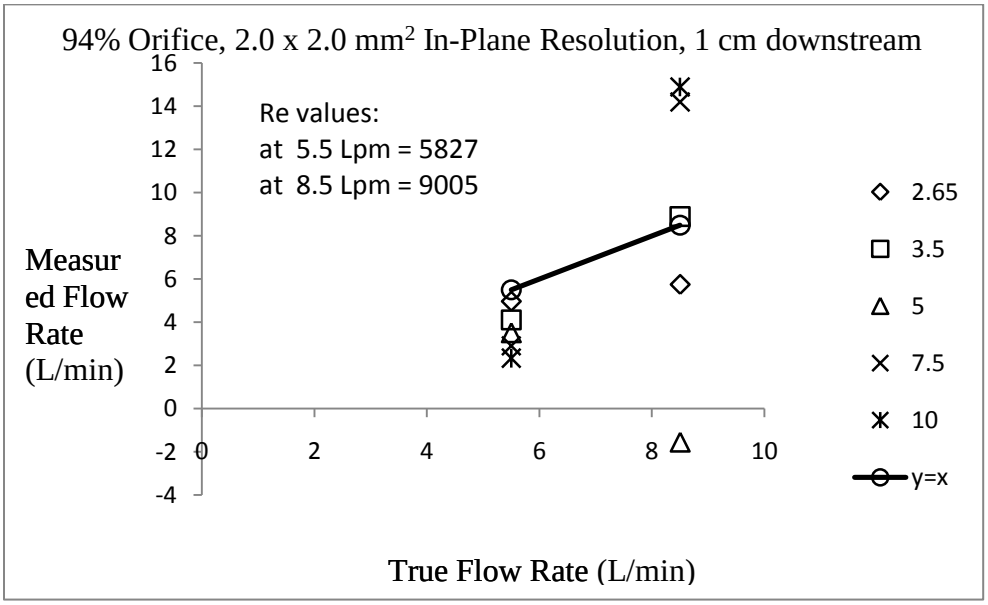

Figure B.16: Relationship between the measured flow rate and the true flow rate for all TEs, at 1.0 cm from the 94% orifice; In-plane resolution = 2.0 x 2.0 mm^2.

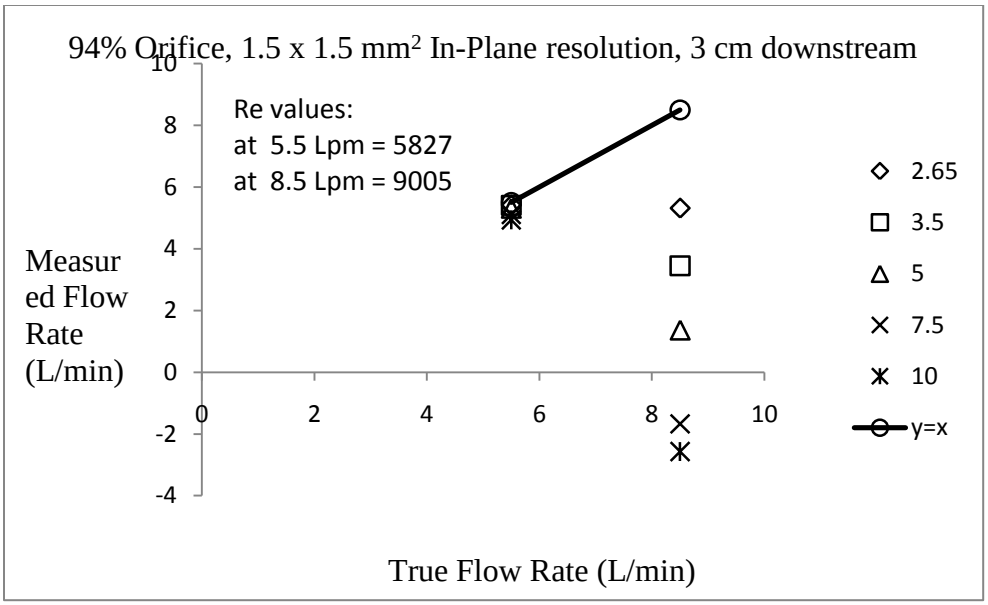

Figure B.17: Relationship between the measured flow rate and the true flow rate for all TEs, at 3.0 cm from the 94% orifice; In-plane resolution = 1.5 x 1.5 mm^2.

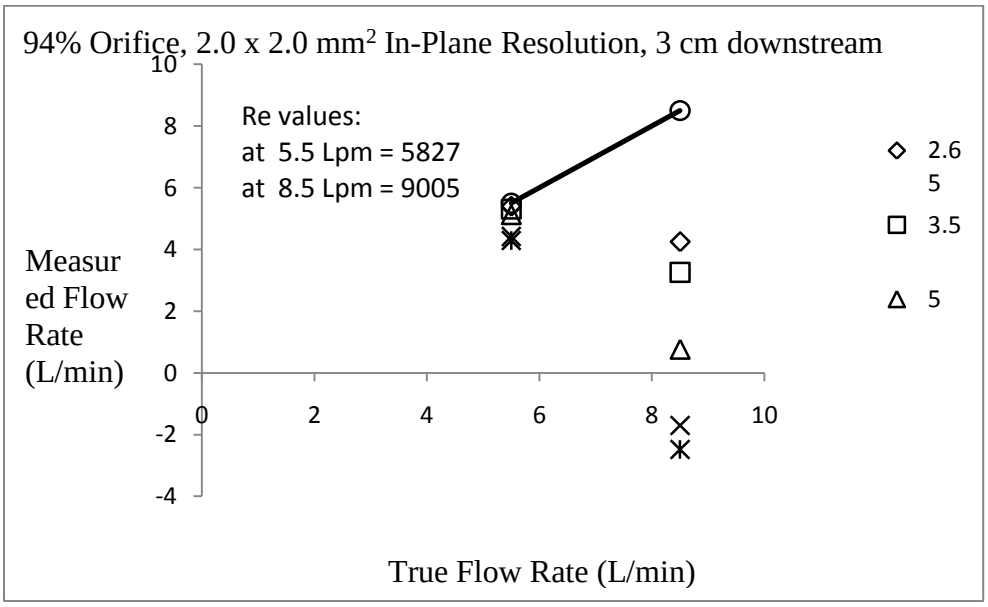

Figure B.18: Relationship between the measured flow rate and the true flow rate for all TEs, at 30 cm from the 94% orifice; In-plane resolution = 2.0 x 2.0 mm^2.

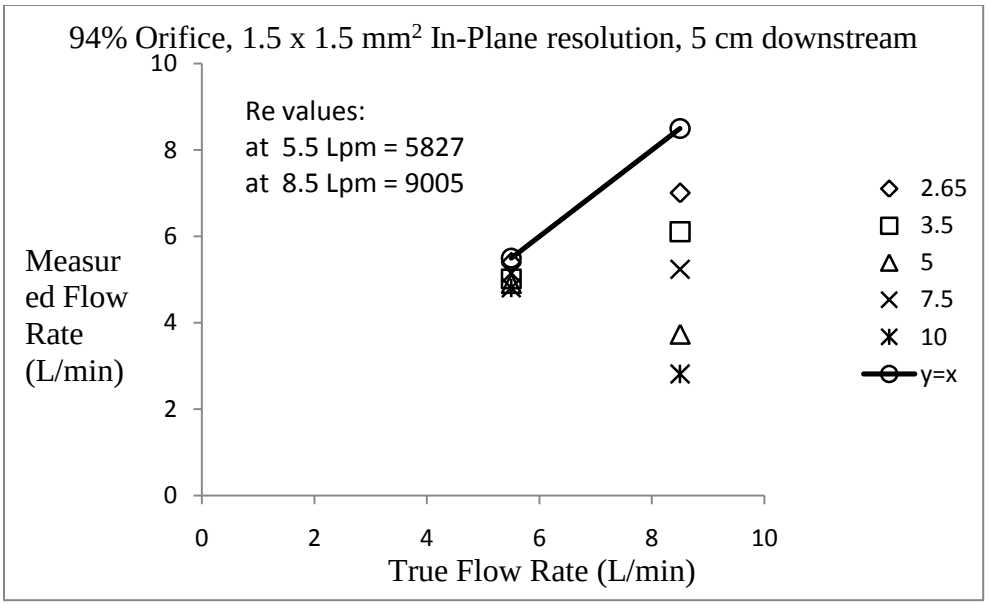

Figure B.19: Relationship between the measured flow rate and the true flow rate for all TEs, at 5.0 cm from the 94% orifice; In-plane resolution = 1.5 x 1.5 mm^2.

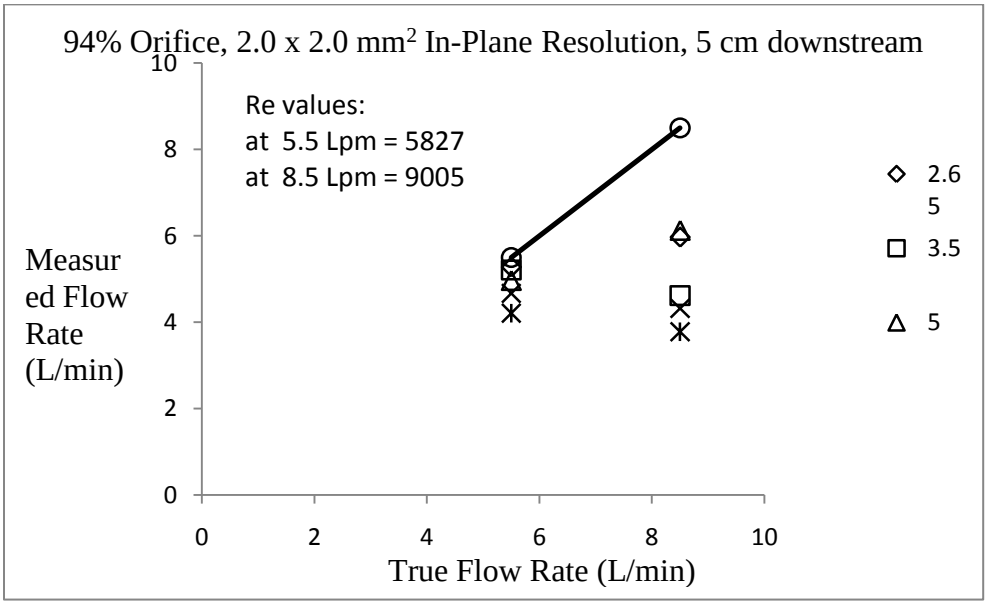

Figure B.20: Relationship between the measured flow rate and the true flow rate for all TEs, at 5.0 cm from the 94% orifice; In-plane resolution = 2.0 x 2.0 mm^2.